Ion release from silver/polymer nanocomposites

Dissertation

zur Erlangung des akademischen Grades

Doktor der Ingenieurwissenschaften

(Dr.-Ing.)

der Technischen Fakultät

der Christian-Albrechts-Universität zu Kiel

Nisreen Alissawi

Kiel, Germany

May 2013

First examiner	Prof. Dr. Franz Faupel
Second examiner	Prof. Dr. Christine Selhuber-Unkel
Date of examination	12.07.2013

To my family & Sven-Olaf

who have given me their love & support throughout my life

& believed that I could do it

Abstract

The tuning of silver ion release is very important for biomedical applications of silver nanocomposite materials to reduce the potential toxicity effects towards human cells and the environment.

The present work is based on developing different metal/polymer nanocomposites using several physical vapor deposition (PVD) techniques. Since the properties of the nanoparticles strongly depend on their size, distribution and shape, the determination of their exact morphology is important in order to understand and control their physical properties. Thus, in this work the metal nanoparticles are deposited on the surface of the polymer films or buried under a polymer barrier instead of being embedded into the polymer matrix. The model system consists of ensembles of silver nanoparticles (AgNPs) on sputtered polytetrafluoroethylene (PTFE) thin films. Sputtered PTFE films are suitable to host the AgNPs due to the high crosslinking and since PTFE is a hydrophobic polymer so the quick depletion of the AgNPs could be avoided. Besides, PTFE is known for its high resistance to chemicals, transparency, good dielectric properties and biocompatibility.

We examined the morphology, the composition and the optical properties of these nanocomposites using various analytical methods to characterize them and to study the potential of the silver ion release of the samples after immersion in water for several periods of time. Inductively coupled plasma mass spectroscopy (ICP-MS) is used to measure the concentration of silver ions in water. Changes in the microstructure and the optical properties of the nanocomposite films upon immersion in water allow demonstrating the kinetics of the silver ion release. Different approaches to tune the silver ion release process are studied and demonstrated in this work. Adjusting the release of silver ions through variation of the initial amount of silver nanoparticles, particle size control and through barrier thickness control is presented. Tuning the silver ion release by alloying with gold is also discussed. Furthermore, we study the release of silver ions from Ag/PTFE nanocomposites covered by thin films of plasma polymerized hexamethyldisiloxane (HMDSO) and we show how varying the oxygen flow during the

plasma polymerization process can adjust the silver ion release potential of the nanocomposites due to changes in the properties of the formed plasma polymerized HMDSO thin films.

Declaration of authenticity

I, the undersigned, **Nisreen Alissawi**, declare that this dissertation is my original work, gathered and utilized especially to fulfil the purposes and objectives of this study, and has not been previously submitted, in whole or in part, to any other university for any academic degree. Except where otherwise indicated, this thesis is my own work.

Signature

Place and date

Declaration of co-authorship and co-contribution:

Papers and publications incorporated in thesis

I, **Nisreen Alissawi**, declare here the nature of my contribution to the work in the following publications:

1. Paper entitled, '*Tuning of the ion release properties of silver nanoparticles buried under a hydrophobic polymer barrier*', **N. Alissawi**, V. Zaporojtchenko, T. Strunskus, T. Hrkac, I. Kocabas, B. Erkartal, V.S.K. Chakravadhanula, L. Kienle, G. Grundmeier, D. Garbe-Schönberg, and F. Faupel, reused in chapter 5 with permission from (Journal of nanoparticle research 14: 928-939). Copyright (2012), Springer.

I prepared all the samples, performed the characterization measurements using UV-vis, XPS, ICP-MS, samples preparation for TEM, SEM, all data analysis, figures and histograms, and wrote most of the text as a first author.

2. Paper entitled, '*Combined in situ electrochemical impedance spectroscopy-UV/Vis and AFM studies of Ag nanoparticle stability in perfluorinated films*', K. Yliniemi, B. Özkaya, **N. Alissawi**, V. Zaporojtchenko, T. Strunskus, B.P. Wilson, F. Faupel, and G. Grundmeier, reused in chapter 5 with permission from (Materials chemistry and physics 134: 302-308). Copyright (2012), Elsevier.

I prepared the whole measured samples and wrote the part related to the samples preparation and helped in writing the results and discussion part.

3. Paper entitled, '*Effect of gold alloying on stability of silver nanoparticles and control of silver ion release from vapor-deposited Ag-Au/polytetrafluoroethylene nanococomposites*', **N. Alissawi**, V. Zaporojtchenko, T. Strunskus, I. Kocabas, V.S.K. Chakravadhanula, L. Kienle, D. Garbe-Schönberg, and F. Faupel, reused in chapter 6 with permission from (Gold Bulletin 46: 3-11). Copyright (2012), Springer.

I prepared all the samples, performed the characterization measurements using UV-vis, XPS, ICP-MS, samples preparation for TEM, all data analysis, figures and histograms, and wrote most of the text as a first author.

4. Paper entitled, *'Plasma polymerized HMDSO coatings to adjust the silver ion release properties of Ag-nanocomposites'*, **N. Alissawi**, T. Peter, T. Strunskus, C. Ebbert, G. Grundmeier, and F. Faupel, submitted to Journal of nanoparticle research (2013), used in chaper 7.

I did most of the samples preparation, performed the characterization measurements using UV-vis, XPS, samples preparation for ICP-MS, samples preparation for TEM, all data analysis, figures, and wrote most of the text as a first author.

Acknowledgments

I express my sincere gratitude to Prof. Dr. Franz Faupel for giving me the opportunity to do this interesting doctorate work under his supervision. I am deeply thankful to Dr. Vladimir Zaporojtchenko, whom we sadly lost in August 2012, for his guidance at all stages in carrying out my work. Without his encouragement and belief in me, I could not have persisted in my work and finished what we had planned together. Many of his instructions, which indeed influenced my whole attitude, I will remember forever.

Thanks go too to Dr. Thomas Strunskus for his kind support, his contributions in my work and the insightful discussions about research. Special thanks to Dipl.-Ing. Stefan Rehders for his friendship and the magnificent technical assistance he offered though out my whole work. I am grateful also to Dipl.-Ing. Rainer Kloth for his assistance in all computer-related issues. Many thanks to my friends and colleagues Dipl. Phys. Tilo Peter for his share in the part dealing with HMDSO plasma polymerization and Dr. Oleksandr Polonskyi for his continuous encouragement and suggestions which helped me through out the writing process.

I am extremely grateful to the entire chair for Multicomponent Materials for the stimulating and innovative research environment they generated besides the friendly atmosphere and the nice coffee and cake times. Working with you guys has been great fun. I would really like to thank all of you who helped me directly or indirectly in completing my work successfully. I appreciate as well the help of all students who worked with me or did their bachelors or masters work within this project.

I would like to thank all colleagues from the group of Prof. Lorenz Kienle for performing the TEM measurements. Thanks also to Dr. Dieter Garbe-Schönberg and Dipl.-Ing. Ulrike Westernstöer for their help in performing the ICP-MS measurements. Thanks to Dipl. Phys. Saleh Habouti for the SEM characterization. I share the credit of my work as well with our collaborative colleagues from the group of Prof. Dr.-Ing. Guido Grundmeier at Paderborn University.

I will always be thankful to my former master's research supervisor, Prof. Dr.-Ing. Mady Elbahri as he has been helpful in providing advice many times during my work. I owe my hearty gratitude to Prof. Dr. Hanna Hallak from the Department of Physics at Bethlehem University in Palestine who has been always my friend, guide and philosopher.

Last but certainly not least, I am indebted to my mom and dad, my brother Naser and his family, my sister Nadia and her family, and my brother Nabeel for their everlasting love, continual support and encouragement. My hard-working parents have sacrificed their lives for us and provided unconditional love and care. I love them so much, and I would not have made it this far without them. Special thanks to the newest additions to my family, Sven-Olaf, my future-husband as well as his wonderful family in Germany who all have been supportive and caring. Many thanks to all my friends back home and the ones I met in Germany, who made my stay here joyful and rich through getting to know them.

Nisreen Alissawi

May 2013

Kiel

List of initials and acronyms

2D	Two dimensional
Abs.	Absorbance
Ag	Silver
Ag^+	Silver ion
AgNPs	Silver nanoparticles
ATP	Adenosine triphosphate
DC	Direct current
DI	Deionized
DNA	Deoxyribonucleic acid
EIS	Electrochemical impedance spectroscopy
FCC	Face-centered cubic
HMDSO	Hexamethyldisiloxane
ICP-MS	Inductively coupled plasma mass spectroscopy
NPs	Nanoparticles
POM	Polyoxymethylene
PTFE	Polytetrafluoroethylene
PVD	Physical vapor deposition

QCM	Quartz crystal microbalance
RF	Radio frequency
ROS	Reactive oxygen species
sccm	Standard cubic centimeter per minute
SEM	Scanning electron microscopy
SPR	Surface plasmon resonance
TEM	Transmission electron microscopy
UV-vis	Ultraviolet-visible light spectroscopy
XPS	X-ray photoelectron spectroscopy

Table of contents

Chapter 1

Introduction

Silver and its compounds have been known for centuries for their broad-spectrum antimicrobial activity against different microbial and they have been used in many medical applications besides food packaging, textile fabrics and for water treatment [1–3]. In comparison with silver salts and the bulk silver, silver nanoparticles (AgNPs) have been better candidates in medical applications due to their slower dissolution rate compared to silver salts [4], [5] and due to their higher interaction efficiency compared to bulk silver [2], [6]. This strongly antimicrobial action is proven to be dominant through release of silver ions from the AgNPs as a cooperative oxidation process requiring both dissolved dioxygen and protons [7–11], with some evidence that the silver nanoparticles themselves can damage the microbial cell membranes too [1], [12–15].

Numerous practical applications of metal NPs require them to be well dispersed into or on the surface of various substrates and matrices without the formation of large aggregates and without high chances of their undesirable transfer into the environment. The stabilization of AgNPs in polymer matrices has recently gained great attention and many methods were developed to prepare Ag/polymer nanocomposite coatings where the silver ion release and the antibacterial effect of the nanocomposites were found to be

dependent on the silver nanoparticle content and on the method employed [2], [8], [16–26].

Because of the marked increase of antibacterial nanocomposites in the last decades, there is significant interest in studying Ag ion release from AgNPs to optimize the nanocomposite performance and to reduce the negative effects on human cells and environment [1], [10], [12], [13], [27], [28]. An important issue concerning Ag ion release is its kinetics; fast or slow release, high or low dose, short or long-term action. All these points are of great interest while searching for novel, efficient antibacterial surfaces and improving AgNPs technologies through controlled release formulations. This is important in order to get a dose control to achieve the desired bactericidal effects on specific targets with no toxic effects on human health or the environment [10]. The understanding of Ag biocide and environmental effects is complicated because of the multifunctional dependence of Ag ion release not only on the nanoparticles' morphology and concentration but also on the particle size distribution in the host materials as well as on their properties. Many previous studies on ion release kinetics of AgNPs focused on environmental factors' dependence, such as dissolved oxygen, pH, temperature, and the presence of natural organic matter [9]. Also the dependence of ion release kinetics on the primary particle size and concentration was investigated [12], [27], [29]. The properties of the polymer matrix play also a major role in the release process due to differences in the water uptake of each matrix [8], [23], [30], [31]. Moreover, several bimetallic/polymer nanocomposites were developed showing promising properties in the silver ion release studies [19], [32–34].

Despite the intensive research that has been carried out so far, there are still no systematic studies of controlled release taking into account how the composite's morphology (nanoparticles' size, concentration, and distribution) affects the mechanism and the kinetics of the interfacial ion transfer reactions of the metal nanoparticles. The lack of understanding is partly due to the fact that metal nanoparticles embedded in a polymeric matrix are not directly accessible concerning their interfacial structure and reactivity. This makes it hard to investigate the geometrical arrangement of the nanoparticles in the host matrix; thereby the morphology of the nanocomposite and their functional properties

can not be tailored. This has been approached in the present work by the usage of well defined model systems consisting of two dimensional (2D) silver nanoparticle ensembles which are either directly accessible or covered by polymer layers of well defined thickness and composition. By 2D we mean that the nanoparticles are deposited on the surface of the polymer instead of being embedded inside the matrix (i.e. 3D). This nanocomposite system was prepared by thermal evaporation deposition of AgNPs with different nominal thicknesses on top of a highly crosslinked sputtered polytetrafluoroethylene (PTFE) thin film or sandwiched between two polymer films. Thin films of sputtered PTFE were chosen as they are possible to be prepared using our home-made sputtering chamber which is a good way to produce a highly crosslinked polymer matrix that is suitable as a host for the AgNPs. Moreover, since PTFE is a hydrophobic polymer, the water uptake is small, so that a quick depletion of the AgNPs should be avoided [35]. Besides, PTFE is widely used in metal-polymer nanocomposite systems due to its high resistance to chemicals, transparency and very good dielectric properties [36]. In the composite studies of PTFE with metal atoms, it was found that PTFE stabilizes the composite, reduces the defects and increases the contact angle for water management applications [37]. Moreover, PTFE has been considered by many researchers as being biocompatible as its low surface energy results in a poor bacteria adhesion, thus the formation of bio-films on the Ag/polymer film could be avoided which is an important issue for medical devices [38].

Characterization of the nanocomposites was performed simultaneously in terms of the release of Ag ions and the control of the morphology transformation of the nanocomposite system by using a combination of different analytical techniques such as transmission electron microscopy (TEM), UV-visible spectroscopy (UV-vis), X-ray photoelectron spectroscopy (XPS) and inductively coupled plasma mass spectrometry (ICP-MS). A strong correlation was found among the results obtained by the different techniques. Based on these results, I discuss the influence of the nanocomposites' morphology and the polymer barrier on the Ag ion release kinetics.

Additionally, silver ion release kinetics from composites consisting of silver-gold (Ag-Au) alloy NPs of 5 nm average size with various compositions was investigated and

compared to composites of only pure AgNPs. The results show that gold alloying strongly improves the oxidation resistance of the AgNPs. The dissolution of Ag slows down quickly after first exposure to water and reaches a saturation state. No concentration gradient is established within the NPs upon Ag depletion due to the high atomic mobility in the small NPs.

In the last part of this work, coatings of plasma polymerized hexamethyldisiloxane (HMDSO) were deposited on the Ag/PTFE nanocomposites. The structure of the plasma polymerized HMDSO film was tailored by varying the oxygen flow during the polymerization process and the silver ion release potential and the water uptake properties were investigated. Results showed a strong relation between the oxygen content and the properties of the plasma polymerized HMDSO coatings. ICP-MS, water uptake and wettability results showed a strong water diffusion dependence on the oxygen content in the coating films. This indicates that by tailoring the properties of the plasma polymerized coatings films, one can tune the silver ion release properties of Ag/polymer nanocomposites. Changing the thickness of the barrier showed also another way of tuning the release of silver ions from the nanocomposites.

This dissertation is composed of eight chapters. The first one gives an introduction into the subject of the Ag containing nanocomposites and the silver ion release process. Chapter two deals with the main theoretical background associated at all stages of this work, starting with the silver nanoparticles and its chemical potential, optical properties and the alloying of silver with gold on the nanoscale. Besides, the dissolution of the NPs and in particular the silver ion release process and the corresponding antimicrobial effects of AgNPs were discussed too. Then the Ag/polymer nanocomposites and the growing and nucleation of the NPs on top of the polymer surface as well as the properties of the sputtered PTFE films and the plasma polymerized HMDSO films were explained. Chapter three describes all the techniques which were employed in this work for the deposition or the characterization of the samples. The fourth chapter is dealing with the experimental procedures which were followed to prepare and characterize all the sample systems. Results and discussions were then shown in three separated chapters as follows: chapter five demonstrates the synthesis of Ag/PTFE nanocomposites and their silver ion

release properties as well as the barrier effects on the silver ion release potential, chapter six deals with the synthesis of Ag-Au alloy/PTFE nanocomposites and their silver ion release potential, and chapter seven shows the deposition of plasma polymerized HMDSO barriers with various oxygen content and various thicknesses on top of Ag/PTFE nanocomposites and how that affects the silver ion release kinetics. Finally, chapter 8 summarizes the whole work and gives an outlook.

Chapter 2

Theory

2.1 Silver nanoparticles

Silver nanoparticles contain 20 - 15,000 silver atoms are generally smaller than 100 nm [39–41] and have unusual physical, chemical and biological properties. They have been utilised in many consumer products and applications as can be seen in Table 2.1, exploiting their strongly bactericidal action and making AgNPs the largest and fastest growing class of nanomaterials in product applications [3].

Table 2.1 Major products in the market containing AgNPs [3]

Nano-Ag containing prodcuts	Percentage
Creams and cosmetics items	32.4
Health supplements	4.1
Textiles and clothing	18.0
Air and water filters	12.3
Household items	16.4
Detergents	8.2
Others	8.6

Nanoparticles (sometimes referred to as ultrafine particles) generally have been defined as particle-types in the size range below 100 nm, in at least one dimension [42]. The smaller size of the NPs, results in unique chemical and physical characteristics leading to

advanced magnetic, electrical, optical, mechanical and structural properties compared to the original bulk substrate [43]. They show behavior which is intermediate between that of a macroscopic solid and that of an atomic or molecular structures [6], [44]. They display deviations from bulk solid behavior such as reductions in the melting temperature which results from the effect of the surface free energy, and changes in the lattice parameter (usually reduction) which results from the effect of the surface stress. Both the surface stress and surface free energy are caused by the reduced coordination of the surface atoms [45].

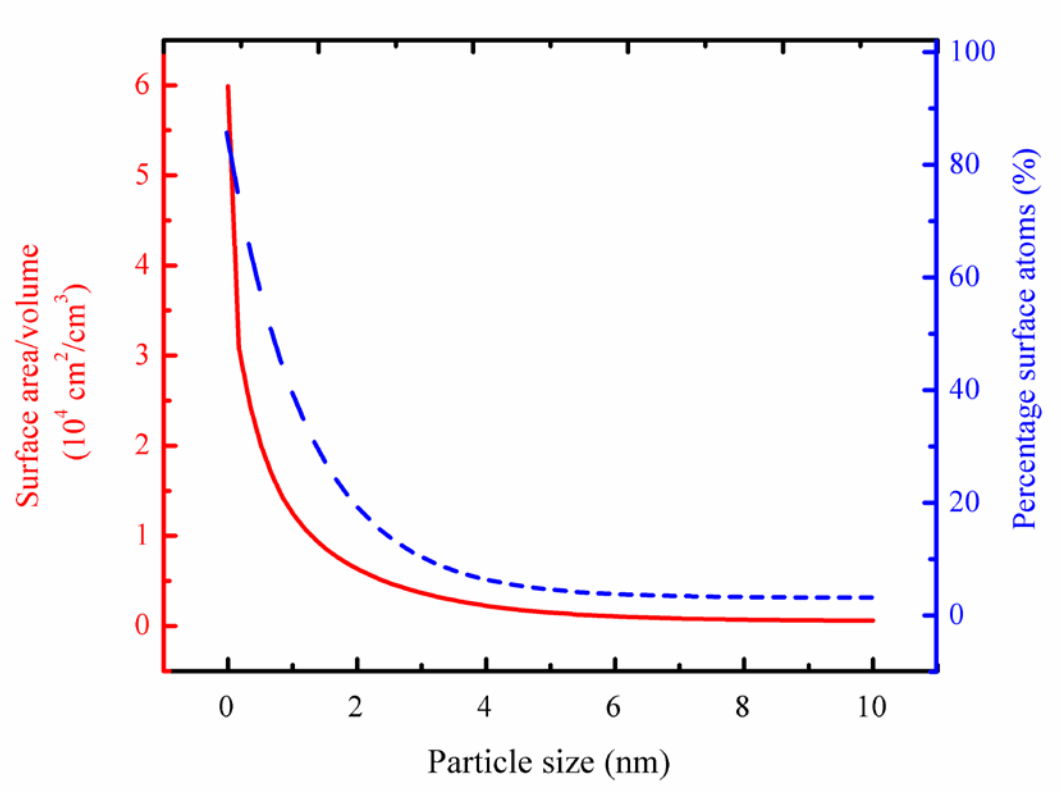

Figure 2.1 Surface area to volume ration and percentage of surface atoms (%) as a function of particle diameter (for gold NPs), based on [6]

The decrease in the size has a number of important attributes including large surface area to volume ratio as shown in Figure 2.1, high surface concentrations of corner and edge atoms and low coordination numbers (the number of nearest neighbors) of surface atoms, causing an increasing reactive surface area and as a result the surface free energy of the particle will change as a function of particle size, thus influencing the thermodynamics of

chemical reactivity. Besides, as size decreases, atomic structure variations occur, in terms of changes in bond lengths, bond angles, and vacancies and other defects near and on surfaces, and unique electronic properties (e.g., quantum transition) as the band structure, well known in bulk materials, begins to resemble discrete energy states of small molecules [6], [46–50]. Depending on the material and its size range, one or a combination of all of these factors will contribute to the size-dependent change in the properties and chemical reactivity of that material [50].

2.1.1 The chemical potential of NPs

The chemical potential μ is a thermodynamic quantity which expresses the amount of energy change per unit mass or mole in a thermodynamic system, if mass or particles would be introduced or removed, assuming fixed entropy and volume, i.e., $dU = \mu dn$, where dU and dn reflect the change of the internal energy and mole, respectively, of a homogeneous system [51].

In bulk systems, the contribution of the surface energy to total energy content is inconsequential. However, at nanoscale, the surface energy forms a major part of the total energy and has to be included in the calculations of chemical potential [52]. This effect is governed by Gibbs-Thomson equation (2.1) which states that the surface chemical potential is inversely proportional to the radius of curvature of the particle. For a one component system the Gibbs-Thomson equation relates the chemical potential $\mu_v(r)$, of the vapor in equilibrium with a spherical droplet of radius r to the chemical potential $\mu_v(\infty)$, of the vapor in equilibrium with a flat surface of the same substance at the same temperature through

$$\mu_v(r) - \mu_v(\infty) = \frac{2\gamma}{r}\Omega_0 \tag{2.1}$$

where γ is the (isotropic) specific surface free energy of the droplet (or the surface tension) and Ω_o is the molecular volume in the condensed phase. This equation is readily derived by considering the transport of material from the flat surface to the droplet so as to increase the radius of the droplet [53].

On applicability of the thermodynamics to nanoparticles, the size dependence of the surface tension has to be taken into account; the effective surface tension (the specific excess free energy) [54].

2.1.2 Optical properties of NPs

The optical properties of nanoparticles, in particular metal NPs, are totally different from the bulk behavior due to quantum size effects that give rise to extra ordinary spectra of electron energy levels which are predicted to be discrete [55].

The optical properties of metal nanoparticles have long been of interest starting with Faraday's investigations of colloidal gold in the middle 1800s. Later on, Gustav Mie presented a solution to Maxwell's equations that describes the extinction (scattering + absorption) spectra of spherical particles of arbitrary size. Since then, it has been recognized that the interaction of light with free electrons in a gold or silver nanoparticle can give rise to collective oscillations commonly known as surface plasmons (SPs) or surface plasmon resonance (SPR) [56–58].

When light is incident on a colloid of small metal particles the oscillating electric field of the light produces a force on the mobile conduction electrons in the metal, which induces a dipole moment in the particle as illustrated in Figure 2.2.

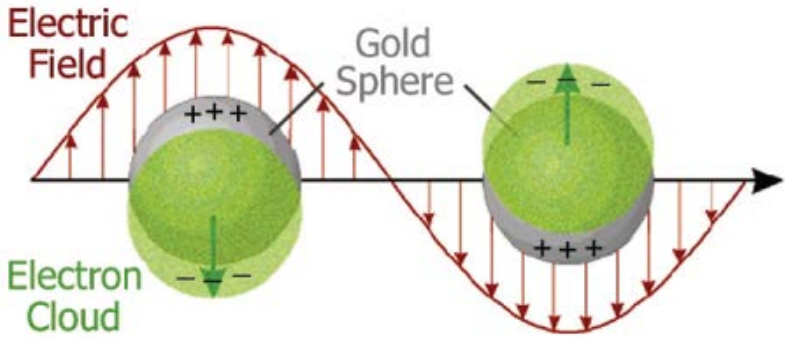

Figure 2.2 Schematic of plasmon oscillation for a spherical gold colloid, showing the displacement of the conduction electron charge cloud relative to the nuclei, reused with permission from [56], copyright (2005), Cambridge University Press

The redistribution of charge provides a restoring force on the displaced electrons arises from Coulomb attraction between electrons and nuclei which results in oscillations of the electron cloud relative to the nuclear framework and results in an associated resonant frequency. When the particle is small compared to the incident wavelength (radius $r \approx 5$ nm or less for visible light), a simple analytical formula for the polarizability, a, of the particle can be derived

$$a = 4\pi r^3 \frac{\varepsilon_m - \varepsilon_d}{\varepsilon_m + 2\varepsilon_d} \tag{2.2}$$

where ε_m is the relative permittivity of the metal and ε_d is the relative permittivity of the surrounding dielectric [56–58].

Understanding the color of different metallic nanoparticles comes from recognizing that the relative permittivity (refractive index n; since $\varepsilon_m = n^2$) of metals varies with frequency, or equivalently, with wavelength. The optical response of the particle is strongest when the denominator in equation (2.2) is closest to zero ($\varepsilon_m = -2\varepsilon_d$) [58].

These oscillations are found to depend on the shape, size and the dielectric constants of both the metal and the surrounding matrix [59]. Well separated gold and silver nanoparticle systems are unique because their densities of free electrons are in the proper range to give their NPs a broad, intense absorption band in the visible regime of the spectrum [56]. The number, the bandwidth, the position and intensity of SPR bands of metal NPs depend on the metal, the shape, the size, the size distribution, the interparticle separation, the surface state, the surface coverage and the surrounding environment of the nanoparticles [56], [58], [60]. As there is a decrease in the size of the NPs, there is a blue-shift in the SPR and a narrow size distribution of the particles yields a sharp plasmon peak [59]. Shape dependence has also been reported [56]. Different shapes have different number of resonance bands according to their shape. In addition, the distance between the nanoparticles affects the dipole-dipole interaction between them which affects the SP bands. The surface plasmon band broadens and shifts to higher wavelength when the interparticle distance gets smaller [61]. Moreover, nanoparticles are often produced on

surfaces and there is an interaction with the substrate influences their plasmon resonance properties. A detailed study of the effect of substrate index of refraction on the plasmon wavelength shows that the SPR wavelength of a silver sphere on a substrate shifts to the red as the sphere goes from free to being embedded. Moreover, the surrounding solvent affects the plasmon resonance wavelength of spherical nanoparticles as the particle plasmon wavelength λ_p varies with the index of refraction of the surrounding solvent [57]. Thus, as different molecules absorb radiation in different wavelengths, and as SPR peaks are highly sensitive to the particle size, shape, and environment of surrounding of nanoparticles, qualitative information about the status of the nanoparticles can be obtained by surface plasmon resonance absorption peak in the spectra [62].

Because of this high sensitivity, UV-vis technique was used throughout this work to study the optical and physical properties of the AgNPs and Ag-Au alloy NPs and changes in the optical spectra due to silver dissolution after immersion of samples in water was examined.

2.1.3 The dissolution of AgNPs and silver ion release

The silver ion release potential of different silver materials can be distributed between the silver sulfide (highly insoluble, hence a low potential for silver ion release) and the silver nitrate (completely soluble, maximum potential for silver ion release) extremes, as illustrated in Figure 2.3. Materials that store discrete silver ions in a matrix show a high release potential, a bit less than silver nitrate. Silver salts such as silver chloride show a lower release potential than the ion-based materials. At the other extreme, bulk silver metal has a potential closer to the silver sulfide. As the size of silver metal decreases, the surface availability per mass of silver increases and both the solubility and dissolution kinetics of silver vary as a function of size, thus the potential for silver ion release increases and moves toward the silver nitrate extreme but the silver salts and silver-ion materials still show higher potential than the nanosized silver metal materials [4].

The state of the nanoparticles, i.e., whether they present as isolated particles, aggregate, or dissolve in aqueous solutions depends on the size and shape of the metal nanoparticles, the manufacture's preparation, the capping agent as well as environmental conditions

such as pH, ionic strength, ionic composition, presences of dissolved organic matter (DOM), etc. [1], [49], [52], [63–65]. High ionic strength promotes NPs aggregation, that reduces the effective surface area of the NPs exposed to the solution, thereby decreasing silver ion dissolution [49], [52], [63].

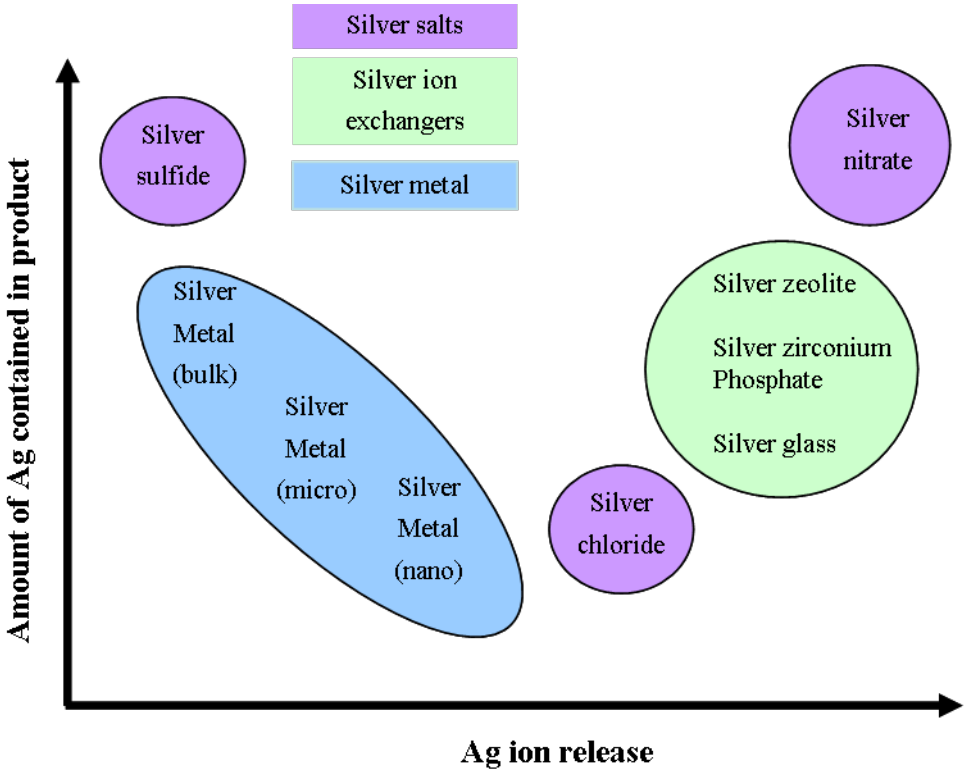

Figure 2.3 Silver ion release and amount of silver required in products for different biocidal silver formulations, based on [4]

The dissolution of a solid in an aqueous solution is considered to take place in two steps: (i) a reaction at the solid–liquid interface, the so called 'interfacial transport' and (ii) transfer of the dissolved matter away from the reaction site. The slower of these steps exercises a dominating influence upon the rate of dissolution [66].

The dissolution of AgNPs to form Ag ions occurs only after they are oxidized by dissolved oxygen, a process that is facilitated by high proton concentration (H^+) at low pH. As AgNPs are introduced to water solution, the NPs undergo the following redox reaction and release Ag ions [9], [11], [67], [68]

$$2\mathrm{Ag_s} + \frac{1}{2}O_{2_{aq}} + 2H^+ \leftrightarrow 2Ag^+_{aq} + H_2O_{aq} \quad (2.3)$$

From this equation, one can see that removing dissolved oxygen from water completely inhibits the release of dissolved Ag ions, which shows the role of oxygen in surface oxidation [9], [67]. In the presence of dissolved oxygen, Ag ion solubility is enhanced when pH is decreased, demonstrating the importance of protons [7–10], [64], [67–69]. Besides, as pH decreases, deagglomeration and dissolution of metal NPs increase [49], [70].

The dependence of ion release kinetics on the primary particle size and concentration has been investigated and it has been revealed that the ion release rate increases with increase in the concentration of AgNPs and is inversely proportional to the AgNP radius [27], [31]. Moreover, the dissolution of the silver NPs is size-depedent, as the solubility increases exponentially as the particle size decreases [49], [67], [70]. Besides, there is a size dependence of the redox properties for metal and metal oxides on the nanoscale [49]. A negative shift in the peak potential (E_p) for Ag oxidation with size was observed due to a negative shift in the standard redox potential (E°) as the size decreases [29], as shown previously in equation (2.1).

The shape of the NPs affect also its potential to oxidize as the NPs in general are not spherical but instead have faceted structures with different interaction energies depending on shape and different surface planes, and thus, different dissolution tendency [49].

The ion release rates were found to increase with temperature in the range 0 - 37 $^\circ$C [9], as temperature leads to an increased degree of dissolution [71]. Other factors that affect the silver ion release from silver nanoparticles are the presence of complexing agents and natural organic matter as these affect the aggregation and dissolution of the AgNPs [63], [69].

Besides, in the preparation of silver polymeric nanocomposites, crucial parameters such as particle shape and size distribution, degree of particle agglomeration, silver content and interaction of silver surface with the polymer host have to be considered as they play

a major role in the Ag ion release process and they determine the antimicrobial efficiency of these polymeric nanocomposites [72].

The essential steps of silver ion release from silver/polymer nanocomposites are the diffusion of water into the matrix, the formation of silver ions due to the reaction between the silver and water molecules, then the migration of these ions through the matrix polymer leading to the release into the aqueous environment. Among these three steps, the production of silver ions is faster compared to the water diffusion and the Ag ion migration processes which can make them be the rate determining stages of the entire release mechanisms [16]. Differences in the water uptake of the polymer matrix were found to lead to different Ag ion release behavior [8], Water uptake (φ) of polymer films increases the dielectric constant of the coating. Dielectric constant, on the other hand, is related to the capacitance by the following equation

$$C = \frac{\varepsilon \varepsilon_{\circ} A}{d_{TOT}} \tag{2.4}$$

where C is the capacitance, ε is the dielectric constant of the coating, ε_o is the dielectric constant for the vacuum, A is area and d_{TOT} is total coating thickness. Hence, capacitance of the coating increases together with water uptake and thus the coating capacitance (C_p) can be estimated from electrochemical impedance spectroscopy (EIS) data at high frequency values (f) using the absolute value of impedance ($|Z|$)

$$C_p = \frac{1}{2\pi f |Z|} \tag{2.5}$$

The effects of the polymer coatings on the kinetics of silver ion release were also demonstrated by plasma polymer coatings with embedded AgNPs [23], [30], [31]. A good control over the rate of release of ions was demonstrated by depositing a thin plasma polymer overlayer and adjusting its thickness [23], [30].

So material properties like the crystallinity, cross linking, matrix polarity, and presence of additives affect the diffusion of water molecules and Ag ions through the matrix and influence the rate of silver ion release.

2.1.4 The bioavailability and toxicity of AgNPs

Silver is probably the most powerful antimicrobial agent that exhibits a strong toxicity toward a broad spectrum of bacterial strains that are found in industrial processes as well as in the human body. Because of these characteristics, silver in various forms is ideally suited for a wide range of applications in consumer, industrial, and medical products [1], [2], [40], [72], [73]. Although silver salts and complexes are effective antimicrobial agents, their use may result in unwanted adsorption of ions in cells [72]. Therefore, silver nanoparticles seem to be better candidates in medical applications due to their slower dissolution rate compared to silver salts [4], [5] and due to their higher interaction efficiency compared to bulk silver as discussed in section 2.1.1.

It remains unclear if the toxicity of AgNPs is the result of Ag ions or it is either attributed to the NPs themselves [1], [7–10], [12–14], [27], [34], [39], [41], [74]. For example, Sotiriou and Pratsinis [12] found that when Ag nanoparticles less than about 10 nm in average diameter were employed, the antibacterial activity of nanosilver was dominated by the high concentration of the released Ag ions, while when relatively larger Ag nanoparticles were used, the concentration of the released Ag ions was lower then the antibacterial activity of the released Ag ions and silver nanoparticles was comparable. Another *in vitro* study of antibacterial activity of silver nanoparticles revealed high antibacterial activity at concentrations that are comparable with concentrations of ionic silver revealing same antibacterial effect. However, such low concentrations of silver NPs did not show acute cytotoxicity to mammalian cells - this occurs at concentrations higher than 60 mg/L of silver, while the cytotoxic level of ionic silver is much more lower (~ 1 mg/L). Moreover, the silver NPs are toxic to eukaryotic organisms at the concentrations higher than 30 mg/L of silver. On contrary, ionic silver retains its cytotoxicity and ecotoxicity even at the concentration equal to 1 mg/L [75]. Dhas et al. [76] reported that both silver particles and released ions are involved in the toxicity as the bacterial growth inhibition caused by the metal ions released from 100 mg/L nanoparticles was nearly 30 % of the overall growth inhibition caused by the 100 mg/L nanoparticles with an effective hydrodynamic diameter of 44.3 nm. On the other hand, Xiu et al. [77] have proven that Ag ions are the definitive molecular toxicant as they tested the toxicity of

glycol-thiol-coated AgNPs (PEG-AgNPs) with sizes ranging from 3 to 11 nm under strictly anaerobic condition.

This uncertainty has also lead to lack of understanding of the mechanism of the antimicrobial activity of silver. The most common proposed mechanisms of the antimicrobial activity of silver nanoparticles are: (i) gradual release of free silver ions, followed by disruption of adenosine triphosphate (ATP) production and deoxyribonucleic acid (DNA) replication, (ii) silver nanoparticles direct damage to cell membranes, and (iii) silver nanoparticles and silver ion generation of reactive oxygen species (ROS) [1], [39–41], [72]. Definitely, silver has multiple actions against various bacteria. To some extent it may be explained why silver seldom gets resisted [41]. Although, a silver resistance has been documented [78] and some studies showed that the continuous exposure to AgNPs leads to moderate adaptation of bacterial species [76].

Several studies reported that AgNPs size [12–14], [79], shape [80], surface charge and coating [76], [77], [81], and solution chemistry [63] affect the toxicity of AgNPs. Additionally, the antimicrobial activity of AgNPs changes with respect to temperature, pH, concentration and time [82], [83]. This can be due to the fact that the bioavailability and toxicity of AgNPs are often linked to the stability of the NPs (remaining unagglomerated) and their ability to deliver soluble metal ions to the specific biological organisms. Accordingly, what affects the AgNPs stability, will indirectly affect its toxicity [1], [52], [81], [84].

The over use of AgNPs in commercial products leads to its release into the environment which is estimated to be 270 tonnes/year [85]. This destabilizes the ecosystem functioning as AgNPs and dissolved silver ions in the environment could be persistent and toxic to other higher organisms and human cells in different concentrations [1], [3], [39], [86]. Therefore, there is a significant interest in optimizing the NPs performance and in reducing the negative effects on human cells and environment. Hence, and in view of the fact that several practical applications of AgNPs require them to be well dispersed into or on the surface of various substrates and matrices without the formation of large aggregates, many methods were developed to prepare Ag nanocomposite coatings where

the silver ion release and the toxicity of AgNPs were reduced by embedding or coating with a polymer or ceramic matrix as the immobilization of silver on these substrates seems advantageous since it will not allow the direct uptake of the particles from mammalian cells [2], [8], [13], [16–18], [23], [30], [31], [72]. Hrak et al. [28] have evaluated the antimicrobial and cytotoxic properties of silver/titania nanocomposite coating with special emphasis on the differences between the activities on the surface versus in solution and have demonstrated that the therapeutic window of high antimicrobial activity without associated cytotoxicity is largely extended at the surface.

In this work, we are mainly focusing on investigating the silver ion release process from silver/PTFE nanocomposites while the antimicrobial activity was previously investigated as shown in Figure 2.4.

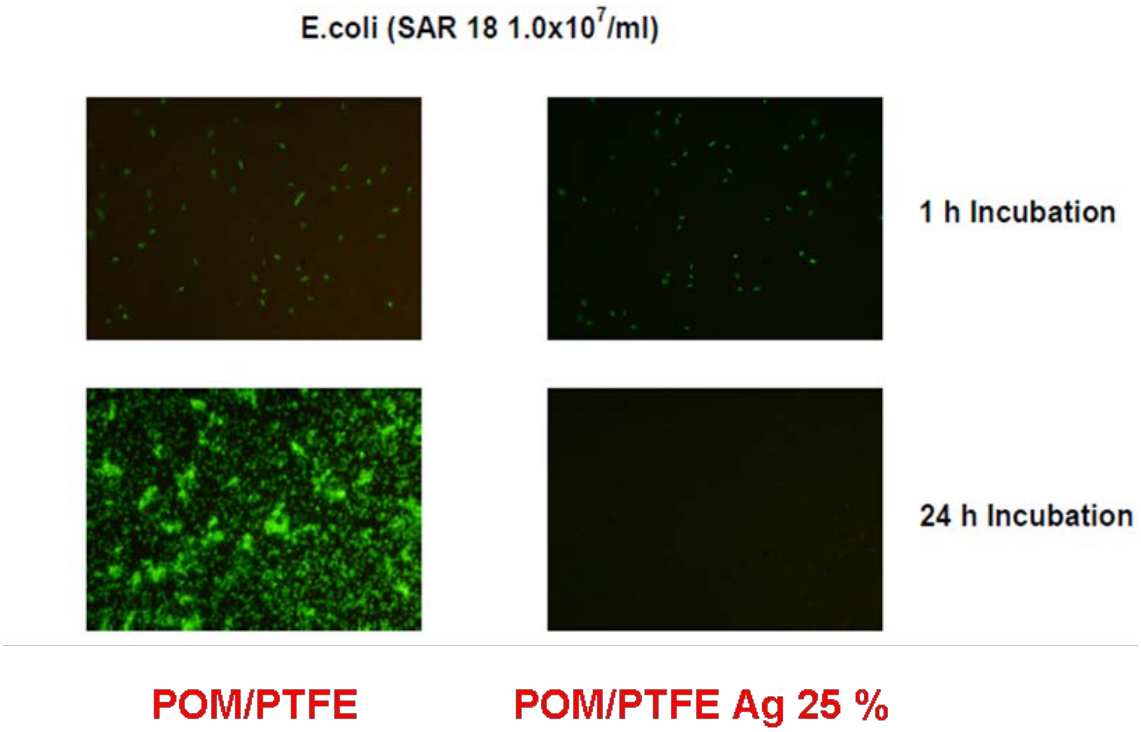

Figure 2.4 Florescence microscopy images from the growth of E. Coli SAR18 after 1 and 24 hours (h) on polymer substrate (POM) with pure PTFE coating, and 25 % Ag/PTFE nanocomposite incubated with 1×10^7 bacteria/ml. The glowing color in the images represents the bacteria grown in the respective areas, based on [21]

A Florescence test from the growth of E. Coli SAR18 on Ag/PTFE nanocomposites was done showing significant inhibition of the growth of E. Coli over time (1 to 24 hours). To compare and remove the effects from the PTFE substrates, the bacterial growth studies were performed on the polyoxymethylene (POM) coated with pure PTFE as well. From Figure 2.4, the glowing of the bacteria grown can be seen on the POM substrates with pure PTFE. As one can clearly observe, the growth of bacteria is not significant for the nanocomposites. The antibacterial efficiency of the coatings against different bacteria was demonstrated at extremely small silver consumption of ≈ 0.1 $g.m^{-2}$, and it was found that the release of Ag ions correlates with the antibacterial efficiency [21].

2.1.5 Ag-Au alloy NPs

Silver and gold are noble metals in the same group of periodic table with similar atomic radii and same crystallographic structures (face-centered cubic; FCC) which make them fully miscible in each other in the solid solutions of any composition [87].

For an ideal solid solution the energy E may be independent of the arrangement of the Nv_B B atoms in the matrix of Nv_A A atoms where N is the number of atoms ,v_i is the mole fraction of component i, and $v_A + v_B = 1$. Then ω^M is the number of distinguishable arrangements of the themselves indistinguishable A or B atoms on the lattice sites. The arrangements are obtained by performing all possible exchanges for the N atoms excluding those between the A atoms amongst themselves and between the B atoms among themselves. Thus

$$\omega^M = \frac{N!}{(Nv_A)!(Nv_B)!} \tag{2.6}$$

Using Stirling's formula, the entropy of mixing (shown in Figure 2.5) is

$$S^M = +k \ln \omega^M = -Nk(v_A \ln v_A + v_B \ln v_B) \tag{2.7}$$

where k is Boltzmann's constant.

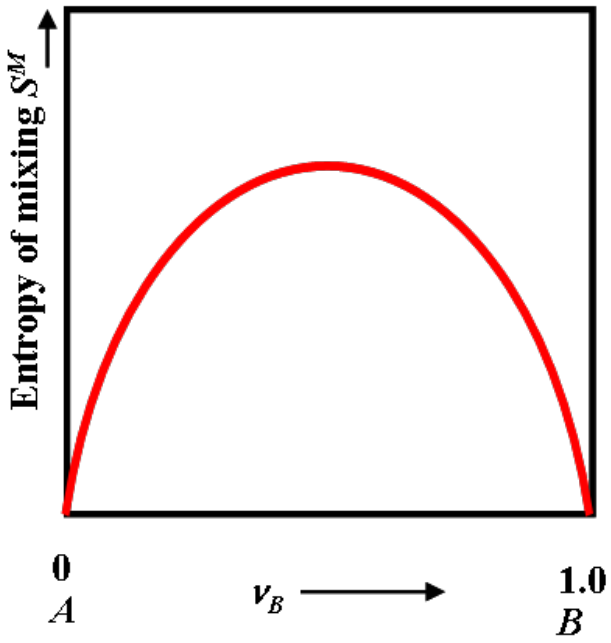

Figure 2.5 Entropy of mixing of an ideal solution as function of the mole fraction v_B, based on [88]

A usual phase diagram presents information on the phase stability of silver and gold as bulk materials with respect to temperature and composition. However, because the properties of nanoscale materials are different from those of bulk materials, a separate phase diagram is needed for nanoparticles. Yeo et al. [89] has constructed a phase diagram of 2 nm Ag-Au alloy NPs over the entire composition range by molecular dynamics simulation combined with other analysis methods. A complete solid-solution phase diagram of the binary Ag-Au system similar to the bulk phase was obtained, but the details were quite different. The freezing temperature was lower than that of the bulk state by several hundred degrees for all compositions and three different solid-state structures; amorphous, icosahedron or crystalline (FCC), were proposed in relation to the Au composition. The overall shapes of the nanophase diagrams are similar to that of the bulk.

In many publications, the production of bimetallic NPs in the form of layers, core-shell, alloys, nanotubes etc. has been reported [90–98]. Ag-Au alloy nanoparticles have been synthesized by various reduction techniques [90], [94], by laser-induced alloying [99], and by thermal evaporation [26], [91].

On the nanoscale, bimetallic NPs have properties that are different from the particles of their constituents not only due to size effects as in pure NPs, but also as a result of the composition of different metals [59], [97]. One example is the optical properties as the combination of Ag-Au NPs provides continuous adjustments of their localized surface plasmonic absorptions with respect to structure, particle size and composition distributions. The alloying of Ag-Au NPs results in an optical absorption spectrum which shows a single plasmon resonance peak, whereas two bands would be expected for the case of phase separated NPs [59], [95]. Alloy formation of Ag-Au NPs caused a plasmon maximum in the UV-vis spectrum between the absorption maximum of Ag and Au that varies with respect to composition distribution. The plasmon peak position is red shifted as a result of an increase in Au composition due to the continuous change of the *d*-band energy level that contributes to the interband transition term in the dielectric function, and a damping of the absorbance maxima is seen attributed to the higher electron scattering by foreign atoms upon alloying and the gold *d-sp* interband transition [59], [94], [100]. The position of the plasmon absorption peak of these alloy NPs, however, depends linearly on the composition of the alloy particles when expressed in terms of the gold fraction as previously reported [90], [93], [99], [100] and shown in Figure 2.6 .

The usage of noble metals with silver has shown different silver dissolution behavior. An early study done by Forty [101] examined the oxidation reaction of a bulk silver/gold alloy system in aqueous environment under the phenomena of selective dissolution. Silver is less noble than gold and releases easily from the gold alloy system, by leaving a high content of gold residue behind and creating surface vacancies and disordered areas near the surface. When all the surface of alloy is dominated by gold atoms, alloy becomes passivated and volume and surface diffusions start to play an important role.

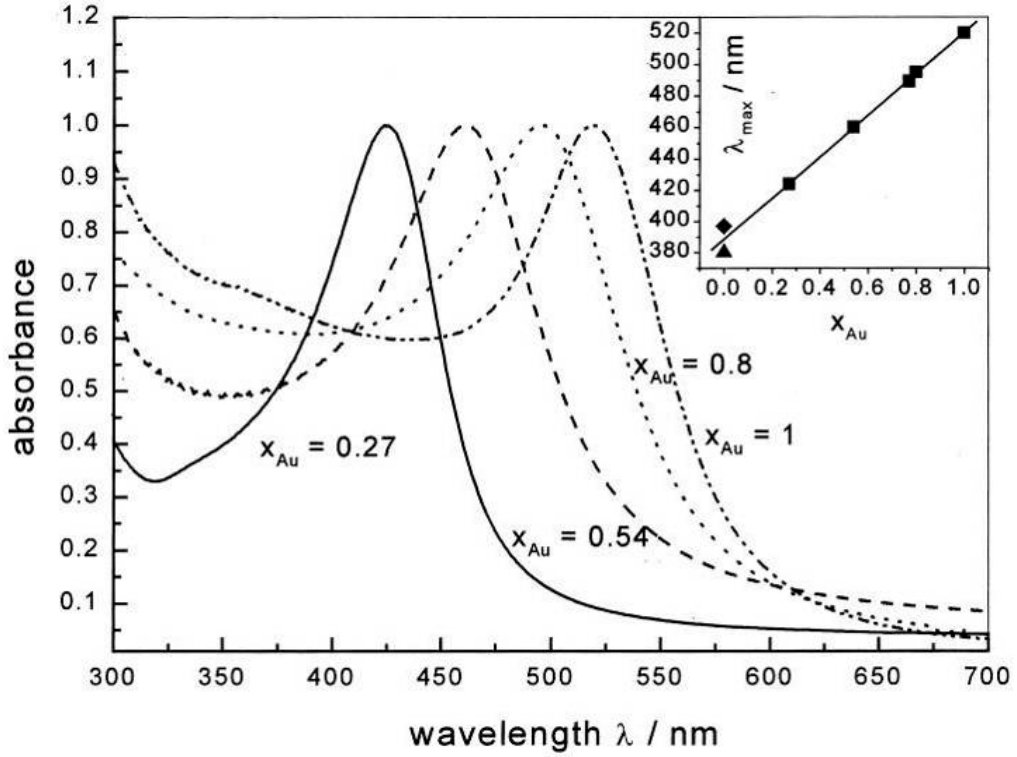

Figure 2.6 UV-vis absorption spectra of Au and Au-Ag alloy NPs with varying gold mole fraction X_{Au}. The spectra have been normalized at the plasmon absorption maximum. The inset shows how the absorption maximum of the plasmon band depends on the composition. The solid line is a linear fit of the absorption maximum to the Au mole fraction. The squares correspond to the experimental data while the triangle and diamond are two literature values for pure AgNPs, reused with permission from [90], copyright (1999), American Chemical Society

Recently, several bimetallic/polymer nanocomposites were developed showing promising properties in the silver ion release studies as it has been demonstrated that galvanic coupling of silver with platinum [32], [33] or gold [19] strongly increases the silver ion release, as due to different standard oxidation-reduction potentials of the two dissimilar noble metals, when they are in contact with each other in an electrolyte, one of the metals oxides or corrodes with respect to electron transfer between the metals. This corrosion process is called galvanic corrosion (galvanic coupling) [102]. Galvanic coupling within an electrolyte enhances the dissolution of less noble metal ion in alloys, thin films or sputtered targets [20], [32]. More noble metal acts as a cathode and less noble metal acts as an anode in the electrolyte thus it provides ion transfer between anode and cathode. Lower difference in standard potential means weaker galvanic effect. Metals that have lower reduction potentials can easily oxidized to their ions by loosing electrons and these

electrons will reduce the other metal. Barcikowski et al. [103], [104] have examined copper/silver and gold/silver nanocomposites containing nanoparticles dispersed in a polymer matrix without direct contact generated by laser ablation in liquids. In the Cu/Ag system, they found that electrochemical oxidation reaction between the two different metals enhanced the ion release of the less noble Cu by the ion mediated electrochemical reaction and silver ion release was retarded. Whereas in the case of Au/Ag nanocomposite films, no effect on silver ion release was observed due to the absence of mobile gold ions. On the other hand, Besner et al. [99] have observed a strong increase in the oxidation resistance with the increase in the Au fraction inside the Ag-Au alloy NPs which could probably result from significant modifications of the electrochemical properties of the NPs. Ag and Au significantly differ in their electronic properties. In this respect, colloidal AgNPs are known to act as an electron storage (donor) medium. Consequently, they would easily dissociate through an anodic reaction to release an electron and an Ag ion. In contrast, Au is known to possess some electron acceptor properties. The addition of Au atoms inside the AgNPs would then contribute to the formation of internal electron traps, inhibiting the dissolution of the AgNPs and the release of Ag ions. Hence, the formation of nanoalloys which exhibit more stability in comparison to Ag and higher plasmonic response in comparison to Au could also be beneficial for surface-enhanced Raman scattering (SERS) applications.

In this work, Ag-Au alloy NPs were prepared by simultaneous thermal evaporation technique and deposited on top of a sputtered PTFE thin film and silver ion release properties of these nanocomposites were investigated and compared to composites with only pure AgNPs as will be discussed in the next chapters.

2.2 Silver/polymer nanocomposites

Polymer nanocomposites are advanced functional materials composed of nanoparticles dispersed inside the polymeric matrix and/or coated by polymer. As a result, the produced material combines the suitable properties of both partners [72]. They have attracted considerable attention in recent years as a result of their high performance, improved properties compared to the constituent's parts, design flexibility, lower costs, high

stability, and uniquely large applicability of nanocomposites in various industrial fields [2], [72].

Numerous practical applications of silver nanoparticles require them to be well dispersed into or on the surface of various substrates and matrices without the formation of large aggregates. From this point of view, polymers are a good choice because of their chemical and structural nature with the long polymeric chains allowing incorporation and fine dispersion of nanoparticles [2], [15], [17], [72], [105]. Additionally, the suitable functional groups of polymers can be used as targeted reactive sites for the controlled one-step synthesis of nanoparticles [72].

Many methods were developed to prepare Ag/polymer nanocomposite coatings where the silver ion release and the antibacterial effect of the nanocomposite were investigated. The toxicity of AgNPs was reduced by embedding or coating with a polymer matrix as the immobilization of silver on polymer substrates seems advantageous since it will not allow the direct uptake of the particles from mammalian cells and reduce the chances of their appearance in the environment [2], [8], [13], [15–18], [23], [30], [31], [72]. Lately, our group applied different vapor phase deposition techniques to produce AgNPs and other noble metals and alloys together with an organic or ceramic component as a method to investigate the antimicrobial effect and the silver ion release potential [19–22], [24–26].

In this work, and through the combination of several vacuum deposition technologies, polymer films with metal NPs on top of them were fabricated in what we call it a two dimensional model system due to the fact that the particle ensembles are on the surface of the polymer and are not embedded inside the matrix (i.e. 3D). The prepared matrix is a thin film of RF sputtered PTFE and the coatings are either sputtered PTFE or plasma polymerized HMDSO as will be discussed in the following sections.

2.2.1 Nucleation and growth of noble metals on polymer surface

Noble metal deposition on polymeric surfaces plays an important role in today's industries. Thus, metal-polymer interfaces should be well investigated in order to obtain desirable product and process conditions. Polymers and metals have different structures;

the building blocks of metals are small and uniformly distributed and the atoms can be arranged into densely packed crystalline regular structures by metallic bonding. On the other hand, polymers are made up of large covalently bonded repeated units that are held together by weak Van der Waals interactions in an open structure. They have high entanglement of the chain and because of this they can not have regular structures. Cohesive energy of the metals is typically two orders of magnitude higher than that of the polymers [106]. Thus these differences cause lower interaction between polymer and metal compared to metal-metal interaction. This phenomenon leads to a strong aggregation of metal atoms and low solubility of metal atoms in polymer [106].

In this work, the synthesis of the metal NPs/polymer interfaces by evaporation of the metal onto the highly crosslinking sputtered PTFE surface takes place between highly cohesive energy metals (Ag and Au) and a low cohesive energy polymer (PTFE) which leads to a very low interaction between the metal atoms and the polymer matrix. Figure 2.7 shows the basic processes that play role in the initial stages of deposition of metal atoms onto untreated polymeric surface [107]. In adsorption stage, noble metal atoms are initially adsorbed on the polymer surface by the thermal energy gained from evaporation. Condensation coefficient (C) of metals on polymer (often also denoted as sticking coefficient) is the ratio of the number of adsorbed metal atoms to the total number of metal atoms arriving at the surface and it depends on the deposition parameters and strongly on the type of the polymer [108]. For PTFE polymer, C is very small even more at elevated temperatures [109].

After adsorption, metal atoms diffuse on polymer surface for a while until they desorb or get trapped at defect site or at a cluster. Defect sites on polymer surface trap the metal atoms by binding tightly the atoms themselves. Thus, atoms need higher energies to overcome the energy barrier for their release. Because of this, desorption of the metal atom can occur only when the atoms diffuse on the free polymer. Surface diffusion process can be considered as a random walk process which is also a temperature dependent process thus strongly depends on the temperature of the substrate. Diffusion of metal atoms into the bulk polymer plays minor role because aggregation tendency of metal atoms into clusters are higher than diffusion of atoms. Forming a stable nucleus

depends on the total nucleation energy; the free energy change (G) as a function of nucleus size (R). Figure 2.8 illustrates that nucleation must occur at a critical size R^* and that the energy barrier to nucleation G^* can be reduced by a decrease in the interfacial term or by an increase in the volumetric driving force [88], [110].

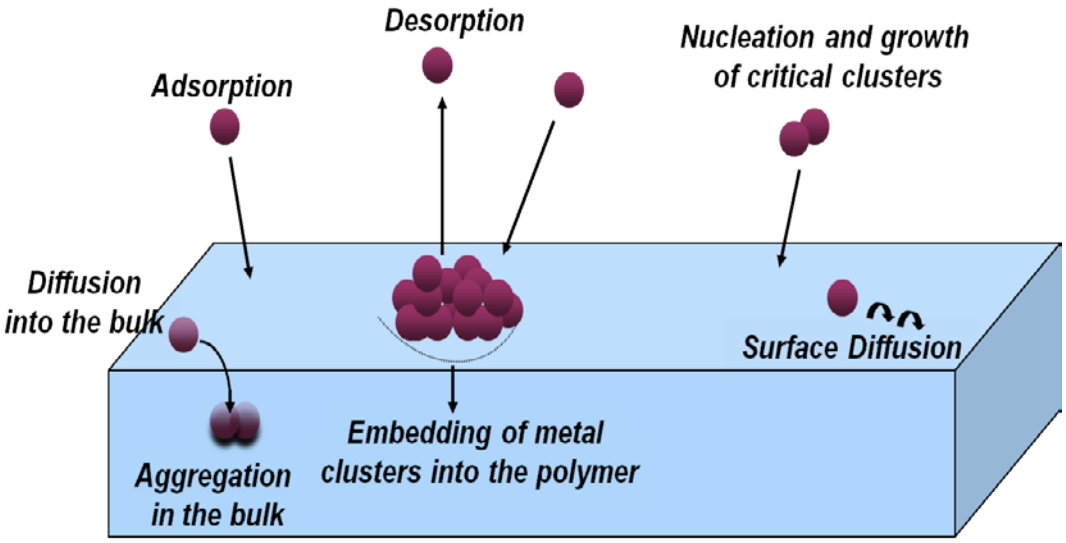

Figure 2.7 Basic processes in the initial stages of metal/polymer interface formation within PVD, based on [107]

By definition, critical cluster is the cluster with one atom less than the first stable cluster. Once clusters are formed, they grow by capturing the metal atoms that diffuses on polymer surface. The agglomeration of the clusters can be seen, if the clusters are mobile on polymeric surface. To obtain homogenous nucleation, the number of diffusing adatoms on the polymer surface should be increased by using higher deposition rates and also, the effects of defect site on the polymer should be considered since they create non-homogenous nucleation. Small clusters are highly mobile on polymer surface thus they have higher aggregation tendency on the polymer than embedding into the polymer. However, embedding of metal clusters into the polymer bulk can occur by higher mobility of the polymer chains that can be obtained by increasing the temperature to near or higher than the glass transition temperature of the polymer. It can be concluded that deposition rate, substrate temperature and defect sites play important role in deposition of

metal atoms on polymeric substrate. These parameters should be optimized well in order to obtain homogenous metal-polymer composites [107].

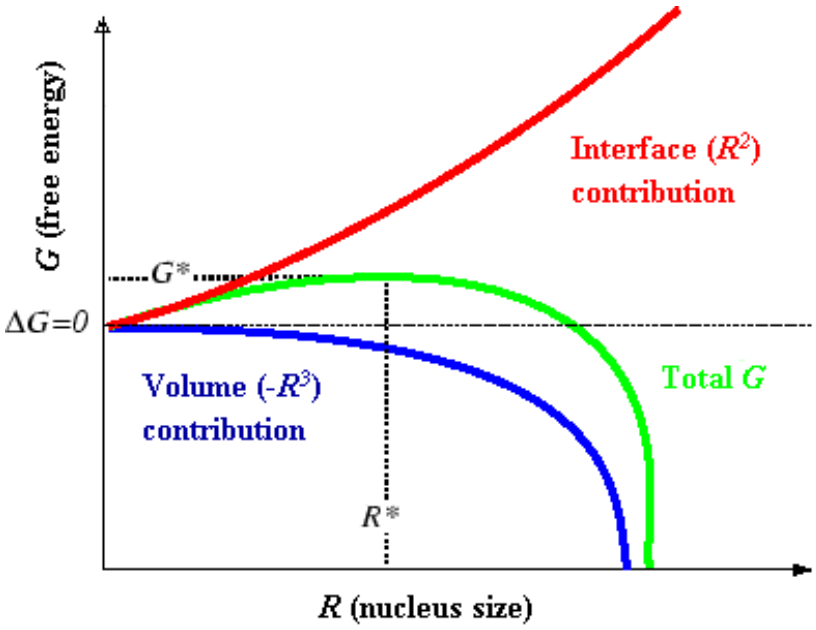

Figure 2.8 Free energy contributions associated with the formation of nuclei of different radii, based on [88], [110]

Figure 2.9 shows the growth stage within Au film by the change within structure and the importance of the growth by the effect of the deposition method. Deposition of Ag and Au films on a dielectric material shows similar growth stages. In the beginning, small metal nuclei are formed at certain sites of the substrate and by continuous deposition the nuclei grow by surface diffusion and impingements, creating larger irregular metal islands. By further deposition, the irregular metal islands undergo large-scale coalescence which results in the formation of metallic network. By this, voids between metallic paths become smaller and more regular. It can be seen that for large scale coalescence, critical thickness around 10 nm is needed for conventional evaporation (c.e.) whereas for ion assisted evaporation (which uses simultaneous bombardment of energetic atoms, sputtering) critical thickness around 4 nm is needed. Finally, a uniform continuous metal film is formed. It can be said that reasonable uniform noble metal films can be formed at a thickness higher than 10 nm by conventional evaporation and sputtering [111].

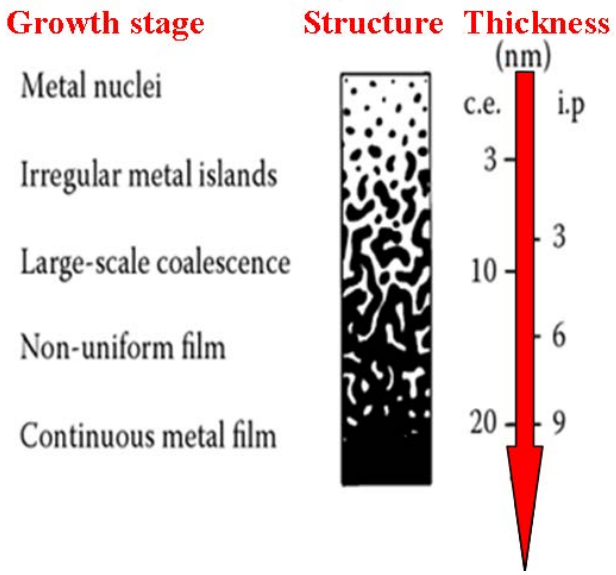

Figure 2.9 Survey over growth stages, structures, thickness scale for thin Au film deposited on glass by c.e. (conventional evaporation) and i.p (ion assisted evaporation), based on [111]

Depending on the thermodynamic parameters of the deposit and the substrate surface, thin films may grow in three different modes described as: (a) Island type, called Volmer-Weber type, (b) layer type, called Frank-van der Merwe type, or (c) mixed type, called Stranski-Krastanov type. In almost all practical cases where nonreactive metals are deposited, the growth takes place by island formation [112]. Surface energy plays a dominant role in thin film formation and the type of growth mode it takes. We have to consider the surface energy of the substrate free surface γ_s, substrate film interface γ_i and film free surface γ_f [113]. When there is no strong bonding between film and substrate to reduce γ_i, we will have the island or Volmer-Weber mode which is characterized by three dimensional islands as atoms have stronger affinity to each other than to the substrate.

2.2.2 RF Sputtered polytetrafluoroethylene (PTFE)

Polytetrafluoroethylene (PTFE) is a synthetic semi-crystalline thermoplastic polymer that is composed of carbon (C) and fluorine (F) as shown in Figure 2.10.

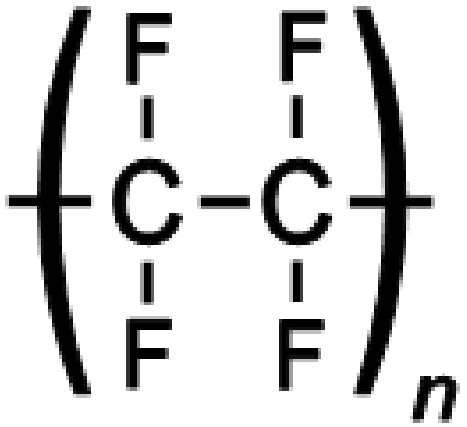

Figure 2.10 Structural formula of PTFE monomer

The conventional PTFE is known for having the lowest surface energy and a low dielectric constant, being highly hydrophobic, having highest chemical resistance, low moisture absorption, high thermal stability among other organic polymers. Due to its unique properties it has been used widely in chemical, medical, semiconductor, filtration, electrical, aerospace, automotive and petrochemical industries [114]. However, to overcome the poor adhesion with other materials problem, it was important to prepare PTFE-like films on various substrates using different techniques. Fluorocarbon polymers films prepared by RF sputtering of PTFE in different gases or by plasma polymerization have attracted attention in the 1970s forward [115–122].

The motivation was to prepare good dielectric films, low friction, protective and non-wettable coatings [116]. The RF sputtering and deposition of PTFE films suggested mechanism is via the plasma polymerization of the sputter-generated tetrafluoroethylene (TFE) monomer and the rearrangement of the sputter-generated $-(CF_2)_x-$ oligomeric segments [122]. A model of a fluorocarbon plasma polymer film obtained by PTFE RF sputtering was suggested by Biederman et al. in which the C-C bonds are predominantly perpendicular to the sample plane and the C-F bonds are predominantly parallel to the sample plane [115], [116].

The results showed that the chemical and molecular structure and composition and several properties of the deposited films are strongly depending not only on the technique employed but also on the specific design of the apparatus in use [121] and the sputtering gas in process [122]. The sputtered PTFE films were found to be amorphous and showed fluorine (F) deficiency in their composition which resulted in a slight increase in the dielectric constant of the films. However, the structure was found to be influenced by the substrate temperature and processing gas [115]. The friction coefficient for the sputtered films was higher than that of the bulk polymer and the average refractive index of the sputtered film was less than that of the bulk PTFE which could be arise if the deposited film had a lower density than the bulk polymer [121].

The crystallinity of the deposited polymer and the untreated target material are not similar. The results from different characterization methods suggest that the partially crystalline structure of the chain is destroyed in the sputtering process of PTFE [36], [122]. During the adsorption of monomers, molecular fragments and radicals on the substrate, they form a crosslinked structure that results in amorphous structure [123]. An XPS spectrum of an argon plasma sputtered PTFE films prepared previously by our group [36], Figure 2.11, shows that the sputtered polymer films have a completely different structure from the pristine PTFE as the C 1s core-level spectrum for pristine PTFE has only one peak at the binding energy 292.0 eV due to the CF_2 groups in the polymer chains. The element ratio of fluorine to carbon is 2:1. After sputtering the spectrum shows three additional peaks which are related to CF (290.2 eV, 28.1 % fraction of C 1s peak), CF_2 (292.0 eV, 31.7 %), CF_3 (293.9 eV, 22.6 %), and C-CF_x (287.9 eV, 17.6 %) species. The additional peaks are in agreement with pronounced crosslinking as reported earlier [115] for sputtered films. The crosslinking might be seen as an advantage in this case as it ensures higher mechanical stability of the polymer around the metal. The density of the sputtered PTFE was determined gravimetrically as 2.1 g/cm^3, which is close to the density given by the pristine polymer supplier (2.2 g/cm^3) taking into account the measurement error. The resistivity of the sputtered polymer is more than 10^7 Ω cm and the refractive index n of the sputtered polymer measured with ellipsometry is n =

1.374, so that we get for the dielectric constant $\varepsilon_\infty = n^2 = 1.88$, which is close to the reported refractive index of PTFE $\varepsilon_\infty = 1.89$.

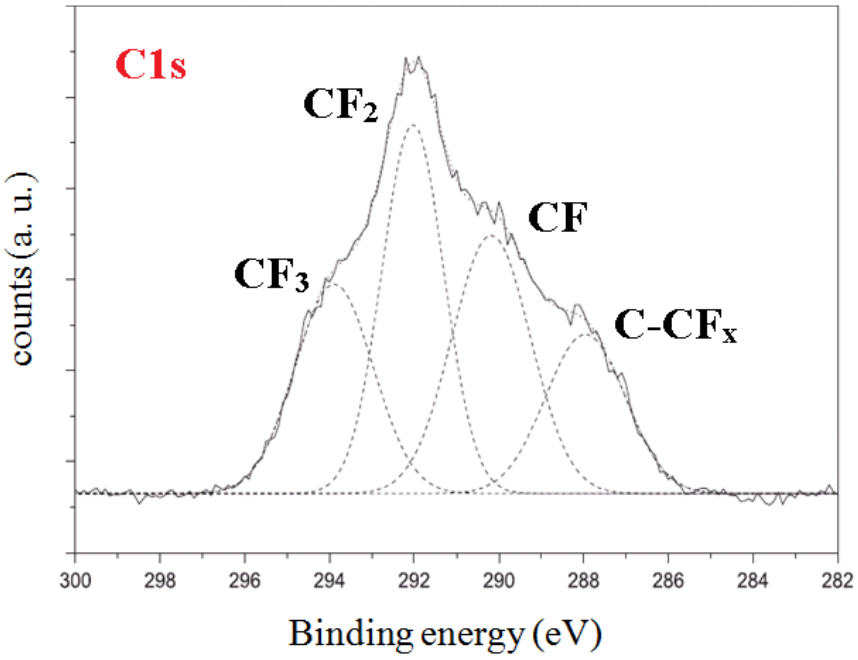

Figure 2.11 XPS C 1s spectrum of sputtered PTFE without Ag, based on [36]

Further investigations were done by Hassel et al. [124] as uniformity of sputtered PTFE films was checked by EDX in the scanning electron microscope by measuring the fluorine content of the film. The absence of pinholes was shown by deposition of ion-enriched water on top of the film. No current could be measured through the film after applying a voltage to the droplet and metal. Contact angle measurements were conducted and the super hydrophobicity which based on the surface structure and the surface functionality was tuned by the RF sputtering of PTFE on different surfaces.

In this study, thin films of RF sputtered PTFE were chosen as it is possible to be prepared using our home-made sputtering chamber which is a good way to produce a highly crosslinked polymer that is suitable as a host for the AgNPs. Moreover, since it is a hydrophobic polymer matrix, the water uptake is small, so that a quick depletion of the AgNPs should be avoided [35]. Besides, PTFE is widely used in metal-polymer nanocomposite systems due to its high resistance to chemicals, transparency and very good dielectric properties [36]. In the composite studies of PTFE with metal atoms, it was

found that PTFE stabilizes the composite, reduces the defects and increases the contact angle for water management applications [37]. Moreover, PTFE has been considered by many researchers as being biocompatible as its low surface energy results in a poor bacteria adhesion, thus the formation of bio-films on the Ag/polymer film could be avoided which is an important issue for medical devices [38].

2.2.3 Plasma polymerized hexamethyldisiloxane (HMDSO)

In plasma polymerization, organic monomer precursors (vapor or aerosol) are introduced into the plasma zone and converted by the plasma into charged or neutral molecular fragments and atomic species. All these fragments recombine on the surfaces that confine the plasma and form a thin film [125]. Plasma polymerized films are generally amorphous, pinhole-free, highly crosslinked and are therefore insoluble, thermally stable, chemically inert and mechanically tough. Furthermore, they are very adhesive to different substrates [125–127].

An important example of plasma polymerization is the deposition of polymer-like or quartz-like thin films with varying concentration of hydrocarbons ($SiO_xC_yH_z$) from siloxane monomers. Hexamethyldisiloxane (HMDSO, $C_6H_{18}Si_2O$); a silicone-oxygen-silicone core with three methyl groups attached to each silicone as shown in Figure 2.12; is often preferred as precursor since it is generally sufficiently volatile near room temperature, relatively non-toxic and non-flammable, cheap and available from commercial sources, in addition to its highly organic character as well as its high vapor pressure [125], [127].

The chemical composition of the HMDSO plasma-polymerized thin films can be adjusted over a wide range from polymer-like properties with various applications as adhesion interfaces to glass-like films with applications corrosion protective layers or anti-scratch coatings on plastic substrates, coatings for biocompatible materials and low-*k* dielectric layers for microelectronic applications [125–129].

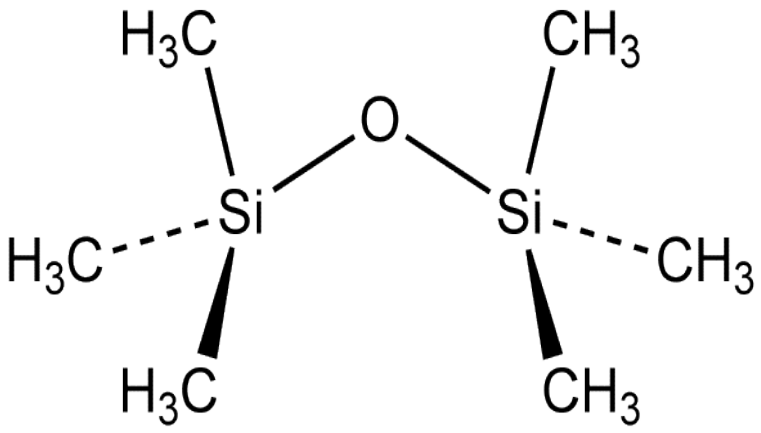

Figure 2.12 Chemical structure of hexamethyldisiloxane (HMDSO)

In this work, different barriers of a $SiO_xC_yH_z$-polymer matrix were grown by plasma polymerization of HMDSO, with tailoring the composition and properties of the matrix. More details about the preparation parameters and the composition of the prepared films were investigated by Peter et al. [130].

Chapter 3

Techniques

3.1 Deposition techniques

Thin films are created by the deposition of layers of a material within few nanometers to about ten micrometers range onto bulk materials (substrate) to achieve properties unattainable or not easily attainable in the substrates alone. Deposition phenomena proceed by removal and transportation of the atoms from the source material and then deposition onto the substrate forming a film layer [110], [113]. This is carried out in ultra high vacuum or a minimum of high vacuum conditions depending on the target material and the method. By decreasing the pressure, the mean free path, i.e. the average distance that a molecule travels in a gas before encountering collisions with other molecules of the evaporated particles within the deposition chamber increases. Higher mean free path means lower probability of collision between molecules than the probability of molecule-wall collision, which can avoid the significant reduction of deposition rate and prevent contaminations to deposit on the substrate. In addition, vacuum conditions are necessary to prevent oxidation of any reactive metals, e.g., the filament in a thermal evaporator at the presence of oxygen [113].

Many techniques have been developed to produce films at nanometer level, namely physical vapor deposition (PVD) and chemical vapor deposition (CVD). PVD is based on condensation of a vaporized material onto another surface and CVD is based on deposition of the desired product resulting from the chemical reaction between the substrate and gaseous precursor [110].

In this work various physical deposition techniques were used: thermal evaporation of silver and gold, RF sputtering of PTFE and plasma polymerization of HMDSO.

3.1.1 Thermal evaporation of silver and gold

Thermal evaporation is a physical deposition process that consists of evaporation of the source material by the heating system and condensation of the vaporized material on to the substrate under vacuum. The vapor expands in the chamber under vacuum and condenses on the substrate that has lower temperature than the evaporation source [113]. Since temperature affects the equilibrium vapor pressure of the materials, there is a strong dependence of the evaporation rate on temperature [110]. In thermal evaporation, high deposition rates can be obtained due to exponential behavior of the vapor pressure of the material to be evaporated and the source temperature [131]. The twisted-wire coil, dimpled boat and the heat-shielded crucible are the most common sources for thermal evaporation [113]. The geometry of the evaporation source affects the geometry of the vapor cloud which results in an angular distribution of the evaporant flux and the film thickness uniformity and coverage are govern by the geometric placement of source and substrate [110].

The advantages of thermal evaporation technique are the easy usage and the low costs instrumentation. Also, metals, alloys and large number of compounds can be evaporated by this technique and deposition parameters can be independently controlled. On the other hand, it is difficult to coat large and irregular shaped substrates because of the non-uniform deposition and it is hard to maintain stoichiometry [110].

In this work, a home-made thermal evaporation chamber was used to deposit Ag and Ag-Au alloy nanoparticles on the surface of a polymer substrate. Figure 3.1 shows a three

dimensional view of the glass chamber and the evaporator. Two separated crucibles (length = 10 mm, inner diameter = 3 mm) made of alumina (Al_2O_3) and boron nitride (BN) and surrounded by a tungsten (W) heater coil filament were used to evaporate Ag and Au separately. They are both positioned at angle 22.5° with respect to the center line of the chamber. The distance between the top of the crucible opening and the sample holder is 170 mm. The chamber is provided by a rotary pump (Pfeiffer DUO 005 M) which generates the pre-vacuum (10^{-1} mbar) and a turbo molecular pump (Pfeiffer TMU 260) coupled to the rotary pump to create the end vacuum (10^{-6} mbar). The power supply SM7020-D (Delta Elektronika) was used to heat the evaporation source by increasing the current (*I*) and the voltage (*U*) slowly which were controlled automatically by the lab view 8.6 software (National Instruments).

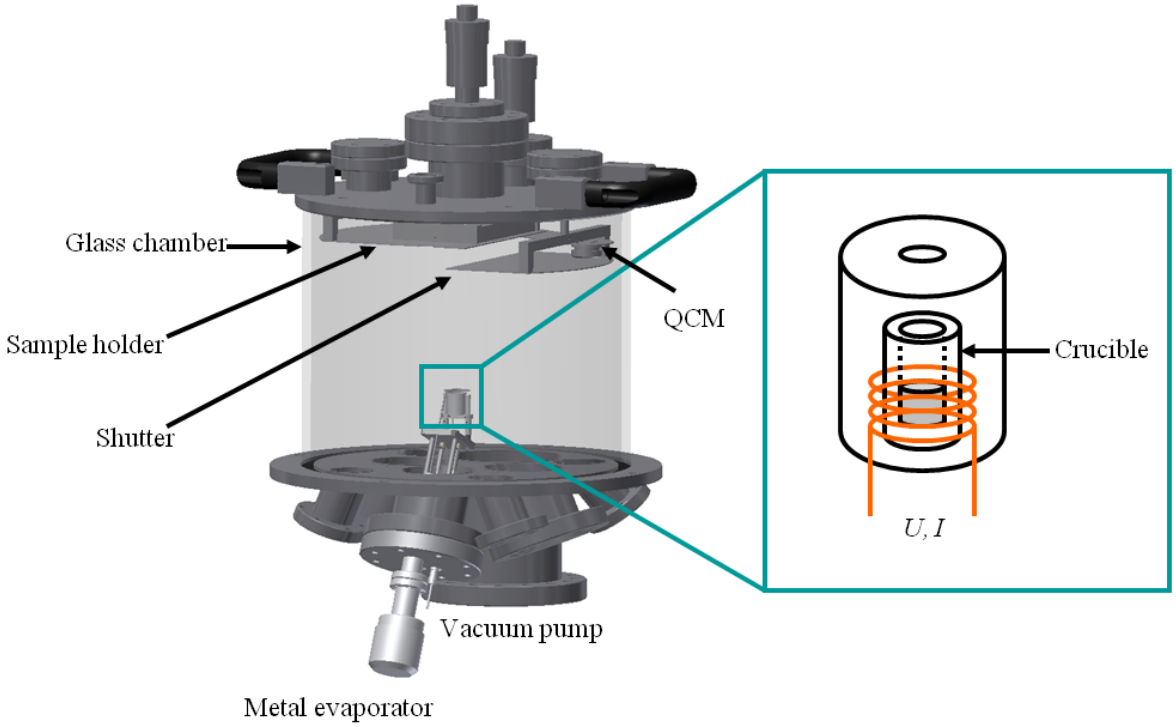

Figure 3.1 3D view of the home-made thermal evaporation chamber and the evaporator constructed by Dipl.-Ing. Stefan Rehders

3.1.2 RF Sputtering of PTFE

Sputtering is a PVD process involving the removal of material from a solid cathode (target) by bombarding with positive ions emitted from a gas discharge. When ions with high kinetics energy are incident on the cathode, the subsequent collisions remove, or sputter, atoms from the material. The process of transferring momentum from impacting ions to surface atoms forms the basis of sputtering. The high-energy strike of the ions leads atoms at the surface of the substrate to be ejected. After condensation, sputtered atoms create a thin film onto the substrate placed in anode. Confinement of the plasma near the target can be improved by the magnetic field of the magnetron sputter source [110], [113].

A sputtering chamber, held at high vacuum, consists of a water cooled grounded anode and a negatively biased target and an inlet for the sputtering gas. To prevent overheating and chemical or thermodynamic changes of the target, the cathode is water cooled Cu backing plate. High voltage is used to ignite the plasma, and the positive gas ions are accelerated towards the cathode. Upon impact, material is removed from the target and deposited onto the substrate placed on the anode. As the target material, PTFE in this case, is electrically insulating, radio frequency (RF) power should be used rather than direct current (DC) bias. In this way, gas discharge is created by an alternating current and the sign of the anode-cathode bias is varied at a high rate so that charge build up on insulating targets can be prevented [110].

Sputtering technique has unique advantages over other techniques: any material can be volatilized by it, compounds are volatilized stoichiometrically, and the film deposition rate can be made uniform over very large areas [113]. As disadvantages, sputtering has slower deposition rates and it is hard to optimize sputtering parameters in order to obtain desired composition within the material [132].

In this work, PTFE target was sputtered to form highly crosslinked thin films onto different substrates using a home-made sputtering chamber shown in Figure 3.2. The deposition chamber was evacuated to base pressure of 10^{-7} mbar, by two different types of vacuum pumps: A rotary pump (Pfeiffer DUO 005 M) was used to generate the pre-

vacuum (10^{-1} mbar) and a turbo molecular pump (Pfeiffer TMU 260) coupled to the rotary pump to create the end vacuum. Monitoring of the deposition rate of the polymer material was done *in situ* by using a quartz crystal monitor. Polymer was deposited by using RF planar magnetron source ION'X 2UHV (Thin Film Consulting) to prevent charging of the target.

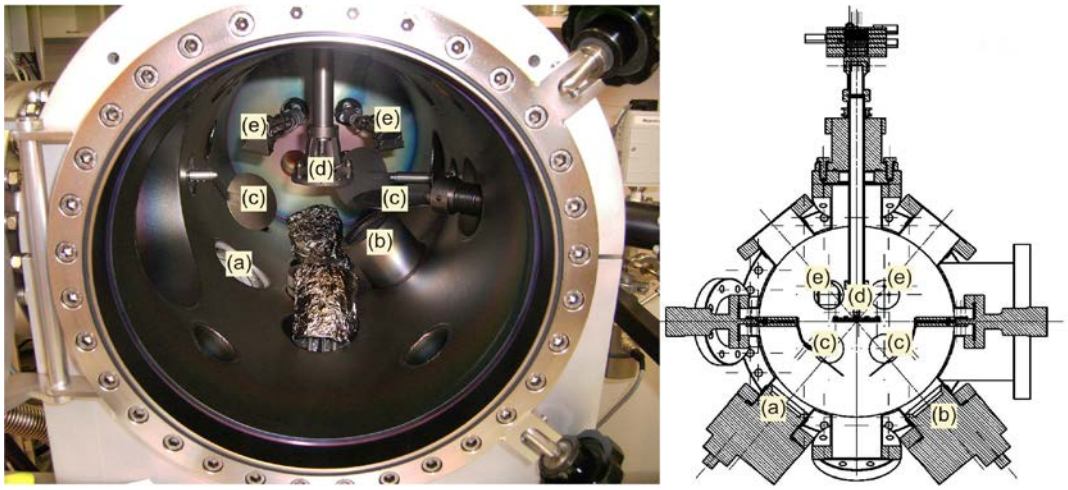

Figure 3.2 Home-made sputtering chamber facility at the Chair for Multicomponent Materials, Kiel University, (a) Metal magnetron (DC) (not used) (b) Polymer magnetron (RF), (c) Shutters, (d) Rotatable sample holder and (e) Quartz crystal monitors [133]

3.1.3 Plasma polymerization of HMDSO

Polymerization of organic monomers in a low pressure plasma results in polymer films which are different from those of conventional polymerization. The films formed by this technique are usually branched, highly crosslinked, insoluble, pinhole-free and adhere well to most substrates [126]. The working principle is the dissociation, ionization and excitation of a monomer precursor in plasma, producing polymer-forming intermediates. These intermediates then polymerize on a substrate, forming a highly crosslinked plasma polymer [134]. The main parameter influencing the processes and by this the deposited polymer are the pressure of the precursor, the inert gas and the power density of the plasma that is used for activation. Typically, the plasma discharge is run using capacitive coupled radio frequency power and a vacuum system, gas flux controllers and matching network are needed. In this work HMDSO plasma polymer coatings were prepared using

a vacuum chamber designed in our chair. HMDSO, the precursor for plasma polymerization, is kept in liquid form in a evacuated glass bottle in an ethanol bath. Using a temperature controller the bath is kept at a temperature between -30 and 10 °C. A stop valve is mounted connecting the bottle to the pipe that leads to the chamber. At the end of the pipe a sensitive needle valve is used to control the flow rate of HMDSO and an electronically controlled pulse valve is used to inject the HMDSO in pulses. The nozzle of the precursor injection system is mounted in about 15 mm distance to the substrate holder. Oxygen (O_2) and argon (Ar) from two separate flow controllers are merged with the HMDSO flow behind the pulse valve before injection. Ar is injected in order to achieve constant plasma polymerization conditions and O_2 is injected to chemically modify the matrix. This enables full control over the atmosphere for plasma polymerization. This mixture of HMDSO, Ar and O_2 is then injected through the nozzle into the deposition chamber in front of the magnetron (Thin Film Consulting), which is powered using an RF-generator (CESAR 136, 600 W, Dressler) and a matching circuit (VM 1000 A, 1 kW, Dressler). The most stable RF-discharge condition was observed with a pulsed injection of the HMDSO at 5 Hz and an opening time of 20 ms [130].

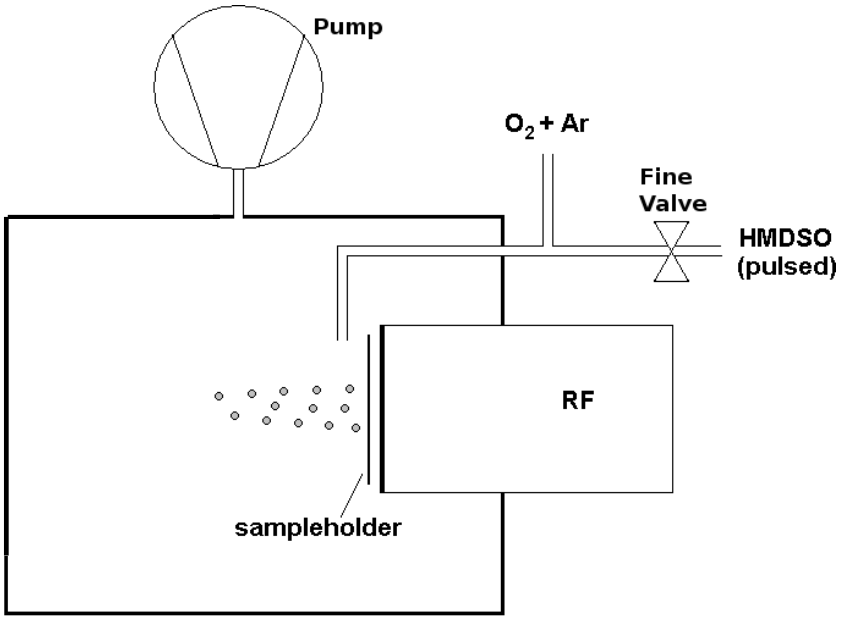

Figure 3.3 Schematic of the experimental setup: the RF power source is mounted next to the grounded sample holder and the injection system for O_2, Ar and HMDSO

3.2 Characterization techniques

3.2.1 Quartz crystal microbalance (QCM)

The technique is employed for *in situ* monitoring of the thickness of films deposited by PVD techniques. A crystalline quartz is piezoelectric, initially oscillates at its natural frequency which is typically 5 MHz [113]. As a material is deposited on the substrate, it is also deposited on the sensor. Depending on the density and the amount of the deposited material, the sensor's frequency will drop from its initial frequency. The rate and thickness can be calculated from this frequency shift. A conventional STM−100/MF quartz microbalance monitoring system was used in this work for film deposition monitor. The calibration procedure is affected by three different parameters, material density, material Z-Factor, and tooling factor. The tooling factor is a deposition system geometry correction (location of sensor relative to substrates), while density (gm/cc) and Z-Factor are material factors. Rate computation is based on the rate of the change of thickness readings, updated four times per second, and then filtered for display. Also the raw measured frequency of the sensor crystal is available from the instrument [135].

3.2.2 Profilometer

Film thickness measurements and calibration processes were carried out using a profilometer. In this technique, a diamond stylus is moved vertically in contact with a sample and then moved laterally across the sample for a specified distance and specified contact force. A typical profilometer can measure small vertical features ranging in height from 5 nm to 800 μm [110]. The height position of the diamond stylus generates an analog signal which is converted into a digital signal stored, analyzed and displayed. The horizontal resolution is controlled by the scan speed and data signal sampling rate. In this work a DEKTAK 8000 is used for our measurements. The radius of the diamond stylus is 12.5 μm and the stylus tracking force is factory-set to 50 mg.

3.2.3 UV-vis/NIR Spectroscopy

Ultraviolet, visible and near infra red (UV-vis/NIR) spectroscopy is the measurement of the attenuation of a beam of light after it passes through a sample or after reflection from a sample surface. These measurements can be done at single wavelength or over an extended spectral range. The spectral range of the instruments is generally from 185 nm to 3000 nm. There is a linear relationship between absorbance and absorber, i.e., concentration of the absorbing molecules, which makes UV-vis/NIR spectroscopy especially attractive for making quantitative measurements and for characterization of optical and electronic properties of materials.

The light source is usually a deuterium lamp for UV measurements and a halogen lamp for visible and NIR measurements and the instrument automatically swaps lamps when scanning between the UV and visible regions. The light beam is separated into its component wavelengths and each monochromatic (single wavelength) beam in turn is split into two equal intensity beams. One beam, the sample beam, passes through a small hole of a container containing the sample being studied. The other beam, the reference, passes through a “blank” sample. The intensities of these light beams are then measured by electronic detectors and compared. The detector converts light to a signal that is analyzed by the computer and the absorbance is calculated by the change in the intensity of the light using the Beer-Lambert law, given in equation (3.9), which tells us quantitatively how the amount of attenuation depends on the concentration of the absorbing molecules and the path length over which absorption occurs [136].

$$A = -\log T = -\log\left(\frac{I}{I_o}\right) \tag{3.8}$$

where A is the absorbance of the sample, T is the transmission of the sample, I is the intensity of the sample beam, and I_o is the intensity of the reference beam. The output data is given with respect to absorbance versus wavelength.

As with other spectroscopy techniques, sample preparation is a very important step to obtain good results. Samples are placed in a small masking apparatus in order to examine

the specific area. It is important not to smudge or leave fingerprints on the curettes. This will cause scattering of the light and lead to falsely high absorption values. A "blank" standard should also be examined.

In this work, the optical properties of the metal-polymer nanocomposites which were deposited on quartz substrates were characterized using Perkin Elmer Lambda 900 UV-vis/NIR, with a deuterium lamp for UV measurements and a halogen lamp for visible and near infrared measurements and also two different detection systems: A Photomultiplier in the UV and visible range and a lead sulfide detector for near infrared. Because noble metals have strong surface plasmon resonances in the visible range of electromagnetic spectrum, the absorption spectra of the nanocomposites were recorded between 300-800 nm with 2 nm resolution in transmission mode and 20 nm PTFE on quartz substrate was used as a reference sample to get rid of any effect of the polymer matrix and the substrate. All the UV-vis plots are presented in this work after linear background correction. Due to the small size of the metal NPs in our model system, the scattering was neglected and only absorption was considered.

3.2.4 X-ray photoelectron spectroscopy (XPS)

X-ray photoelectron spectroscopy (XPS) is a widely used surface analysis technique that can make quantitative chemical state analysis. It can detect all elements except helium and hydrogen. The surface sensitivity of XPS arises from relatively short inelastic scattering mean free path of the photoelectrons. It can make depth analysis between top 2 atomic layers up to 20 atomic layers and it is the least destructive technique between other spectroscopy techniques [137]. Figure 3.4 shows the principle of XPS process which based on the photoelectric effect.

Initially X-ray photon with energy hv hits the surface of the material and this energy is absorbed by an electron with binding energy E_b with respect to the fermi level, resulting in emission of a photoelectron from the atom with a kinetic energy E_k and leaving behind a core hole. The binding energy of the electron can be calculated by

$$E_b = h\nu - E_k - \phi \tag{3.9}$$

where h is Planck constant, ν is frequency of the radiation, ϕ is the work function of the spectrometer and E_k is the kinetic energy of the emitted electron [138].

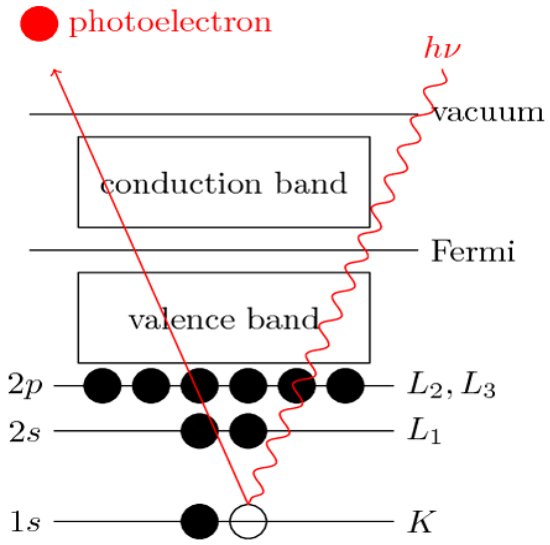

Figure 3.4 Principle of XPS

Therefore, each element has its own characteristic peaks in photoelectron spectrum with respect to their kinetic energies. The Binding energy of an electron also depends on its oxidation state and the local chemical and physical environment which means a quantitative analysis about compositions can be obtained from changes in peak intensity and position in photoelectron spectrum which change according to chemical environment.

The intensity of Ag and Au, as well as other elements, were determined in this work by XPS Full lab from Omicron Nanotechnology GmbH, under ultra high vacuum analytical chamber of a pressure about 10^{-9} mbar. XPS setup consists of an aluminum anode X-ray source (VG Microtech XR3E2), hemispherical electron analyzer (VSW EA 125), a detection system and a data analyser. The intensity of the elements (area under the peak) in XPS spectra were measured and compared by other typical spectra shown in the handbook of X-ray photoelectron spectroscopy [139].

3.2.5 Transmission electron microscopy (TEM)

Transmission electron microscopy (TEM) is a highly used microscopy technique to examine topography, morphology (shape, size), composition and the crystallographic structure of the material. It uses highly energetic electrons as a beam to examine the materials on a very fine scale. TEM can create resolutions up to point 0.1 nm at 300kV by using high resolution TEM. The microscope consists essentially of three parts, the electron gun where the beam is generated, electromagnetic lens system, sample holder and imaging system. The high resolution of TEM mostly depends on highly focused electron beam which is defined as "probe". The probe focuses a very small area on the specimen. The source of probe, the electron gun, emits almost monoenergetic electrons with small wavelengths that are directly correlated with the spatial resolution. Also, for a high resolution sample should be so thin (less than 100 nm) that less scattering can be obtained and electrons can travel across the sample [137]. Contrast formation in TEM plays important role in the image resolution and it strongly depends on imaging mode such as bright field and dark field. In dark field imaging, one or more diffracted beams are allowed to pass the objective aperture because the direct beam is blocked by the aperture. Since diffracted beams have strongly interacted with the specimen, information about planar defects, stacking faults or particle sizes can be obtained. In the bright field mode of the TEM, an aperture is placed in the back focal plane of the objective lens that allows only the direct beam to pass. In this case, the image results from a weakening of the direct beam by its interaction with the sample. By using the occlusion and the absorption of the electrons, contrast is formed in the sample image. Regions with lower diffracted potential appear dark in bright-field imaging depending on the structure factor of the specimen [140].

The morphology of the metal/PTFE nanocomposites deposited on carbon-coated copper TEM grids was analyzed using a Tecnai F30 G^2 microscope working at an accelerating voltage of 300 kV. Bright-field images were obtained by charged coupled device (CCD) and Gatan Image Filter (GIF) cameras.

3.2.6 Inductively coupled plasma-mass spectrometry (ICP-MS)

ICP-MS is a sensitive method to detect a wide range of elements with a concentration down to ng/l (ppt; parts per trillion) and below. The system consists of: sample introduction system, inductively coupled plasma (ICP) source, interface/vacuum, ion lenses, analyzer, detector, vacuum system and RF generator. The sample aerosol is ionized in the plasma and the ions go through the interface, the ion lens, and the quadrupole mass filter to the detector. The RF generator supplies RF power to the work coil to generate plasma. In this work an Agilent 7500cs instrument was used with liquid sample introduction by a PFA micro-nebulizer at the institute for Geosciences/ICP-MS Lab, CAU Kiel. Calibration was against aqueous multi-element solutions using indium and rhenium for internal standardization. The procedure detection limit was 10 ng/l (ppt; parts per trillion) for Ag. All results are blank-subtracted averages of 3 replicate measurements. Analytical quality control was monitored by multiple analyses of procedural blanks, unknown samples, and certified reference materials NIST 1643e, IAEA W4. The analytical error as estimated from replicate sample measurements was typically < 2 % RSD (relative standard deviation) for Ag.

3.2.7 Scanning electron microscopy (SEM)

SEM is a type of electron microscope that images the sample surface by scanning it with a high-energy beam of electrons in a raster scan pattern. The electrons interact with the atoms that make up the sample, producing signals that contain information about the sample's surface topography, composition and other properties [140]. As a result of the interaction between the impinging electrons and the target atoms, X-rays are emitted which are characteristic in energy for the constituent chemical elements. Analysis of X-rays emitted from a sample can be accomplished by an energy dispersive spectrometer discriminating X-ray energies which enables not only the identification but also the quantification of the chemical elements present in the specimen. In this work SEM measurements were performed using SEM (ZEISS Ultra plus/Oxford Instruments) at the University of Applied Sciences (Fachhochschule Kiel).

3.2.8 Contact angle measurements

When a liquid droplet interacts with a solid surface, the droplet attains an equilibrium shape. The droplet can be characterised by an angle formed at its edge where the liquid contacts the solid surface. This angle is called the contact angle. Depending on the type of surface and liquid the droplet may take a variety of shapes. The contact angle θ is given by the angle between the interface of the droplet and the horizontal surface. The liquid is seemed non-wetting when $90^{\circ} < \theta < 180^{\circ}$ and wetting when $0^{\circ} < \theta < 90^{\circ}$. A contact angle $\theta = 0^{\circ}$ corresponds to perfect wetting and the drop spreads forming a film on the surface. In this work we measured the contact angles by the so-called sessile drop technique, simply by putting a drop of liquid on the surface, which is the static kind of measurements. Drops of deionized (DI) water (~ 1 μL) were used to determine contact angles and measurements were conducted on a dataphysics OCA5 contact angle system and recorded with a Teli CCD camera.

3.2.9 Electrochemical Impedance Spectroscopy (EIS)

EIS or alternating current (ac) impedance methods are applied to the characterization of electrode processes and complex interfaces. EIS studies the system response to the application of a periodic small amplitude ac signal. These measurements are carried out at different ac frequencies. Analysis of the system response contains information about the interface, its structure and reactions taking place there [141]. In this work *in situ* UV-vis/EIS measurements were performed by our collaborative group in Paderborn university using an in-house built cell which was illustrated by K. Yliniemi et al. [35]. The cell allows the transmission of light through it for UV-vis spectroscopy measurements and had a three-electrode set-up for EIS measurements. After the set-up was assembled, the electrolyte was injected between the working electrode and laboratory glass used as a window for the UV-vis measurement. The studied sample was used as a working electrode, a Pt coil as a counter electrode, and Pt wire as a pseudo-reference electrode. UV-vis/EIS measurements were performed in 0.2 M phosphate buffer +0.5 mM H_2O_2 (pH = 7.5) solution and commenced after the sample was exposed to the solution for different time points. UV-vis spectroscopy (Evolution 600, Thermo

Scientific) recorded the absorbance between 350-800 nm in transmission mode and a pure ITO glass (in 0.2 M phosphate buffer +0.5 mM H_2O_2) was used as a background. The parameters utilised for the EIS measurements (Compactstat, IVIUM Technologies) were the following: potential (open circuit potential, OCP), frequency (100 kHz to 0.1 Hz), amplitude (0.01 V), equilibrium time (2 s), pre-treatment (OCP, 10 s).

Chapter 4

Experiment

4.1 Samples preparation

4.1.1 Ag/PTFE nanocomposites

20 nm PTFE thin films were deposited on quartz glass (1 x 1 cm^2), silicone (0.5 x 0.5 cm^2) and carbon-coated copper TEM grids by magnetron sputtering of the polymer from a 50 mm diameter target mounted on a water-cooled magnetron head using an ordinary RF discharge. The magnetron was arranged at an angle of 50° to the substrate plane. A rotatable sample holder was used to obtain films with a uniform thickness. All experiments were carried out in a home-made stainless steel vacuum chamber, which was initially evacuated to a pressure below 10^{-6} mbar by a turbo molecular pump in combination with a scroll pump. A conventional QCM monitor was used to control the deposition rate of the polymer which was also controlled by variations of the RF power applied to the magnetron. An RF power of 30 W providing a deposition rate of 5 nm/min was used to give a thickness varied between 10-20 nm which was checked using a profilometer. After that, the samples were then mounted in a home-made thermal evaporation chamber maintained at pressure of the order of 10^{-6} mbar and the AgNPs

were deposited as a 2D ensembles on top of the polymer film by thermally evaporation of silver metal pieces (99.99 %, Goodfellow) filled in a crucible. The voltage input for the evaporator was increased in optimum steps of 5 mV per sec till 5.6 V and a current of 2 A to prevent the evaporator from thermal shocks. The current was maintained at this level for 10 minutes to have a constant deposition rate of 0.3 nm/min. For further studies on the barrier effect, an additional layer of PTFE was sputtered on top of these Ag/PTFE samples as described earlier*. The PTFE barrier covers the AgNPs from top and lateral sides. Films with different thickness ranging from 5 to 50 nm were checked by XPS and our collaborative group did atomic force microscopy (AFM) measurements showing a good coverage for barrier films thicker than 5 nm, even from lateral sides [35]. Figure 4.1 shows the model system used in this study, where the thickness of the PTFE barrier and the amount of AgNPs were varied to examine how they affect the silver ion release rate.

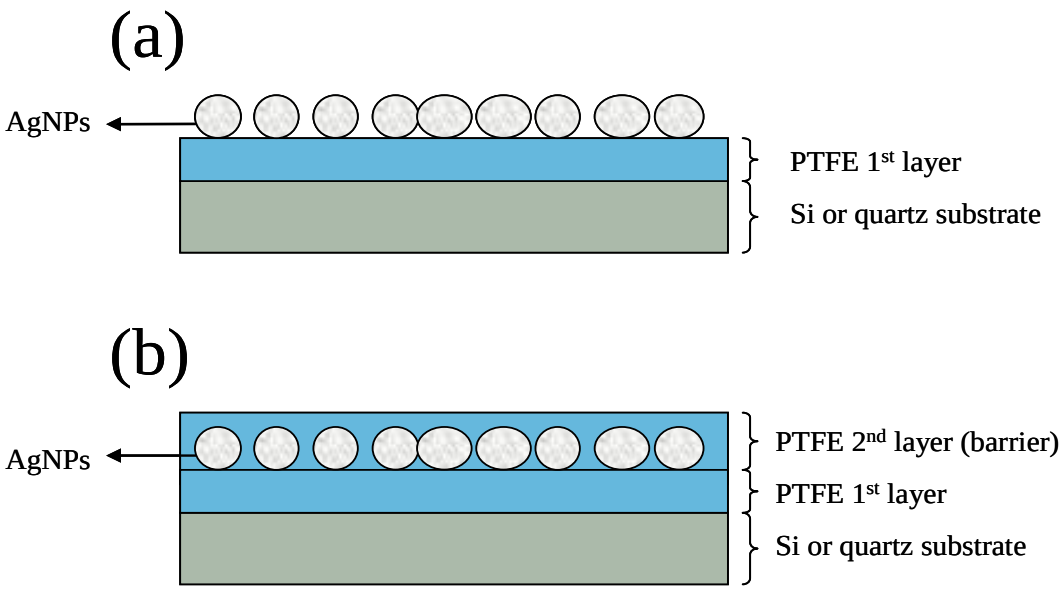

Figure 4.1 Schematic representation of the fabrication of 2D silver nanoparticles/polymer directly accessed (a) or covered with a barrier (b)

* Some researchers claimed that the adhesion of a second layer of PTFE to a previously sputtered PTFE layer may not be good, as the free radicals of the first layer get saturated by either forming bonds with each other or with other atoms in the atmosphere. For the samples studied here the possible influence of poor adhesion of the second layer was checked. In XPS and AFM measurements and in the release behavior of sandwiched NPs no indication for an adhesion problem was observed and therefore no influence on the present results is expected.

4.1.2 Ag-Au alloy/PTFE nanocomposites

20 nm thin films of PTFE were prepared by RF sputtering technique as explained before. Later on, samples were mounted in the thermal evaporation chamber and beads of silver and gold (99.99 %, Goodfellow) were loaded into two separated crucibles and the chamber was evacuated to a pressure below 10^{-6} mbar by the vacuum pump system.

Ag-Au alloy NPs with a 5.5 nm nominal thickness of various compositions were deposited on top of the polymer film by simultaneous thermal evaporation from two separated crucibles. The silver evaporator current was increased slowly in order to avoid thermal shocks by raising the voltage 5 mV/s up to 6.4 V and a current of 2.2 A with a deposition rate of 0.5 nm/min. The deposition rate of gold was varied for the different compositions. For 10 % Au alloy samples, gold evaporator was heated up to 15.8 V and 3.5 A and a deposition rate of 0.05 nm/min was achieved. For 30 % Au samples, the evaporator was heated up to 18 V and 3.7 A and the deposition rate was 0.25 nm/min, while for 50 % Au samples the evaporator was heated up to 18.5 V, 3.8 A providing a deposition rate of 0.5 nm/min. The deposition rate was calibrated and the thickness of the films was monitored using a QCM and a profilometer.

4.1.3 Plasma polymerized HMDSO coatings on Ag/PTFE nanocomposites

Samples of AgNPs on PTFE thin film were produced as already described, then mounted in the chamber where we have a HMDSO source to deposit barriers with different thicknesses by plasma polymerization of the HMDSO monomer. The chamber was then evacuated to a low base pressure (about 10^{-6} mbar) and the deposition was done using an RF generator with 10 W power. The pulse injected HMDSO precursor is mixed with oxygen and argon gases. This mixture of HMDSO, Ar and O_2 is then injected through the nozzle into the plasma. A flow rate of 105 sccm (standard cubic centimeter per minute) of Ar leads to a pressure of 8.8 X 10^{-3} mbar in the main chamber, to which a partial pressure of 3 X 10^{-4} mbar of HMDSO and 1.2 X 10^{-3} mbar of O_2 are added. Different matrices were prepared by changing the O_2 content, which was realized by varying the O_2 flow

rate from 0 up to 20 sccm. The thickness of the coatings was also varied by changing the deposition time.

4.2 Silver ion release measurements

The prepared samples, which were kept in vacuum and darkness, were used to investigate the silver ion release potential. This process is illustrated in Figure 4.2 in the presence of water which is essential for the dissolution of the Ag ions from the surface of the AgNPs.

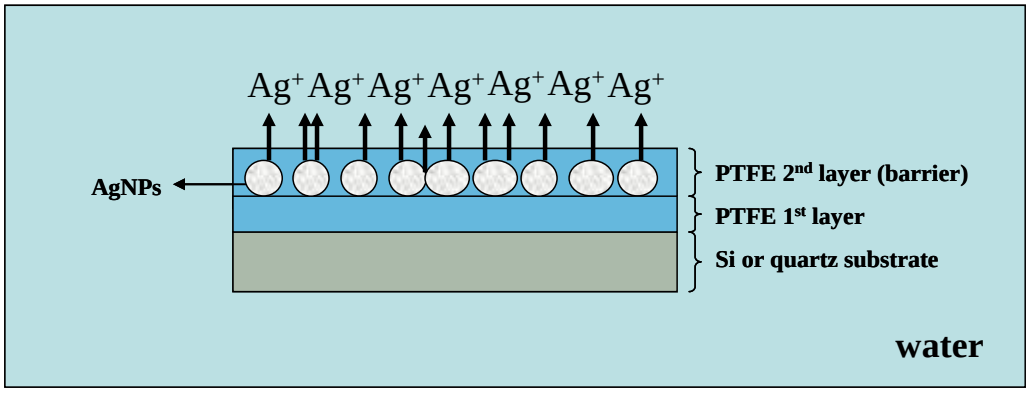

Figure 4.2 Schematic representation of silver ion release from 2D 5.5 nm AgNPs on 20 nm PTFE in water

The silver ion release measurements were performed by observing the changes that occur as samples were immersed in 10 ml air saturated deionized water (pH = 7, σ = 0.06 µS/cm at T = 13 °C) in small bottles made of high density polyethylene (HDPE) at room temperature for different time intervals. A control experiment was done with series of aqueous solutions (Acetic acid pH 4, 6, 7) on 2D AgNP ensembles samples that showed a slight variation in release rates between pH 7 and pH 6 and about ~ 2 times increase in release rate at pH 4. Thus, in this work we did our experiments only in water with pH 7. Samples which were deposited on quartz glass were used for the UV-vis measurements and samples which were prepared on Si were checked by XPS. These measurements were carried out on the samples before and during the immersion time of several days starting from 40 minutes to check the variations. Additionally, TEM measurements were done after immersion of the coated TEM grids in water for several days. The released silver ion concentration in water was checked by ICP-MS. This was done by immersion samples prepared on Si in water and after a definite period, 5 ml of the water were taken

out of the bottle to be analyzed later by ICP-MS and replaced with new 5 ml for the next measuring point of time as shown in Figure 4.3. This procedure has been optimized as we found that removing the whole water could affect the sample by exposure to atmosphere or could change the starting point conditions for the next time step as there were always drops left on the sample or in the bottle. Removing the sample from the water was also not a good option as that could damage the coating or the left water drops would dry and change the surface conditions, e.g. leaving "water rings" on the sample. The half-water-change-method is a suitable method to protect the sample; we don't affect the system too much and we get enough water to repeat the ICP-MS measurements for several times. The calculation of the cumulative ion concentration is mathematically straightforward since the remaining 5 ml of water contain the same amount of silver ions as the 5 ml water that has been removed. It is important to mention that the ICP-MS technique can not distinguish Ag ions from AgNPs. However, since our samples were immersed in neutral water; pH 7, then only oxidation of Ag is expected at this pH as mentioned before [7–10], [64]. Additionally, TEM images and particle size distribution after immersion of samples in water which are shown later in the results chapter showed that especially smaller particles disappear from the matrix which indicates dissolution of the particles in water and ion release. No mechanical detachment of the particles is expected according to our experience with the sample system. Detachment would also mean that larger particles would disappear first instead of smaller ones in contrast to our observations.

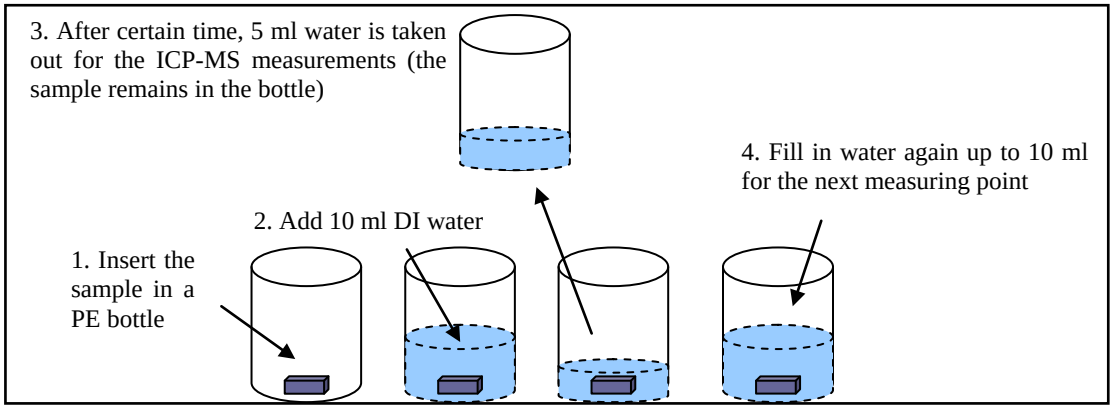

Figure 4.3 The performed half-water-change-method for ICP-MS measurements

Furthermore, EIS was performed by our collaborative group to investigate the water uptake properties samples of PTFE and the HDMSO thin films deposited on the conductive ITO. The measurements were done using a 0.2 M phosphate buffer solution with a pH of 7.5 and an *in situ* cell was used as described previously. The sample was connected as working electrode. Reference and Counter electrode consisted of a platinum wire. The EIS measurements were done with a Gamry Potentiostat Reference 600 over a time period.

Chapter 5

Silver ion release properties of Ag/PTFE nanocomposites

In this chapter the silver ion release properties of a well defined model system consisting of two dimensional silver nanoparticle ensembles with nominal thickness ranging from 1.3 to 8.3 nm and deposited on a 20 nm PTFE polymer and are either directly accessible or covered by another PTFE polymer barrier were investigated. Study of the Ag ion release was accompanied with a control of the composite morphology (Ag nanoparticle size, concentration, and distribution) to understand the mechanism and the kinetics of the interfacial ion transfer reactions of the AgNPs. The surface plasmon resonance of the AgNPs and the variation in the morphology of the nanocomposites as well as the time-dependent release of silver ions after immersion in water were examined by UV-vis, TEM, XPS and ICP-MS.

5.1 Results and discussion

5.1.1 The morphology and the optical properties

A series of TEM images in Figure 5.1 shows the growing of AgNPs on top of the PTFE polymer surface as the amount of silver deposited is increased. For (a) 1.3 nm and (b) 2.8

nm nominal thickness of Ag on PTFE, the formed AgNPs are almost homogenously distributed with an average diameter of about 3-4 nm, while proceeding growth leads to coalescence and formation of larger and more irregular nanoislands. The density of the nanoparticles approximately stays the same but the nanoparticles become bigger and the distance between them gets smaller, as one can see in (c) 5.5 nm and (d) 8.3 nm nominal thickness of Ag on PTFE. The histograms given in Figure 5.2 show the size distribution and the average diameter. As more amount of Ag is deposited, the average diameter increases and the particle size distribution gets broader.

Figure 5.3 presents the optical absorption spectra of the samples deposited on quartz glass with Ag content varying from 1.3 to 8.3 nm. AgNPs exhibit a strong SPR indicated in the absorption spectra. As the mean size and density of the nanoparticles increase, SPRs intensity and optical absorption bands also increase. Since the amplitude of the absorption maxima increases with the deposited amount of Ag, this allows an optical probe of the amount of loaded AgNPs, taking into account the size dependence of the absorption cross-section [142], and the surface density of nanoparticles. The SPR peak is red shifted which is correlated with variation of the nanocomposites' morphology, the changes in the particles' size and shape as well as with decrease of the mean inter-particle distance. The position of the maxima between 450 nm and 460 nm for the 1.3 nm and 2.8 nm Ag/PTFE indicates almost spherical nanoparticles, and the narrow band width indicates a narrow size distribution of AgNPs. Also, the band is symmetric, indicating that negligible aggregation occurs for this amount of Ag while for more deposited silver the peak is red-shifted because the particles become bigger and irregular. Furthermore, the width of the plasmon gets larger due to the wide size distribution of the nanoparticles which can be clearly seen from the conventional TEM images and histograms of Ag (*x*)/PTFE upon the variation of the amount of Ag (*x*) shown before in Figure 5.1 and Figure 5.2. Thus, TEM and UV-vis techniques correlate the optical spectral response with the number, size, and shape of the nanoparticles. This correlation was used for optical monitoring of the variation of the amount of loaded Ag due to Ag dissolution after immersion in water and it was also used as a quick and simple method to study the kinetics of the Ag dissolution process as shown in the next section.

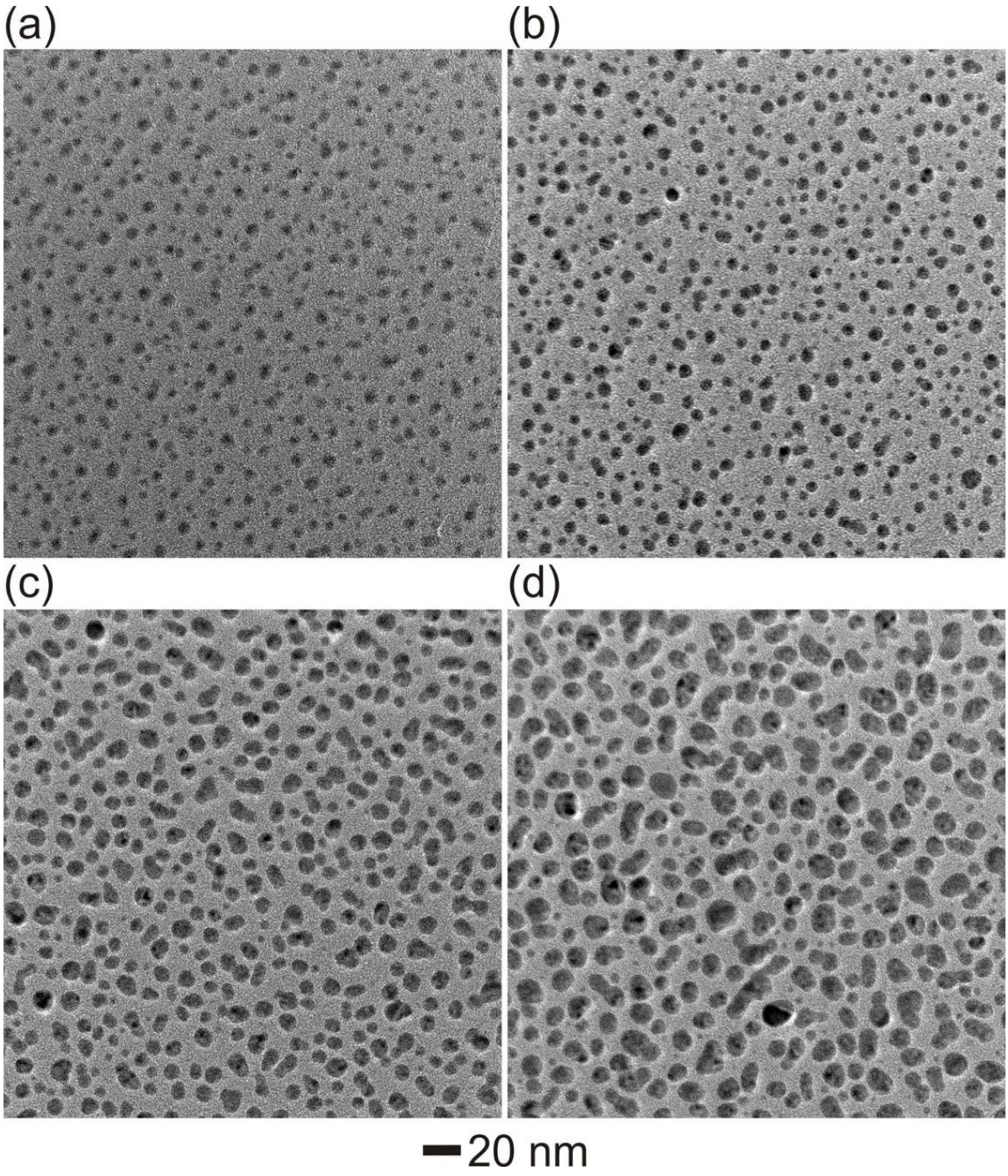

Figure 5.1 BF-TEM images of different amounts of Ag with nominal thickness of (a) 1.3 nm, (b) 2.8 nm, (c) 5.5 nm, and (d) 8.3 nm on 20 nm PTFE film

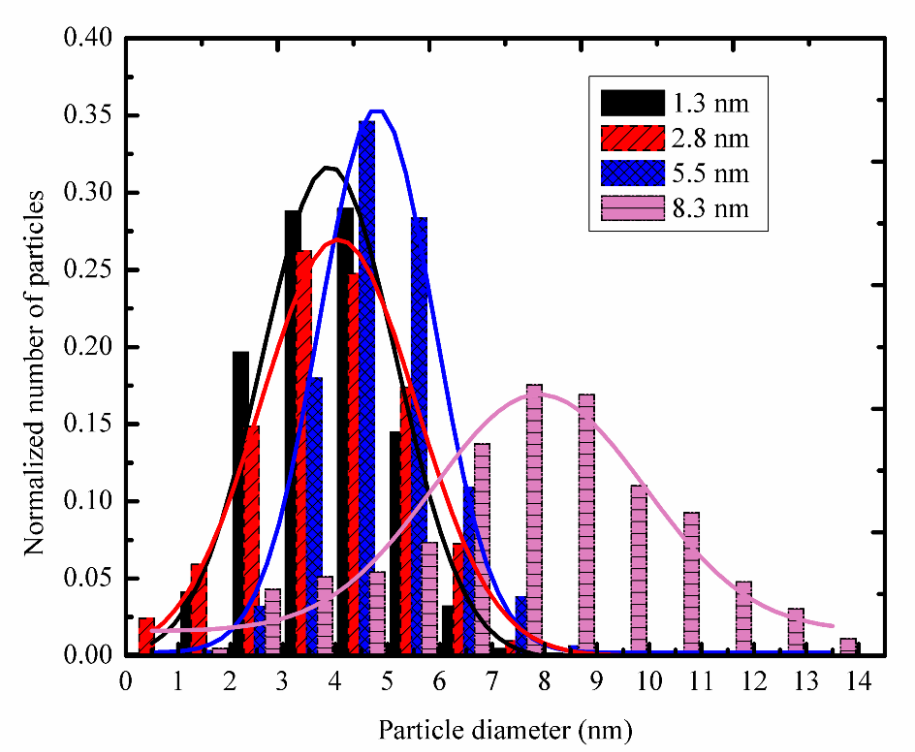

Figure 5.2 Particle distribution for different amounts of AgNPs on PTFE

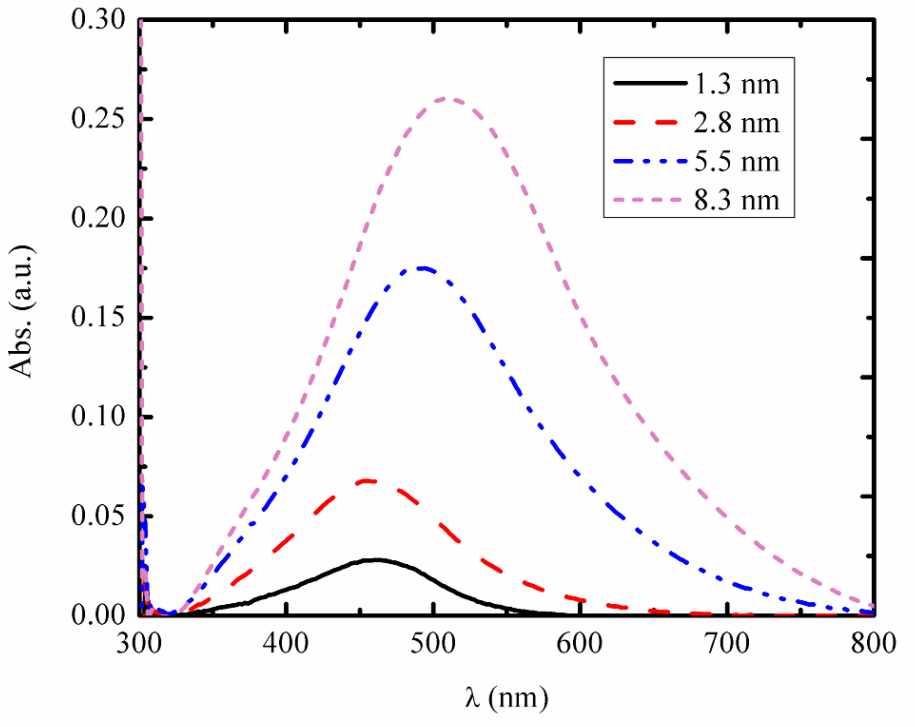

Figure 5.3 UV-vis spectra for different amounts of Ag on PTFE

5.1.2 The silver ion release studies

Since the oxidation of Ag to Ag+ is an important step in the release process of silver ions from Ag surfaces, this suggests surface area dependence and the potential to control release through particle size variation. The macroscopically observed transfer of Ag ions into the environment should depend on the particle size distribution. The latter could be controlled based on the deposition parameters. Therefore, samples with different amount of Ag nanoparticle ensembles were studied by observing the changes that occurred as samples were immersed in water for increasing times. TEM images and changes in particles distribution of sample 5.5 nm Ag/PTFE before and after 1 day in water are shown in Figure 5.4 a, b, and c. Significant changes in the morphology and in the surface amount of AgNPs could be observed before and after immersion in water for one day. The nanoparticles' density looks smaller in the TEM image after one day as a result of the reduction of the initial Ag amount. From the histogram in Figure 5.4 c, one can see a decrease in the amount of the small particles after immersion in water because they are more active than the larger particles, so they were preferentially oxidized and ions were released into the water. Ostwald ripening process, i.e. growth of large particles by dissolution of small particles driven by the particle size dependence of the Ag standard electrode potential, has to be taken into account as it could explain the formation of some new bigger clusters, but this process is more favorable for conductive surfaces [143].

Furthermore, the changes in the morphology of the nanocomposite were characterized by high resolution SEM (HR-SEM) in order to make sure that the Cu-coated grids have no influence on the morphological changes observed, as shown in Figure 5.5 a and b, which confirm again that the TEM results are also in line with the other observations.

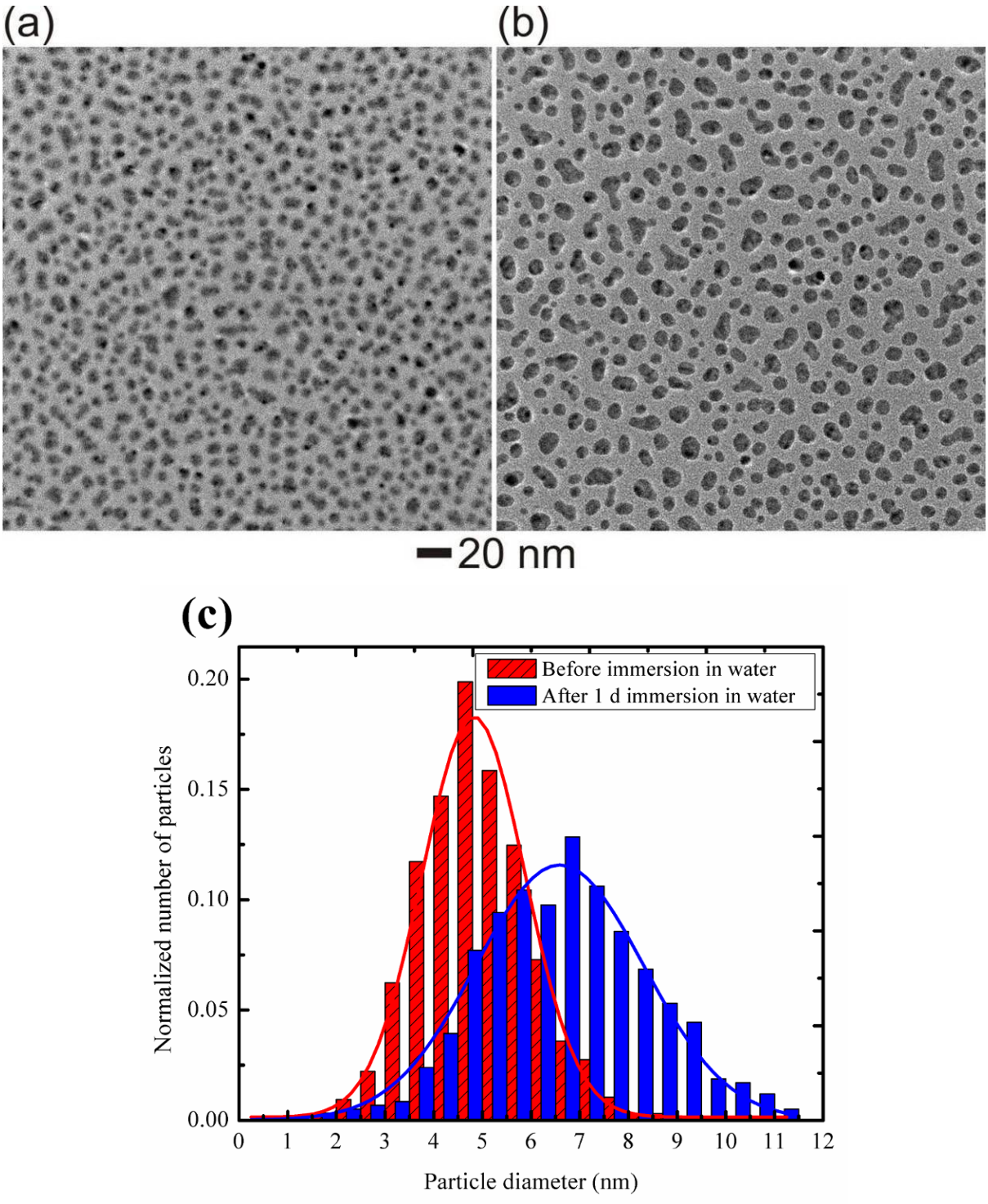

Figure 5.4 BF-TEM images for 5.5 nm Ag/PTFE before immersion in water (a), after 1 day in water (b), and change in particle size distribution (c)

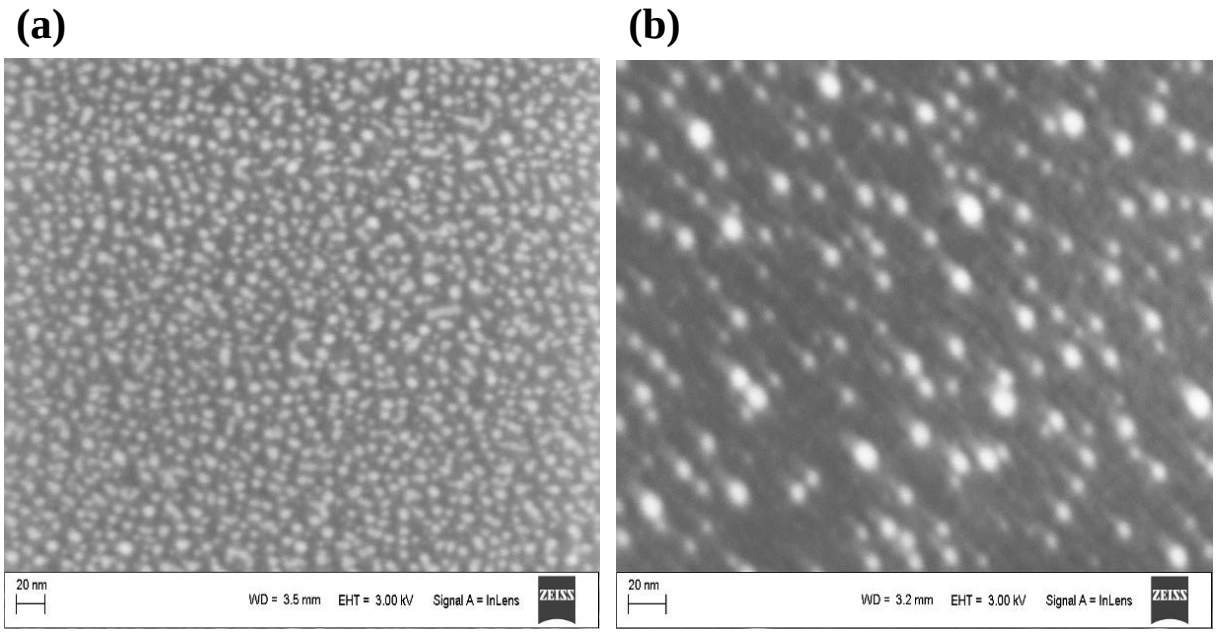

Figure 5.5 HR-SEM images for 5.5 nm Ag/PTFE before (a) and after 1 day in water (b)

The changes can be observed more precisely by UV-vis, Figure 5.6, since the absorption maxima and the peak position are very sensitive to any change in the particles' size and amount. The SPR peak intensity decreased and a blue-shift was also observed due to dissolution of particles after certain time in water. A similar blue-shift was observed in our previous aging experiments on Ag/polymer nanocomposites [144] as well as after agglomeration of small nanoparticles into large nanoparticles by heating the 2D Ag arrangements at 200 $^{\circ}$C. This view is also supported in the work of Peng et al. [142] by optical measurements and theoretical analysis based on the Mie theory [59] for particles with a diameter less then 15-20 nm. The optical results shown in Figure 5.6, support the TEM results (variation of particle size distribution, Figure 5.4 a-c) demonstrating that small particles dissolved faster than large particles. These observations were supported by measuring of the Ag ion release rate for the 2D Ag/PTFE nanocomposites with different Ag loadings.

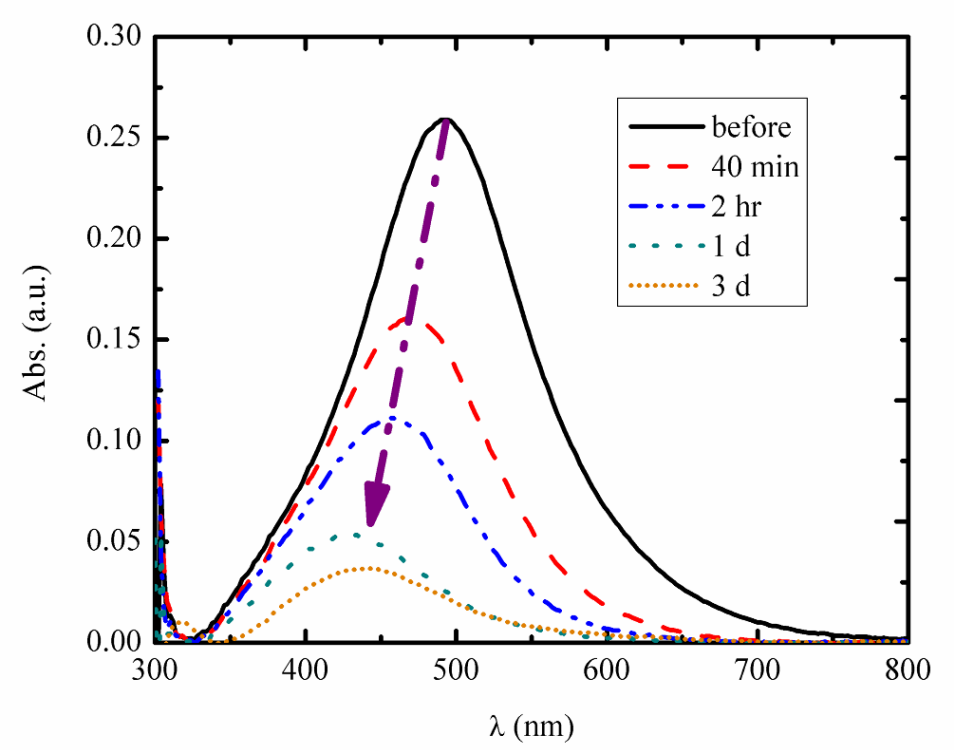

Figure 5.6 UV-vis spectra for 5.5 nm Ag/PTFE at different immersion times in water

Figure 5.7 shows the variation of these rates determined from the change in the SPR maxima of samples with different amount of AgNPs which were immersed in water for different times. Two different phenomena were observed: first of all, the normalized release rate (rate normalized on loading) was significantly higher for the samples with low Ag loading. Secondly, the release rate decreases with time independent of Ag loading, taking into account the nanoparticles' size distribution in Figure 5.2 and assuming a first-order rate reaction, the rate constant after 40 min immersion in water for the nanoparticles with average sizes from 3 nm to 8 nm range between 22 day^{-1} (R_{av} ~ 3 nm) and 1.3 day^{-1} (R_{av} ~ 8 nm). This agrees with the generally accepted assumptions based on the modified Kelvin equation that solubility increases exponentially as the particle radius decreases [49], [145]. Moreover, the decreasing dissolution with the immersion time can also be explained in terms of the initially higher rate constant for nanoparticles with smaller radius. This explanation is supported by the variation of the nanoparticles' size distribution in Figure 5.4 c, since aggregation reduces the surface area of the NPs exposed to the solution. These results prove again that the sample with the

smaller particles has the highest and the fastest decrease in the absorbance maxima (which indicates decrease in the initial amount of silver) since the dissolution of smaller particles is more favorable than that for the larger particles.

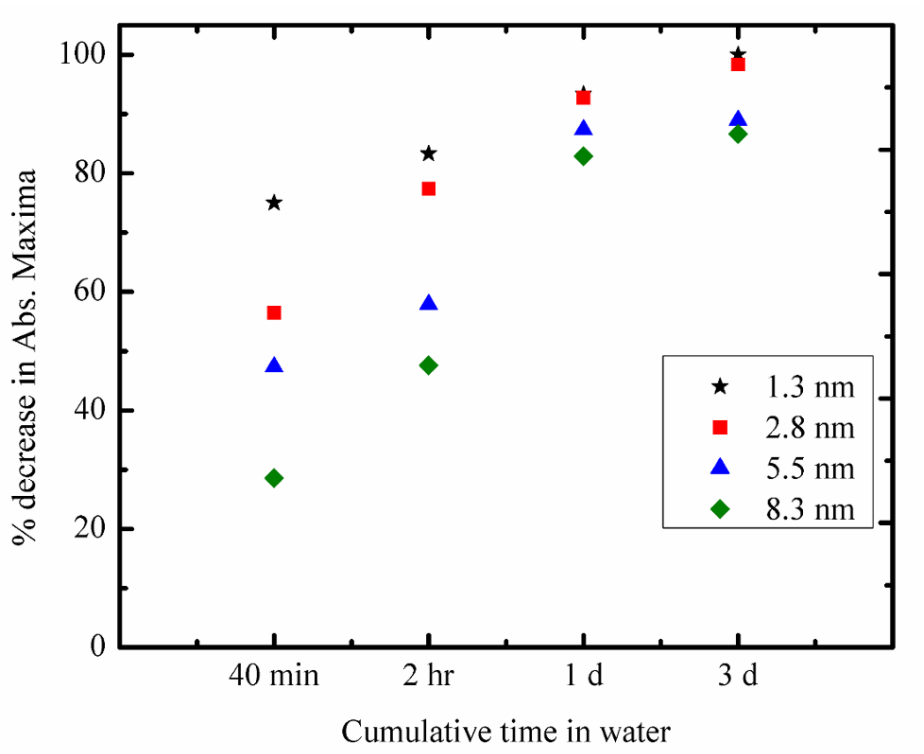

Figure 5.7 Change in absorbance maxima for different amounts of silver due to Ag ion release in water

The concentration of the dissolved Ag in water after dissolution of AgNPs was also directly measured by ICP-MS. The results of samples 2.8 and 5.5 nm Ag/PTFE are shown in Figure 5.8 a and b. A higher amount of AgNPs on the surface of the polymer leads to a higher absolute release (higher ion concentration was detected in the water) as shown in Figure 5.8 a. However, if we compare it to the initial amount of silver, then the percentage relative ion release (amount of released Ag^{+}/initial amount of Ag X 100 %) for 2.8 nm Ag/PTFE is higher than that for 5.5 nm Ag/PTFE, Figure 5.8 b, because it has more amount of smaller particles confirming again that the smaller particles' size leads to a higher dissolution rate.

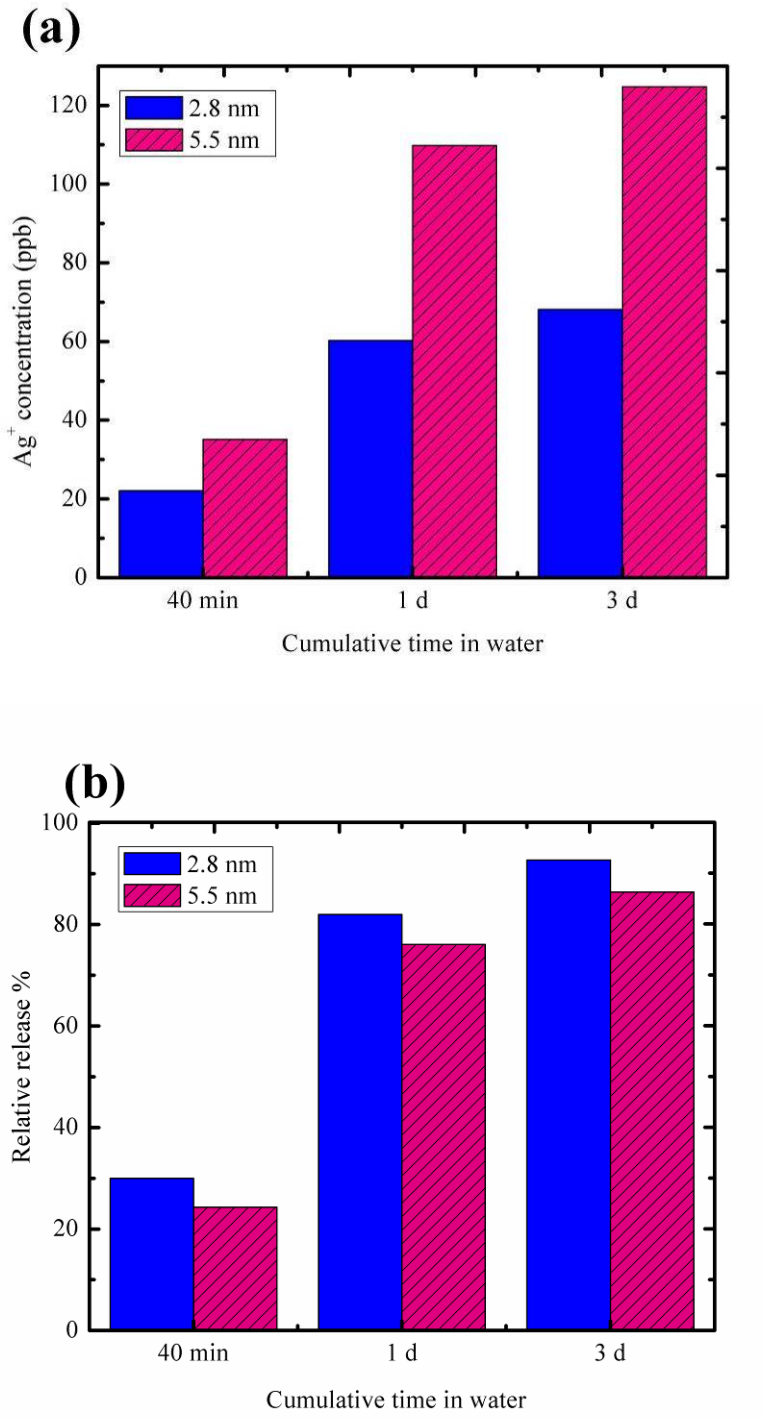

Figure 5.8 ICP-MS results for 2.8 and 5.5 nm Ag/PTFE after immersion in water: (a) the absolute Ag ions concentration in water, (b) the normalized (% relative) release

To understand in detail the kinetics of Ag ion release from Ag/polymer nanocomposites, we compared the data, which was received by measurements of the concentration of Ag ion in water (ICP-MS), with the data from surface loading variation, which was evaluated by XPS and UV-vis techniques for our model samples with effective Ag loading of 2.8 and 5.5 nm. The percentage damping of the plasmon absorption maxima and the change in the Ag intensity from the XPS spectra, as well as the percentage of the relative ion release of these two samples as they were immersed in water for 3 days showed a strong correlation among the different techniques used in this work as shown in Table 5.2.

Table 5.2 Comparison of the percentage Ag released from two different samples after 3 days immersion in water as determined by different techniques

Sample	**ICP-MS**	**UV-vis**	**XPS**
	% Ag released	% decease in abs. maxima	% decrease in Ag intensity
2.8 nm Ag/PTFE	93 %	88 %	78 %
5.5 nm Ag/PTFE	86 %	86 %	69 %

5.1.3 The barrier effect

To stabilize the nanoparticles, i.e. to avoid the Ostwald ripening, and to control the rate of release of silver ions from the samples, a PTFE barrier was deposited on top of the previous system and the effect of the polymer barrier on the Ag ion release rate was studied by UV-vis technique and ICP-MS as shown in Figure 5.9 a and b. Figure 5.9 a shows that the decrease in the absorption maxima (i.e., due to decrease in the amount of Ag) as a result of Ag dissolution after immersion of the samples in water was much less for the sample with a 10 nm barrier than that for the sample with the same amount of silver (5.5 nm nominal thickness) but with no barrier. Besides, for the two samples with the same silver content, Figure 5.9 b shows that the amount of the released Ag ions and the kinetics of the silver release process were different. The sample without the barrier has a quick Ag dissolution directly after being in contact with water and almost 80 % of the initial Ag amount was dissolved in one day and after that the dissolution became slowly and a saturation state has been arrived. While for the sample with 10 nm PTFE

barrier on top of the AgNPs, there was almost no release of Ag ions till the 1st day onwards with only 10 % release of the Ag and the process continues after that linearly but at a much lower concentration level.

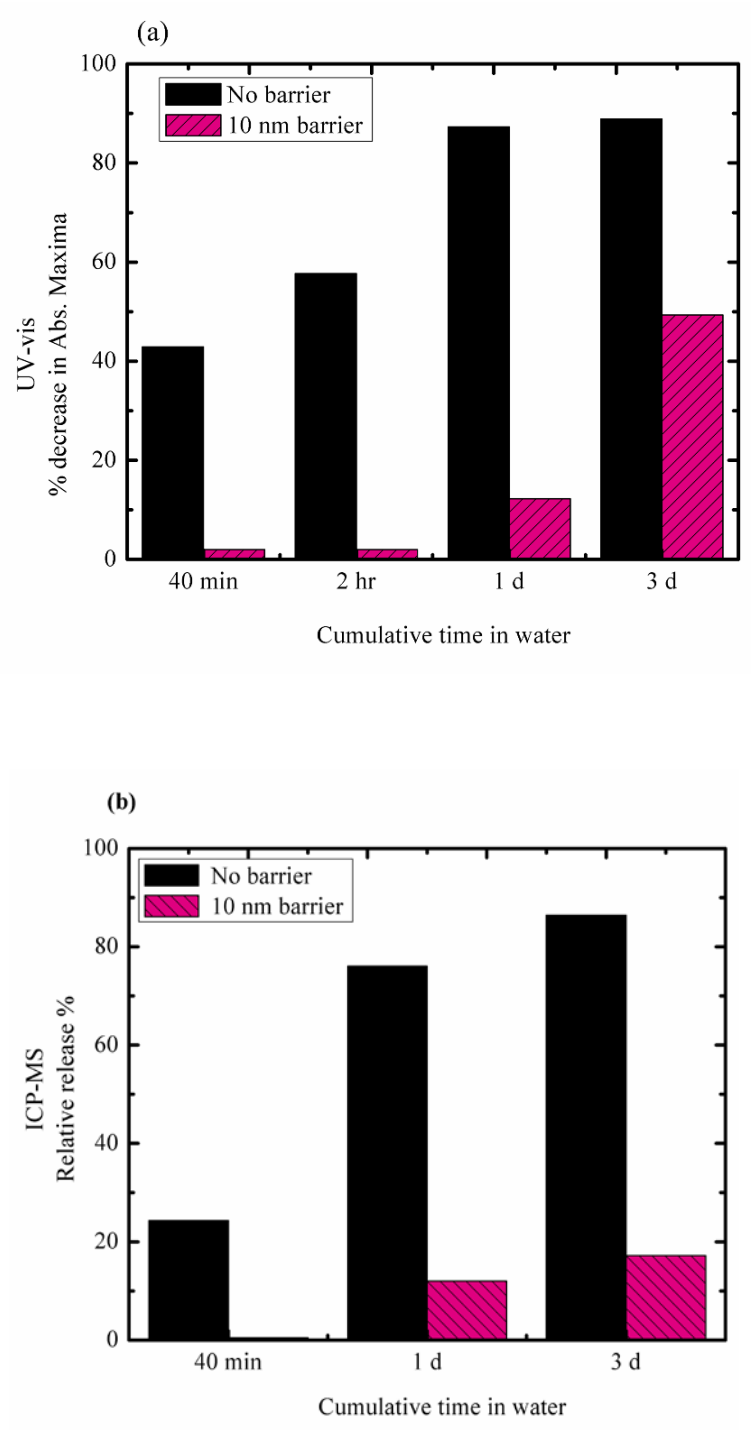

Figure 5.9 % Change in abs. maxima as measured by UV-vis (a) and % relative release as measured by ICP-MS (b) for the 5.5 nm Ag/PTFE samples with and without a PTFE barrier

This can be explained by the fact that PTFE is a hydrophobic polymer and its water uptake and the diffusion coefficient of water in PTFE are very low compared to other polymers. Damm et al. [8], [18], for instance, have investigated the silver ion release behavior of polyamide 6 (PA6)/Ag and polymethylmethacrylate (PMMA)/Ag nanocomposites with the same silver content and morphology. Different silver release properties of the two nanocomposites were found which were explained by the difference in the water uptake properties of the polymer matrices since PMMA is a rather hydrophobic polymer in comparison to PA6. These findings imply that the mobility and solubility of water molecules in the polymer must be taken into account to explain the silver ion release. Thus, in the case of Ag/PTFE nanocomposites covered with a highly crosslinked PTFE barrier, water uptake of the polymer barrier was not sufficient for a high Ag ion release rate similar to that for the samples without a polymer barrier. This means that only when water reaches the surface of the metallic nanoparticles, the oxidation of Ag takes place and the ion release process starts. This explains the slowing down of the rate of the ion release process within the 1st day of immersion the Ag/PTFE samples with barrier film in water.

To study the effect of varying the thickness of the PTFE polymer barrier, 3 samples with the same Ag content (5.5 nm) but different barrier thicknesses were examined by UV-vis as shown in Figure 5.10. One notices that the damping in the intensity of the SPR peak gets smaller as the thickness of the barrier increases. For the sample without a barrier, about 90 % of the initial absorbance maximum was vanished after 3 days of immersion of samples in water due to the Ag dissolution and Ag ion release. Deposition of an additional PTFE polymer film of thickness of 10 nm, achieves a reduction in the damping in the intensity of the SPR peak compared to the nanocomposite sample without such an additional coating. Increasing the thickness of the PTFE overlayer to 20 nm, leads only to 10 % reduction in the initial absorbance maximum which means that the water penetration through the polymer film was retarded due to the high hydrophobicity of the highly crosslinked RF sputtered PTFE polymer films and indicates that a huge control over the Ag ion release rate can be done with thin PTFE films in short time. In comparison with previous studies done by Vasilev et al. [23] using *n*-heptylamine (HA) plasma polymer overlayers of several thicknesses on top of AgNPs loaded films, a 20 %

reduction of the rate of the silver ion release (absorbance maximum) was achieved with a film thickness of 18 nm after 20 days of immersion of samples in buffer solution. This proves again that the properties of the polymer matrix and the thickness of the polymer coatings have a crucial role in the silver ion release process as they affect the water transport through the polymer barrier to the surface of the metallic AgNPs and the subsequent silver ion diffusion through the polymer into the water. This an important issue since excessive dosages of Ag ions may have undesired consequences in medical applications. Moreover, the additional polymer barriers prevent the direct uptake of the AgNPs into the cells and the environment and prevent the bacterial adhesion and the formation of biofilms.

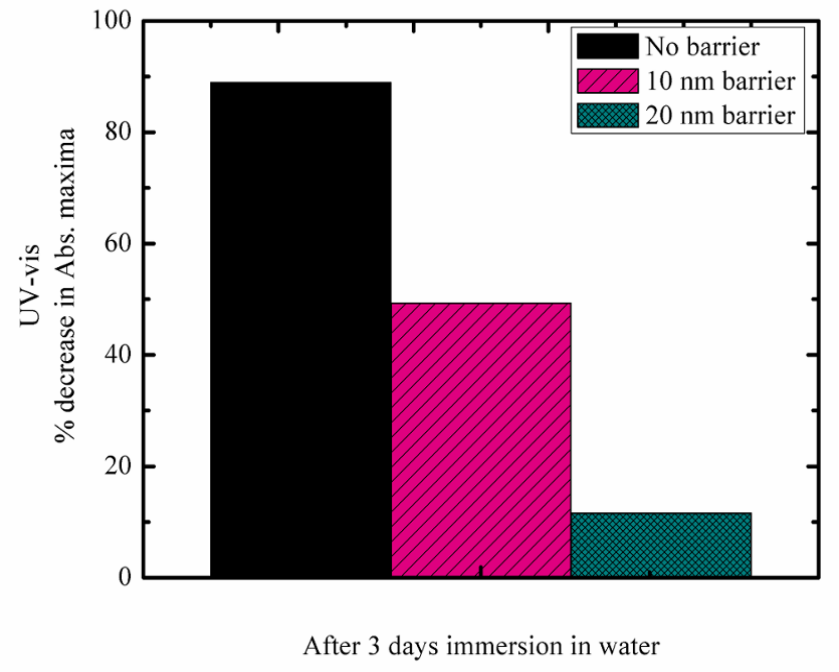

Figure 5.10 % decrease in abs. maxima for different PTFE barrier thickness on 5.5 nm Ag/PTFE

These results are supported by complimentary experiments on similar model samples done by our collaborative group using combined *in situ* UV-vis/EIS [35]. When the decrease in absorbance and the increase in the coating capacitance (C_p) are compared to each other, Figure 5.11 a and c, the correlation between these two parameters is clear: AgNPs dissolution begins when the solution reaches the AgNPs layer of the film. At the long exposure times (200-300 min) one can also detect the increase in the coating capacitance after a plateau area, which - in turn - is assumed to be a saturation point of

the water uptake. However, the polymer barrier film could also delay the silver ion transfer from the nanoparticles' surface into the solution, which also leads to a low rate of ion release [18].

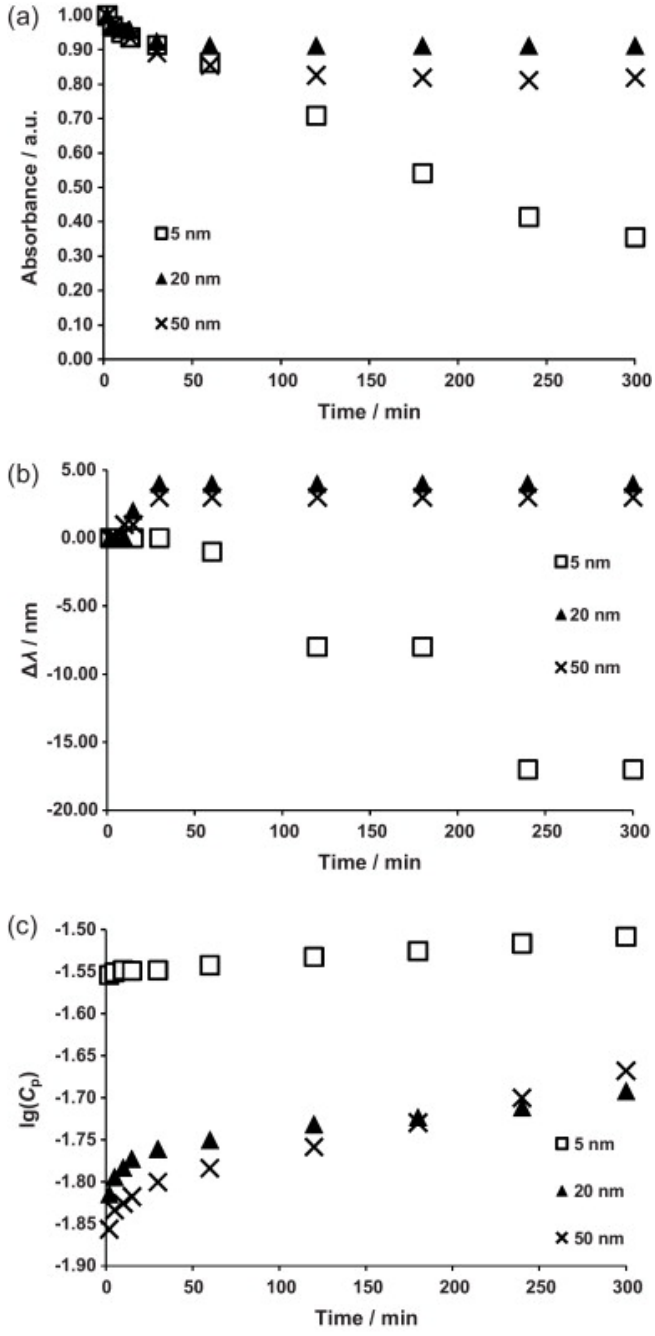

Figure 5.11 Absorbance of the SPR peak (a), shift of the SPR peak (b) and capacitance of the coating at f = 1KHz for PTFE (d)/(5.5 nm) Ag/(75 nm) PTFE/ITO where d = 5, 20 or 50 nm, as a function of exposure time to the buffer solution [35]

5.2 Conclusions

A well defined model of two dimensional ensembles of AgNPs on top of a highly crosslinked RF sputtered PTFE films was prepared using PVD techniques. Depositing the AgNPs on the surface of the PTFE polymer films instead of embedding them in the polymer matrix made them directly accessible and easily investigated regarding the geometrical arrangements of the nanoparticles and their variations. With increasing the amount of the deposited silver with a nominal thickness ranges from 1.3 to 8.3 nm, the average diameter of the nanoparticles increased from 4 to 8 nm and the size distribution broadened. The change in the Ag content (nominal thickness) from 1.3 to 8.3 nm Ag resulted in a SPR shift and a broadening and increasing of the absorbance peak which corresponds to an increasing particle size and a decrease in interparticle distance from the TEM analysis.

To understand the time-dependent release of silver ions from Ag containing nanocomposites after immersion in water for defined time intervals, the composites' morphology variation was examined by different analytical techniques (TEM, SEM, UV-vis, and XPS) and the concentration of the released Ag ions in water was measured by ICP-MS.

Changes in the microstructure of the nanocomposite due to the dissolution of the AgNPs after immersion in water and to Ostwald ripening phenomena and the corresponding changes in its optical properties were good way to study the silver ion release potential. A correlation between changes in the morphology and optical properties of the nanocomposites and the kinetic of the Ag ion release process was found.

Moreover, results showed that the silver ion release potential increases with increasing the silver content of the nanocomposites, and since the oxidation process takes place on the surface of the metallic particles, at a given Ag amount, silver ion release increases with an increasing surface-to-bulk ratio of the particles. Therefore, we varied the amount, the size of AgNPs by controlling the deposition parameters in order to tune the silver ion release properties of Ag/PTFE nanocomposites. It was also shown that the strong

dependence of the silver ion release on the particle size leads to a significant redistribution of the composites' morphology and a suppression of the Ag ion release rate with time.

Finally, results showed that PTFE polymer barrier stabilizes the morphology of the nanocomposites and can be applied to control the Ag ion release rate since the crosslinking and hydrophobic nature of the PTFE polymer reduces its water uptake which results in a less amount of the released Ag ions and a slower release rate in comparison to that for nanocomposites without PTFE barrier. Besides, by changing the thickness of the polymer barrier during the deposition process, the released amount of Ag ions and the kinetics of the release process were varied dramatically. This leads to the conclusion that covering the AgNPs by a polymeric barrier represents a simple and effective way to stabilize a controlled dispersion of protected NPs whilst taking advantage of their physical characteristics.

Chapter 6

Silver ion release properties of Ag-Au alloy/PTFE nanocomposites

In this chapter, nanocomposites containing Ag-Au alloy nanoparticle ensembles with various compositions were deposited on PTFE thin films by PVD. After certain time of immersion of the samples in water, oxidation and dissolution of the AgNPs occurred and changes in the morphology, optical properties and composition of the nanocomposites were examined using TEM, UV-vis spectroscopy and XPS, respectively. The composition-dependence and the time-dependence of the silver ion release were studied and the concentration of the silver ions in water was detected using ICP-MS.

6.1 Results and discussion

6.1.1 The morphology and the optical properties

For Ag-Au alloy NPs, silver and gold were evaporated simultaneously, and a complete alloy formation is expected as gold and silver are in the same group of periodic table, have similar atomic radius and same structures that make them fully miscible in each other in the solid solutions [87]. According to the nucleation and growth model of metal

atoms on polymeric surfaces discussed in section 2.2.1, they grow on the polymeric surface by forming small nuclei at certain sites which grow by the continued deposition of the metal via direct impingement and surface diffusion [107]. Figure 6.1 a and b shows a BF-TEM image for 5.5 nm of 70 % Ag - 30 % Au alloy NPs on PTFE and its corresponding particle size distribution. A uniform distribution could be observed with an average diameter of about 5 nm except for some larger diameter particles having irregular shape contribute to coalescence growth of the particles. The 5.5 nm nominal thickness Ag and Au alloy NPs have almost a similar size distribution and an average diameter of about 5 nm as the pure AgNPs prepared in the same way and same amount as was shown in the previous section.

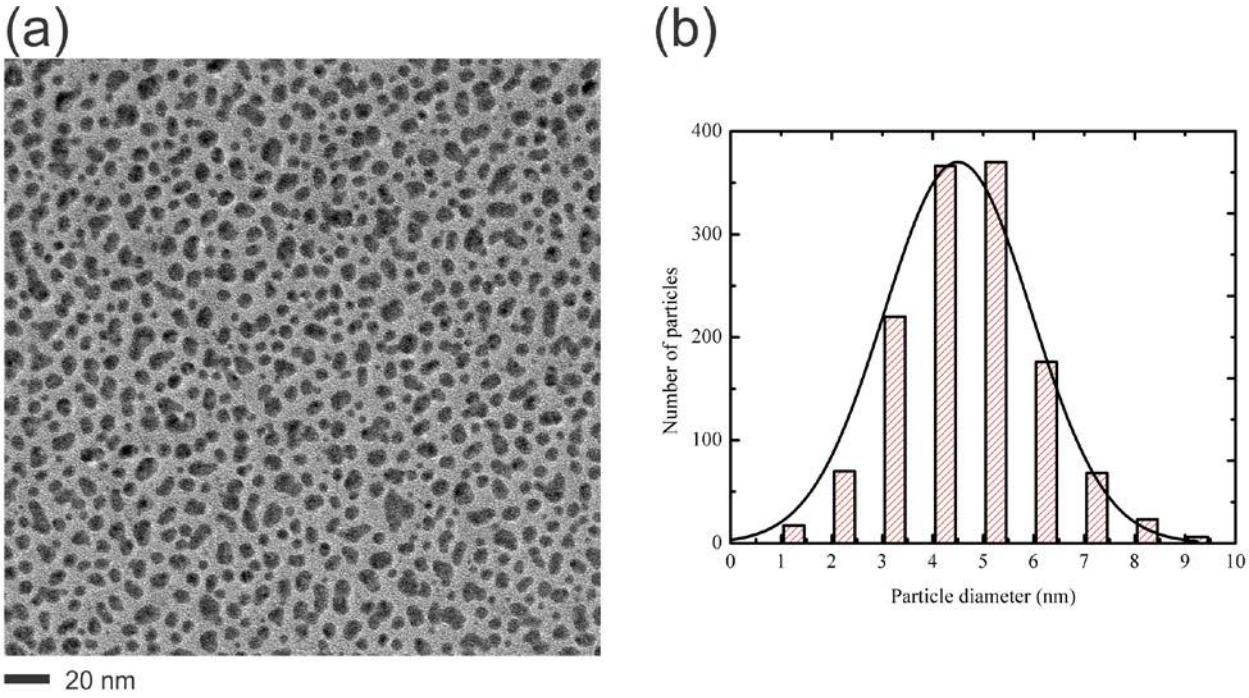

Figure 6.1 BF-TEM image (a) and the corresponding particle size distribution (b) of 5.5 nm 70 % Ag - 30 % Au alloy NPs on PTFE

The absorption spectra obtained by UV-vis for 5.5 nm pure Ag and Ag-Au alloy NPs on PTFE with various compositions are shown in Figure 6.2. The alloying of Ag-Au NPs on PTFE can be concluded from the resulted optical absorption spectra which show a single plasmon resonance peak, whereas two bands would be expected for the case of phase separated NPs [59], [95]. Alloy formation of Ag-Au NPs caused a plasmon maximum in

the UV-vis spectrum between the absorption maximum of Ag and Au that varies with respect to composition distribution. One can see that the plasmon peak position is red shifted as a result of an increase in Au composition due to the continuous change of the *d*-band energy level that contributes to the interband transition term in the dielectric function, and a damping of the absorbance maxima is seen attributed to the higher electron scattering by foreign atoms upon alloying and the gold *d-sp* interband transition [59], [94], [100] as discussed previously in section 2.1.5.

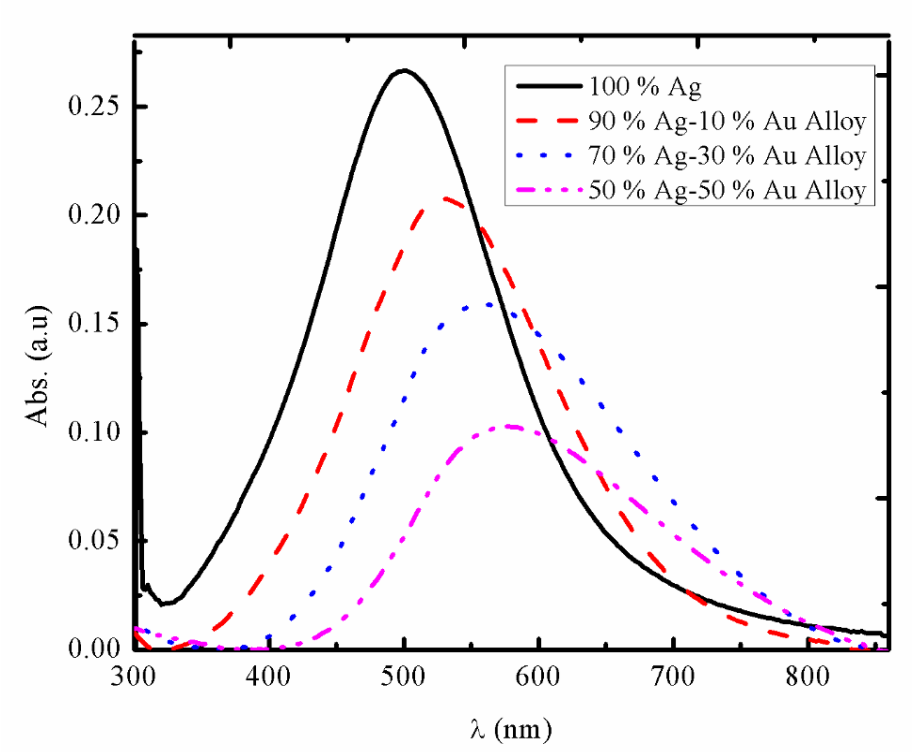

Figure 6.2 UV-vis spectra for 5.5 nm nominal thickness of various composition of Ag-Au alloy NPs

The position of the plasmon absorption peak of these alloy NPs, however, depends linearly on the composition of the alloy particles when expressed in terms of the gold fraction as shown in Figure 6.3, in agreement with what was reported previously [90], [93], [99], [100].

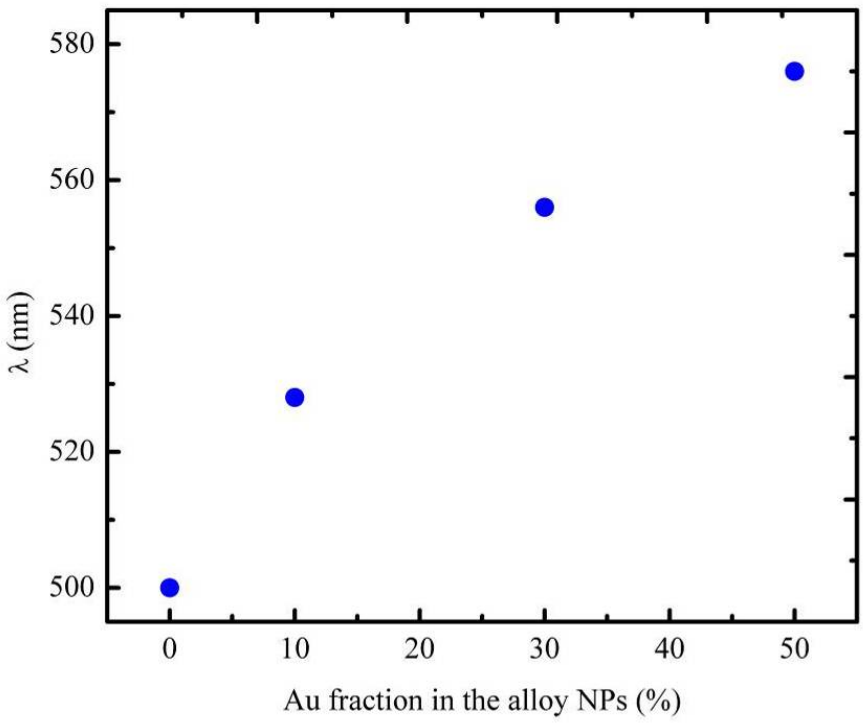

Figure 6.3 The position of the SPR peak (λ) of the alloy NPs with respect to the Au fraction (%)

6.1.2 The silver ion release studies

The Ag ion release kinetics was studied by observing the changes as samples were immersed in water for different time intervals starting from 40 minutes up to 7 days. The concentration of the released silver ions from each sample was measured by ICP-MS where results showed a negligible Au ion concentration. Additionally, UV-vis and XPS measurements were carried out for all samples after immersion into aqueous medium. The cumulative concentrations of the released Ag ions (μg/l.cm^2) normalized to the silver fraction in the alloy nanocomposites were measured at several time periods as shown in Figure 6.4. All silver ion concentrations are the mean values of three ICP-MS measurements.

One notices that the release of the silver ions is not just proportional to the amount of silver present in the nanoparticles. In that case all four diagrams should look the same. But one notes significant differences for short and long release times. In all systems there was a rapid release of Ag ions at the beginning (determined after 40 min) due to the first

interaction of the nanoparticles with water and the Ag dissolution from the surface. The fastest release of the silver is here observed for the pure silver system and the 50 % alloy, while the relative release is smallest for the 70 % alloy system. This can be explained with the entropy of mixing which is most favorable for a 50 % alloy and decreases from there for higher silver fractions [88].

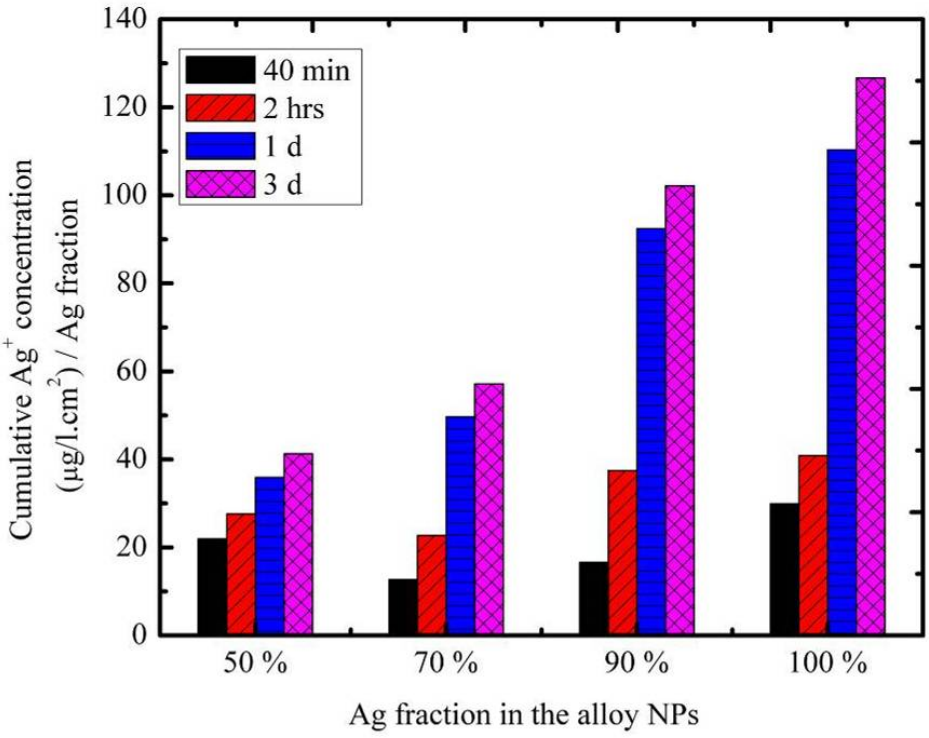

Figure 6.4 Cumulative concentration of silver ions released from Ag-Au alloy systems at different immersion times in water and different Ag fraction

Thus the initial silver release of the 50 % alloy is not slowed down so much and the initial release of the 70 % and 90 % alloy is even below the 50 % alloy. But after one day the relative silver release scales with the amount of silver present and the pure silver shows the largest silver release, whereas the release is significantly reduced for the alloys. Here the slowing down of the silver release is directly correlated with the gold fraction in the alloy. The more gold is present in the alloy the more the release is slowed down. For the 90 % alloy system one observes still a big difference between the release after 2 hours and 1 day, whereas the change for the 50 % alloy system has become already very small. To explain this behavior one has to consider the change in composition caused by the

silver release. For the nanoparticles with initially 90 % silver fraction the composition will move towards 50 % with still a higher silver than gold fraction. Here entropic contributions favor further silver release. The situation is different for the 50 % alloy. Here the entropic contribution due to change in composition is not favorable for further silver release and thus the silver release will be slowed down. Additionally, increasing the Au fraction inside the NPs could lead to a significant change of the electron transfer properties of the alloy NPs with the composition. This interaction between Ag-Au causes depletion and reduces the silver ion release. Thus, a rapid dissolution of Ag occurred only at the first contact of the sample with water and when the composition of the alloy NPs becomes Au rich a saturation state is approached. This could be an advantage for potential applications where the Ag ion release is required to be rapid and effective at the beginning then a slower dissolution rate, leading to a continuous release of Ag ions for long term application.

These results are in agreement with what was shown by Besner et al. [99] as they observed a strong increase in the oxidation resistance with the increase in the Au fraction inside the Ag-Au alloy NPs which was explained by the idea that addition of Au atoms inside the AgNPs would then contribute to the formation of internal electron traps, inhibiting the dissolution of the AgNPs and the release of Ag ions. On the other hand, several bimetallic/polymer nanocomposites were developed where the galvanic coupling of silver with platinum [32], [33] or gold [19] strongly increases the silver ion release. And as mentioned earlier in sec. 2.1.5, Barcikowski et al. [103], [104] have found that electrochemical oxidation reaction between Cu and Ag enhanced the ion release of the less noble metal (Cu) by the ion mediated electrochemical reaction and Ag ion release was retarded. Whereas in the case of Au/Ag nanocomposite films, no effect on silver ion release was observed due to the absence of mobile gold ions. These results show that the way systems with two different noble metals are prepared and whether the noble metals are in direct contact, spatially separated or no contact at all, play a role in adjusting the dissolution of the less noble metal if the stability of the bimetallic NPs is vital for the desired application.

Further investigations were performed by XPS to examine changes which occurred for the 70 % Ag - 30 % Au alloy NPs on PTFE film deposited on Si substrate after immersion in water for several days. Variations in Ag and Au peaks intensities were investigated before and after immersion of samples for several days in water. Intensity of each element and area under the XPS peaks give quantitative information about the elements within the composite. The sensitivity factors of Ag and Au are approximately the same i.e. 5.2 [139], so the alloy composition can be determined from the intensity of XPS signal which is the area under the Ag and Au peaks. Ag and Au intensities were normalized with respect to the carbon intensity in order to eliminate time-dependent changes in the intensity of the XPS spectra, as shown in Figure 6.5.

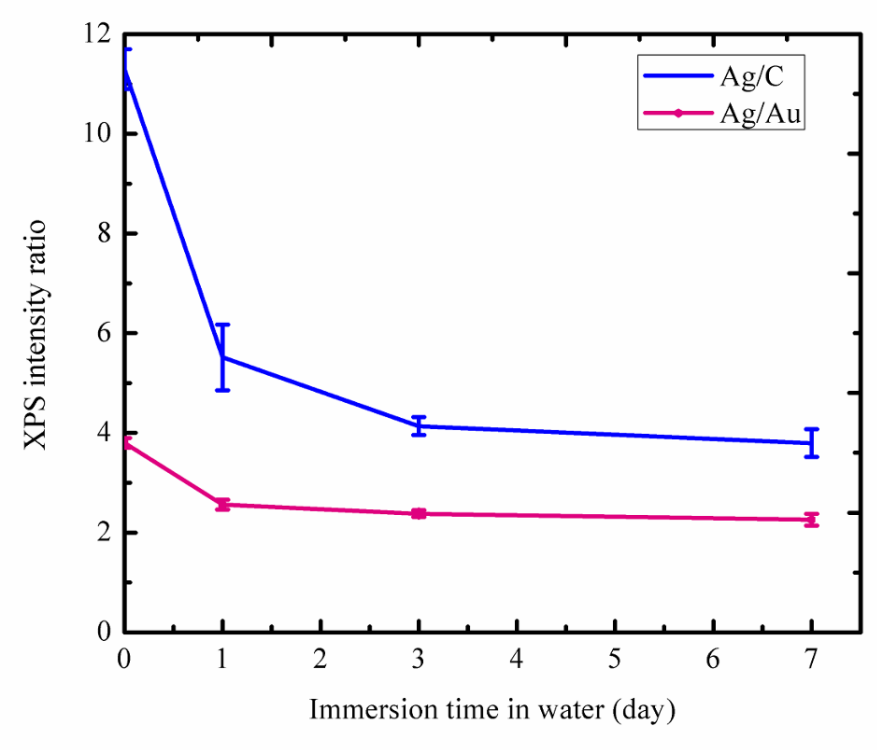

Figure 6.5 Change in the XPS Ag and Au intensities for 5.5 nm 70 % Ag - 30 % Au alloy NPs on PTFE after immersion in water

Before immersion in water, the ratio of Ag to Au was a little larger than the expected value. This could be caused by a slightly higher deposition rate of the silver during the co-evaporation of the alloy NPs. Note that prior to co-evaporation the deposition rates were calibrated independently and no cross influence of the evaporators was taken into

account. In addition the deviation from the expected value could be due to systematic errors in the determination of the peak areas, in particular for the weaker gold lines. Due to dissolution of silver after immersion of samples in water, the Ag/C and Ag/Au intensity ratios decrease rapidly at the beginning and after the first day the decrease in the ratios becomes slower with time indicating the approach of a saturation state. One could speculate that this saturation states occurs because silver ions are released only from the outer layers of the nanoparticles and that a gold shell is formed subsequently by the gold that is left behind.

In order to check this possibility energy dependent XPS spectra were measured on one set of the 5.5 nm layer of the 70 % Ag - 30 % Au alloy nanoparticles on sputtered PTFE. One sample was measured as prepared and the other one after 3 days of immersion in water. By varying the photon energy the probing depth is varied. The spectra were analyzed by normalizing the Au 4f lines (at 84.0 and 87.6 eV) to the same intensity for all spectra and then the decrease of the signal of the Ag 3d lines (at 368.3 and 374.2 eV) due to immersion in water was determined for the different photon energies, i.e. for different probing depths, see Table 6.1.

Table 6.1 Summary of energy dependent XPS analysis

Photon energy (eV)	**Kinetic energy at Ag 3d lines (eV)**	**Inelastic mean free path (probing depth) (nm)**[†]	**Decrease of Ag 3d signal after 3 days immersion in water (%)**
500	130	0.43 (0.86)	55.3±3
650	280	0.61 (1.21)	58.3±3
900	530	0.89 (1.78)	53.5±3
1200	830	1.21 (2.41)	52.8±3
1500	1130	1.50 (3.00)	53.2±3

The data show no significant variation of the silver depletion with XPS probing depth indicating that the silver distribution within the nanoparticles remains essentially

[†] calculated from the data provided by Tanuma et al. assuming a 70 % Ag and 30 % Au composition [151]

unchanged, i.e. it remains alloy like, as illustrated in Figure 6.6. Therefore the formation of a gold shell can be ruled out and the observed slowing down of the silver release of the gold containing alloys must be due to a shift of the chemical potential with increasing gold fraction as has been suggested above and in different words also by Besner et al. [99].

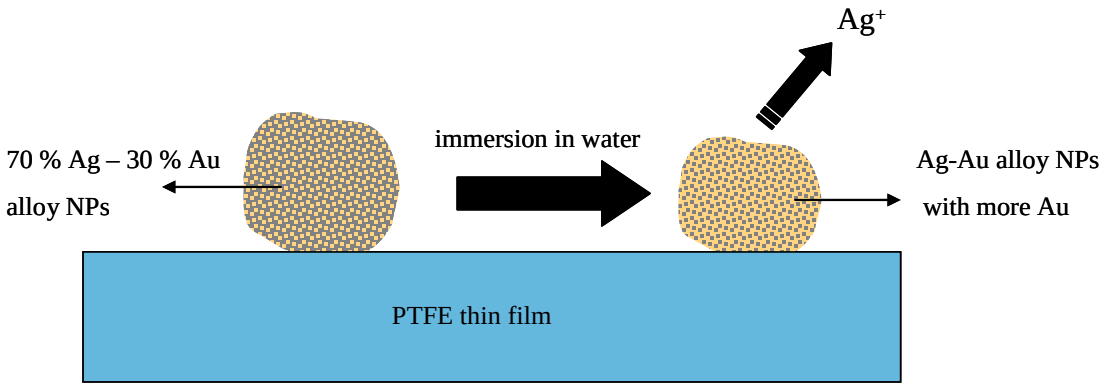

Figure 6.6 Schematic illustration of the Ag ion release process from Ag-Au alloy NPs where the NPs remain alloy-like

At first glance this result could appear somewhat surprising since for bulk Ag/Au alloy systems the dissolution of silver leads to formation of porous gold structures and for larger nanoparticles by a galvanic exchange reaction indeed hollow nanoparticles with a gold shell can be produced [146]. But as suggested by Shibata et al. [96], the situation is different for smaller nanoparticles, in particular if they have defects. Here the vacancies created in the alloy nanoparticles by the released silver atoms should allow a fast redistribution of the silver in a range of several nanometers thus leading to an always almost homogeneous spatial distribution of the silver in the small nanoparticles.

TEM measurements were also done after 3 days of immersion of the sample deposited on the TEM grid in water. Figure 6.7 a and b shows changes in the morphology and in the surface amount of the 5.5 nm alloy NPs of 70 % Ag - 30 % Au before and after immersion in water. The nanoparticles density looks smaller after three days in water and the interparticle distance increases as a result of the reduction of the Ag fraction due to Ag ion release which is more favorable from the smaller particles. Additionally, other NPs may undergo Ostwald ripening process, i.e. growth of large particles by dissolution

of small particles driven by the particle size dependence of its standard electrode potential, in way similar to what we observed before for pure AgNPs [22], [35]. Moreover, no Au shell formation was observed here either. The change in the particle size distribution is shown in Figure 6.8, where the number of particles was normalized to the total number of particles for each case.

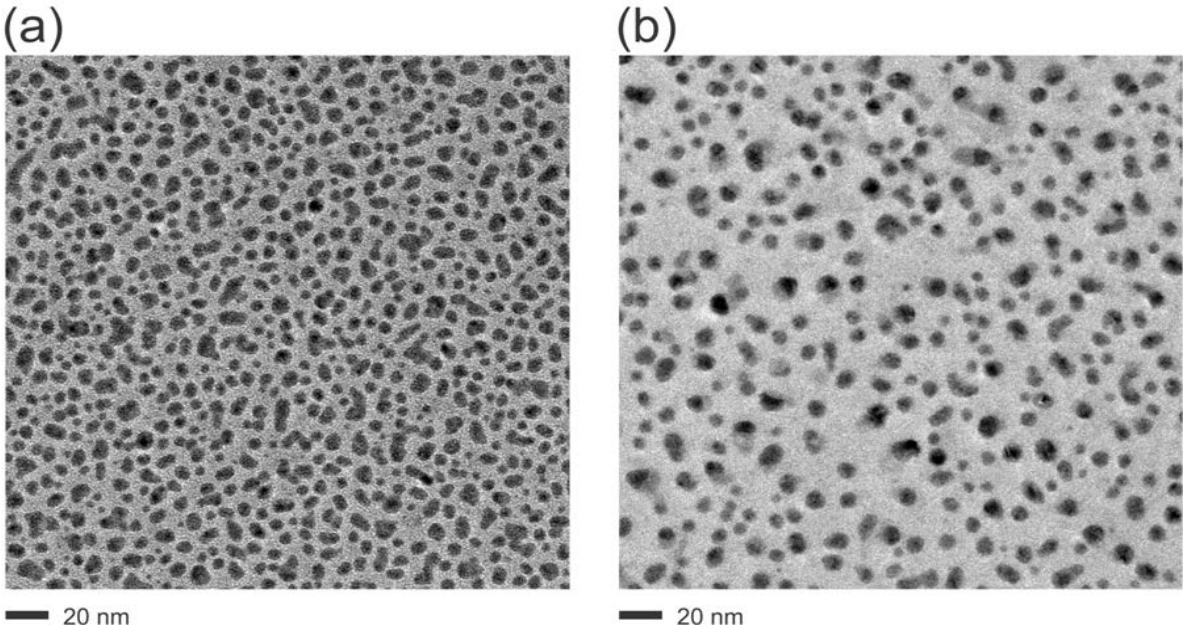

Figure 6.7 BF-TEM images for 5.5 nm 70 % Ag - 30 % Au alloy NPs on PTFE before immersion in water (a) and after 3 days in water (b)

Further investigations were performed using the UV-vis technique by observing the changes in the absorbance spectra of 5.5 nm alloy nanocomposite with various compositions as a function of the immersion time in water as shown in Figure 6.9. After immersion of the samples in water, SPR peak positions and absorbance maxima values were changed due to the oxidation and the release of silver ions into aqueous media. The shape of the absorbance peaks for each time period differs from each other too. One expects a red shift towards the typical gold plasmon absorption band due to the increase of the Au fraction in the nanoalloy [90], [93]. In contrast, a dominant shift to smaller wavelength occurred due to changes in the morphology, size distribution, and the interparticle distance. These changes are similar to the changes that occurred in the pure AgNPs system shown in the previous chapter. However, the rate of the change in the SPR

peak absorbance maxima values and its position after immersion of the samples in water is slower than that for the pure silver due to the increase of the Au fraction on the expense of Ag in the alloy, in accordance with the results from the ICP-MS and XPS measurements.

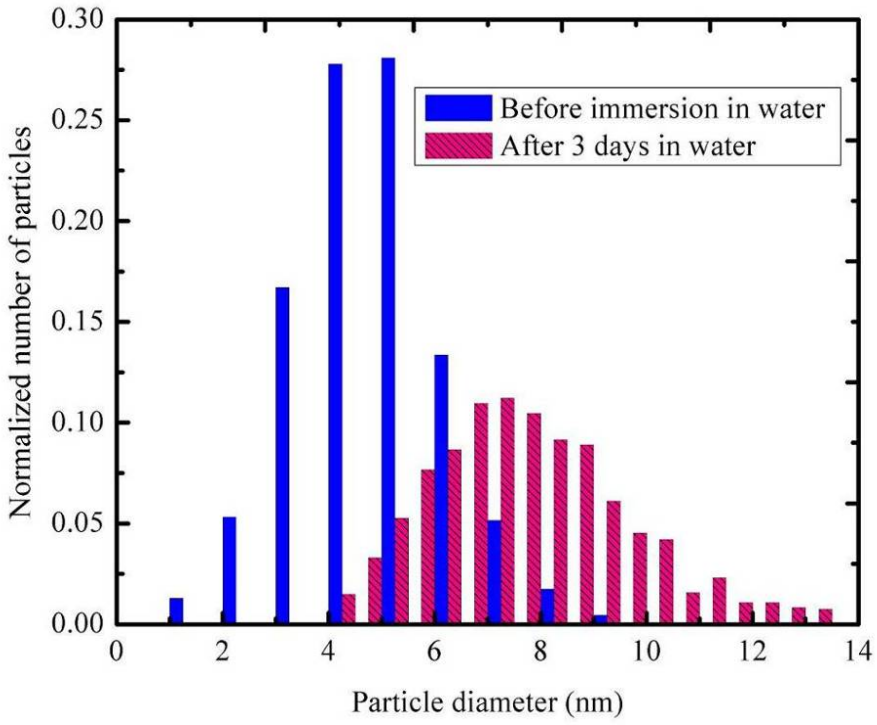

Figure 6.8 Particle size distribution of the 5.5 nm 70 % Ag - 30 % Au alloy NPs on PTFE before and after immersion the TEM grid in water for 3 days

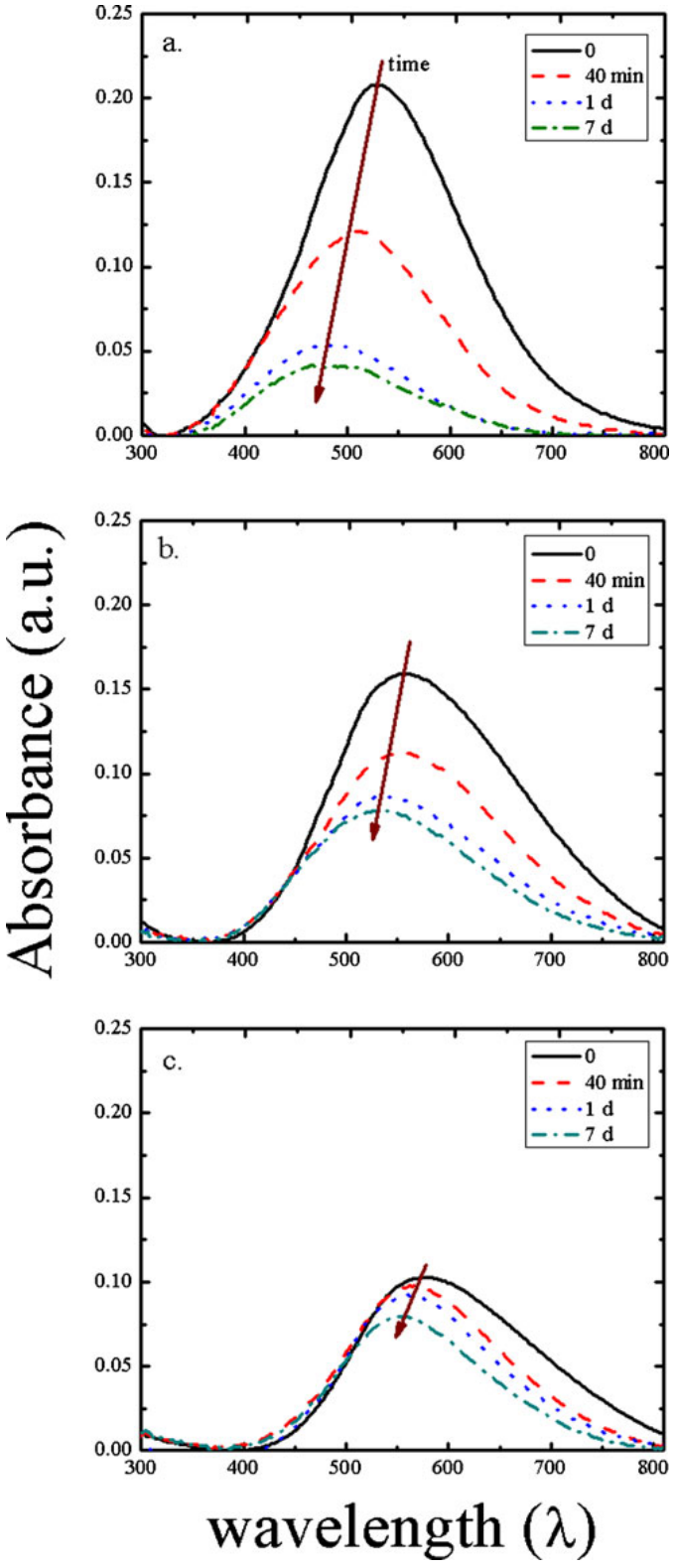

Figure 6.9 UV-vis spectra for 5.5 nm of alloy NPs of 90 % Ag - 10 % Au (a), 70 % Ag - 30 % Au (b), and 50 % Ag - 50 % Au (c) on PTFE at different immersion times in water

6.2 Conclusions

Model systems consisting of two dimensional ensembles of 5.5 nm nominal thickness of Ag-Au alloy NPs on a 20 nm highly crosslinked sputtered PTFE substrate were prepared using PVD techniques to investigate the effect of gold alloying on the silver ion release properties upon immersion in water. The Ag-Au alloy NPs with various compositions were prepared by simultaneous thermal evaporation of silver and gold, and a complete alloy was formed. A uniform particle distribution was observed with an average diameter of about 5 nm. The optical absorption spectra showed a single plasmon resonance peak between the absorption maxima of Ag and Au and its position depends linearly on the gold fraction in the alloy NPs, confirming the alloy formation of Ag-Au NPs.

Results showed that alloying of Ag with Au increases the oxidation resistance of the Ag nanoparticles and results in a reduced absolute silver ion release rate when compared to pure AgNPs. We noticed that the released amount of the silver ions is proportional to the amount of silver presents in the alloy nanoparticles with significant differences for short and long release times. In all samples with different compositions, a rapid dissolution of Ag occurred only at the first contact of the sample with water, and later on a saturation state is approached which is also affected by concentration dependent entropic contributions.

XPS and energy dependent XPS spectra analysis were also performed to examine changes which occurred for the 70 % Ag - 30 % Au alloy NPs nanocomposites before and after immersion of samples in water and results showed that Ag depletion does not lead to a concentration gradient but rather to a homogeneous drop in Ag concentration in the NPs.

TEM measurements for the same alloy system showed changes in the morphology and in the surface amount of the alloy NPs and no Au shell formation was observed here either.

UV-vis spectra showed as well that after immersion of the samples in water, the position and the intensity of the SPR peak of the alloy NPs changed due to the release of silver

ions into aqueous media. A dominant shift to smaller wavelength occurred due to changes in the morphology of the nanocomposites, the particle size distribution, and the interparticle distance. The rate of the change in the SPR peak absorbance maxima and positions slows down with increasing the fraction of Au in the alloy NPs, in agreement with the results from the other measurements. The results suggest that Au alloying can be made instrumental to tailor silver ion release in silver-based nanocomposites.

Chapter 7

Silver ion release properties of HMDSO/Ag/PTFE nanocomposites

In this chapter, the silver ion release and the water diffusion kinetics through plasma polymerized HMDSO barriers with different oxygen contents and different thicknesses were investigated. These layers were deposited on top of our previously described model system which composed of 2D ensembles of AgNPs with nominal thickness of 2 nm on a 20 nm sputtered PTFE thin film. The first PTFE layer was not changed since the deposition of the AgNPs and their growth on PTFE polymer surface have been already well investigated. Therefore, only the second polymer layer on top of the NPs was replaced by HMDSO plasma polymerized film for better understanding of the coatings properties effect on the ion release process. Morphology and optical properties were investigated. Samples were then immersed in water for several time periods and the concentration of the silver ions released from the system into the water was measured using ICP-MS technique. EIS measurements were also performed to explain the water uptake behavior of the plasma polymerized HMDSO thin films.

7.1 Results and discussions

7.1.1 The morphology and the optical properties

The TEM micrograph of the sandwiched sample of 20 nm plasma polymerized HMDSO barrier on top of a 2 nm nominal thickness AgNPs on 20 nm PTFE film deposited on TEM grid is given in Figure 7.1. It shows that the average particle size of the NPs is around 5 nm and some aggregates can also be seen. The particles are with almost a uniform shape and are well distributed on the surface of the polymer film following the same model [107] as discussed previously in sec. 2.2.1. Some fringes can be seen in the image which could be due to structural disorders such as twinning or stacking faults, or due to superpositioning of multiple grains.

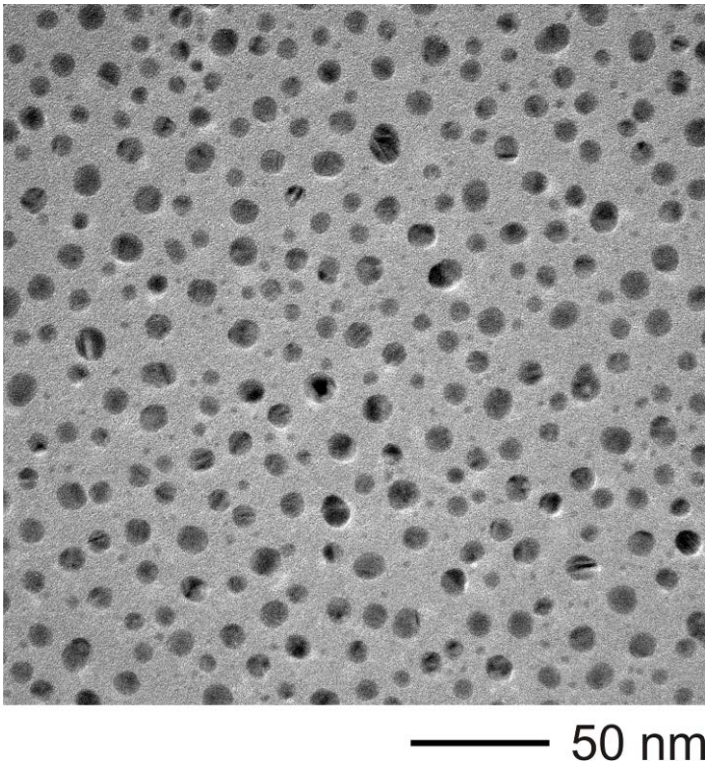

Figure 7.1 BF-TEM image of 2nm Ag/PTFE nanocomposite sample coated by 20 nm HMDSO

The absorbance spectra of several samples coated by plasma polymerized HMDSO films prepared with various O_2 flows were measured by UV-vis spectroscopy as shown in

Figure 7.2. By adding a barrier with no oxygen, the absorbance maximum increases due to the change in the dielectric constant of the surroundings of the nanocomposites [57], [59]. While other barriers of the same thickness but with more oxygen content show a shift and a damping in the SPR peak that can be explained by the oxidation that AgNPs encountered due to the increase in the O_2 flow [147]. In order to prove this, a plasma polymerized HMDSO barrier was prepared with gradient in the oxygen flow, by sputtering the HMDSO without mixing it with O_2 (0 sccm; standard cubic centimeter per minute) at the beginning of the deposition, and after 5 sec, 10 sccm of O_2 was added. The optical spectrum of the nanocomposite with this kind of barrier showed a peak at the same position as that for the sample without a barrier but with higher absorbance due to the dielectric change effect. Therefore, and due to the damping in the absorbance maxima of the nanocomposites with increasing the O_2 flow during the deposition of the coatings, the optical properties were not further investigated after immersion of samples in water and the ion release behavior was only studied by measuring the Ag ion concentration in water.

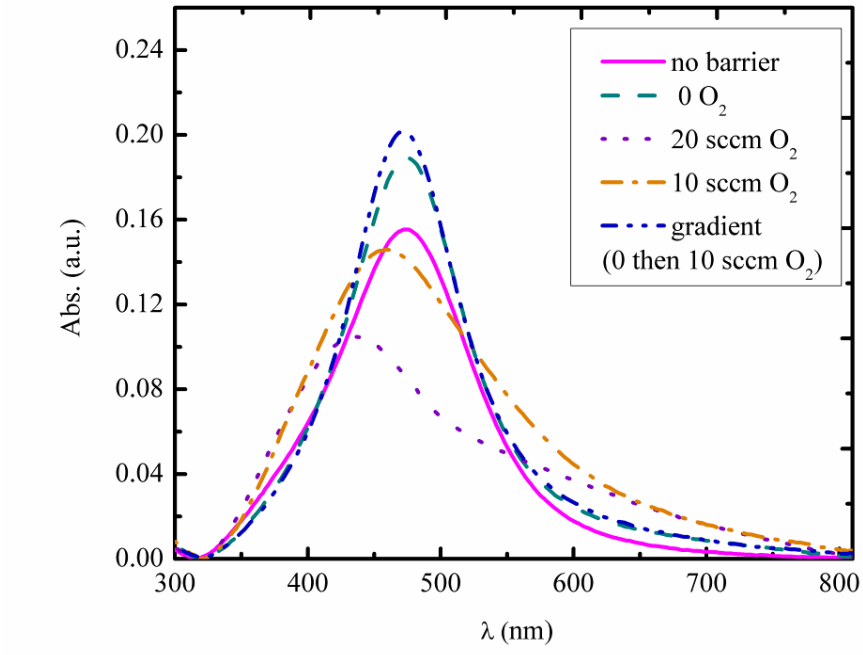

Figure 7.2 UV-vis spectrum of 2 nm Ag/PTFE nanocomposites coated by 20 nm HMDSO film of different O_2 content and compared to a sample without a barrier

7.1.2 The silver ion release studies

In contact with water, the samples release Ag ions over a certain period of time, due to the oxidation of the Ag atoms at the surface of the NPs to Ag ions and the diffusion of the ions through the interface to the sample surface and then into the water. TEM images showing the changes in the morphology of the nanocomposites before and after immersion in water for 7 days are given in Figure 7.3 a and b. The nanoparticles density looks smaller in the TEM image after 7 days of immersion of the samples in water and the interparticle distance increased as a result of the reduction of the initial Ag content after immersion in water because they were oxidized and ions were released into the water. No growth of large particles took place as the NPs are stabilized by the top layer of plasma polymerized HMDSO which prevents the agglomeration.

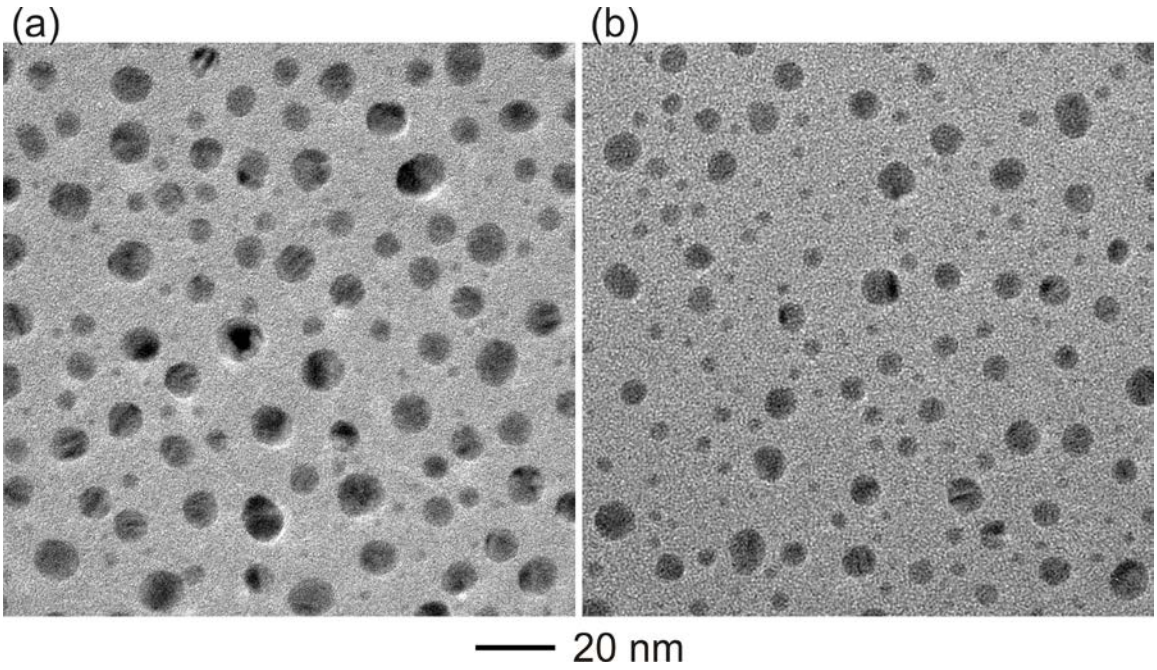

Figure 7.3 BF-TEM images of 2nm Ag/PTFE nanocomposite sample coated by 20 nm HMDSO before (a) and after 7 days in water (b)

Samples of 2 nm AgNPs/PTFE covered with 20 nm plasma polymerized HMDSO layers of different O_2 contents and samples without a barrier were then immersed in water for 7 days and the cumulative concentration of the released Ag ions was directly measured by ICP-MS and shown in Figure 7.4. Since the Ag content and the morphology of the

AgNPs are the same for all samples, then the strong difference in the Ag ion release kinetics after 7 days of immersion of the samples in water proves that the properties of the barrier layer play a role in the Ag ion release process. First of all, if we compare between the nanocomposites without HMDSO coatings and the other samples with coatings, it is clear that the nanocomposites without coating released the highest amount of Ag ions as water has a direct contact with the surface of the nanoparticles so they oxidize and dissolute into the water. By adding the plasma polymerized HMDSO coatings on top of the NPs, a fall in the release has been noticed. However, there were significant differences in the amount of the released ions from the coated nanocomposites despite the fact that the coatings are all of the same thickness of 20 nm. The samples with plasma polymerized HMDSO barrier of no oxygen, released the minimum amount of Ag ions compared to the ones with more O_2. As the oxygen flow was raised from 0 to 20 sccm, the amount of the released ions was increasing as we can see for samples with plasma polymerized HMDSO coatings with 20 sccm O_2.

Lamendola et al. [148] have found that when HMDSO deposition occurs in an oxygen-free environment, no C and CH radicals are in the gas phase and there is a low degree of monomer fragmentation leading to the condensation of HMDSO-like heavy fragments, while when oxygen is utilized, the C, CH and Si radicals are consumed leading to the deposition of a silica-like coatings. Not only the chemical structure is affected, but also the film morphology as AFM results obtained by Morent et al. [125] showed that with increasing the air content in the plasma phase, the roughness of the deposited films increases most likely due to the etching of the deposited films by oxygen atoms present in the discharge.

This indicates that the oxygen addition during the plasma polymerization process has changed the structure of the plasma polymerized HMDSO coatings and influenced the water penetration ability of the HMDSO plasma polymer barrier and thus the silver ion release potential of the nanocomposites. Despite the fact that ions diffusion in polymer matrices is much faster than in silica-like ones , we see here that the silver ion release rate is higher for the silica-like coatings, which indicates that the silver ion diffusion out of the sample is not the diffusion rate limiting step and that the water diffusion in the matrix

is the dominant process. Besides, we can see that the oxidation of the AgNPs during the plasma polymerization process in an oxygen-rich atmosphere did not have an influence on the release potential.

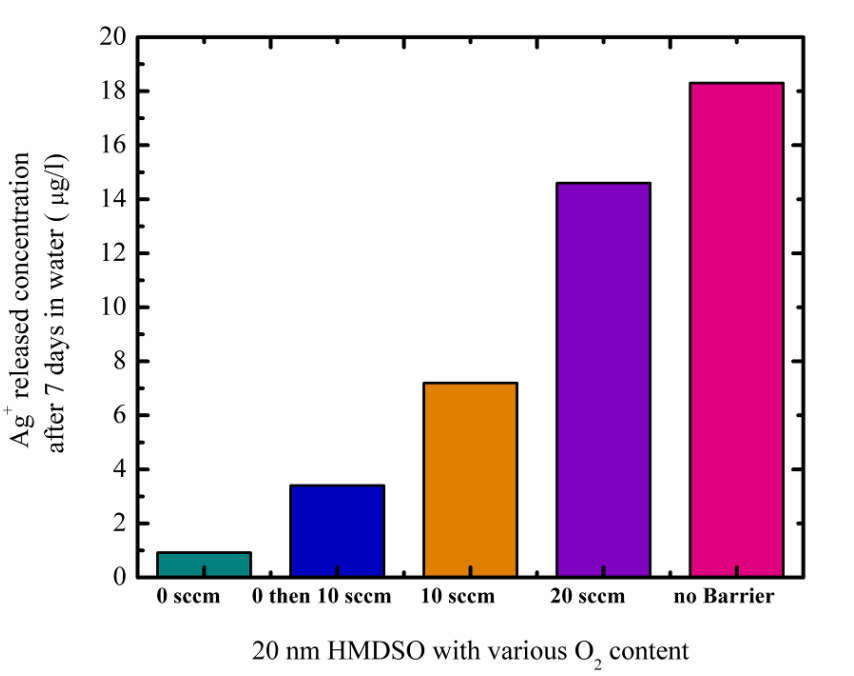

Figure 7.4 The cumulative concentration of Ag ions released from 2 nm AgNPs/PTFE without a barrier or with 20 nm HMDSO barriers of different O_2 content after 7 days of immersion in water

To check the wettability of the plasma polymerized HMDSO films by water, contact angle measurements were performed for 20 nm HMDSO plasma polymer films deposited on Si substrate and Table 7.1 shows the average contact angle of water for plasma polymerized HMDSO films prepared with various oxygen flows.

Table 7.1 Contact angle measurements for plasma polymerized HMDSO with various O_2 content

O_2 flow	0 sccm	10 sccm	20 sccm
Contact angle	101.43°	88.15°	80.20°

It can be seen that for plasma polymerized HMDSO films with no oxygen flow, the water contact angle is larger than 90°, which means that the solid surface is hydrophobic. By increasing the oxygen flow from 0 to 20 sccm, the value of the water contact angle

decreases and becomes smaller than 90°, indicating that the water tendency to wet the polymer surface increases and the solid surface is considered hydrophilic. These results confirm our conclusions that the oxygen flow during the deposition of the plasma polymerized HMDSO films affects their chemical structure and their interaction with water. This means that by increasing the oxygen flow during the plasma polymerization process, the chemical structure of the plasma polymerized HMDSO matrix tends to change from hydrophobic polymer-like coatings to hydrophilic ceramic-like ones.

For comparison of the kinetics of the Ag ion release from the nanocomposites, samples prepared with same barrier thickness but with different oxygen flow were immersed in water for longer time and the concentration of the released Ag ions was measured at several time periods as shown in Figure 7.5

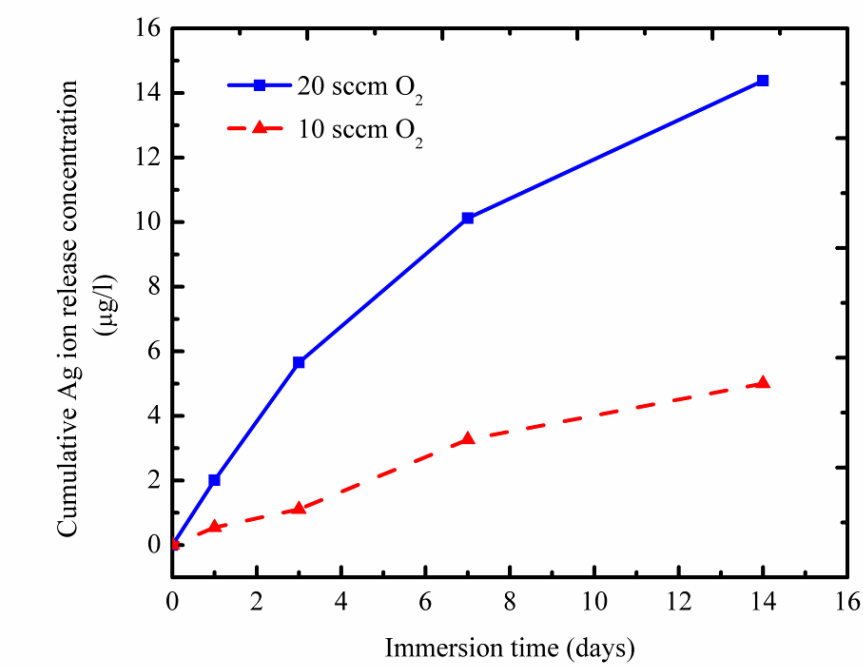

Figure 7.5 The cumulative concentration of Ag ions released from Ag/PTFE nanocomposites coated by HMDSO barrier (20 nm) of different oxygen content versus immersion time in water

One can see that the sample with 10 sccm O_2 plasma polymerized HMDSO barrier releases much fewer amount of Ag ions than the one with 20 sccm O_2 plasma polymerized HMDSO barriers. Moreover, the Ag ion concentration in water increases up

to a saturation value with time where it gets slower after 7 days. In contrast, the Ag ion concentration in water released from nanocomposites with a plasma polymerized HMDSO barrier with more O_2 content increases continuously with time. The amount released by this nanocomposite sample is about 3 times higher than that released from the one with plasma polymerized HMDSO barrier of lower O_2 content, even though they are containing the same amount of silver.

For further study of the kinetics behavior, the released Ag ion amount was normalized to the initial content of AgNPs and plotted versus the square root of the immersion time, as shown in Figure 7.6. The initial amount of AgNPs was found by immersion of the samples for several days in (4 %) HNO_3 acid, and after that the ion concentration was measured by ICP-MS. To check if there is any Ag left after that, the samples were checked by XPS and no signal from Ag was detected.

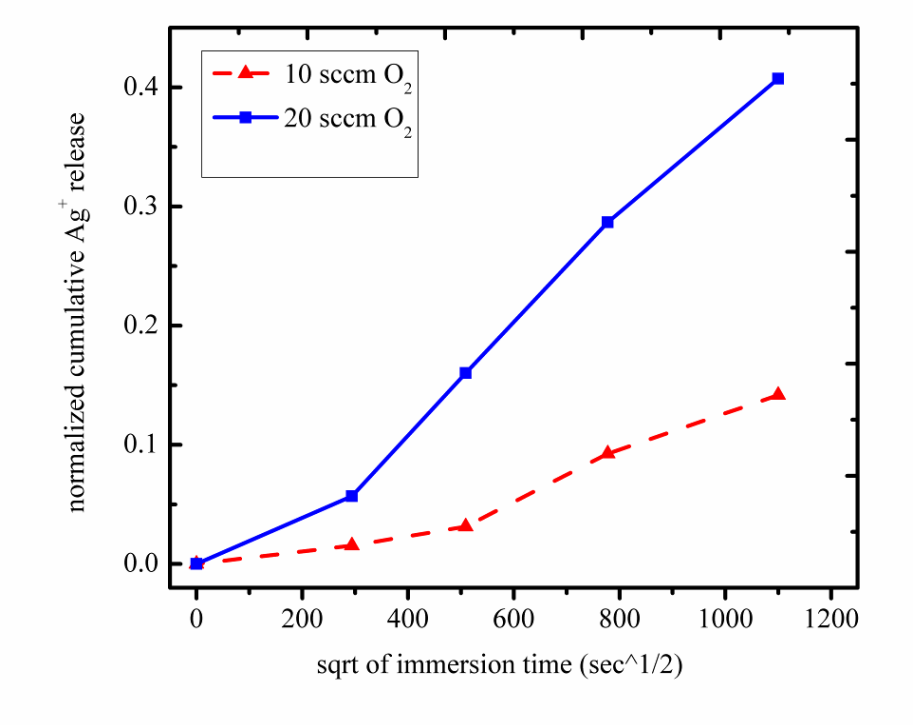

Figure 7.6 The normalized cumulative concentration of Ag ions released from Ag/PTFE nanocomposites coated by plasma polymerized HMDSO barriers (20 nm) of different oxygen contents versus the square root of the immersion time in water

HMDSO plasma polymerized films with more O_2 content are more hydrophilic, with almost a linear diffusion behavior, so water diffuses through it (polymer is plasticized by the water). The deviation from the linear diffusion behavior could be explained by the effect of swelling that may occur when the water molecules diffuse into the matrix which results in a directional transport of water molecules. The released ion concentration increases with time and it took about 1 day for water to diffuse completely from the surface of the barrier till it reaches the interface with the NPs when the Ag ion release process increases with time and these ions diffuse through the polymer into the surrounding immersion water. On the other hand, the samples covered with plasma polymerized HMDSO with low O_2 content, seems to be rather more hydrophobic. The release kinetics rate was very slow at the beginning and the absolute released amount is much less than the other barrier type, with a linear relation only till the 7th day then the Ag ion release slows down.

The difference in the release behavior with immersion time can be explained by the kinetics of the water uptake of the polymer barrier [8], [149], [150]. Therefore, electrochemical impedance measurements were performed over a long time scale (0 to 4068 min) for ITO substrates covered with 20 nm film of plasma polymerized HMDSO with 10 sccm or 20 sccm oxygen, and the capacitance change of the coating together with water uptake can be estimated from EIS data at high frequency values. The coating capacitance (C_p) was calculated using equation (2.5) and the water ingress into the polymer film as a function of exposure time to the buffer solution was also plotted as shown in Figure 7.7 and Figure 7.8. In direct comparison it can be seen that at the beginning of exposure to the electrolyte, the sample treated with 10 sccm O_2 shows higher barrier properties than the sample with 20 sccm O_2. After a time period of 4068 min the impedance of the two samples decreases nearly to the same value indicating that the water has permeated through the plasma polymerized HMDSO layer. For the sample with 10 sccm O_2, it can be assumed that after 2500 sec the limit of water uptake is reached. The further increase in the coating capacitance (Figure 7.8 a) could be caused by delimination of the plasma polymerized HMDSO layer from the ITO substrate. In this case the final value of water uptake is reached after 2500 sec of exposure. Thus, the water uptake of the sample with 10 sccm O_2 shall be approximately 2 % (Figure 7.8 b). When

these figures are compared to the increase in the released Ag ion concentration (Figure 7.5), a relation between these two processes can be seen; AgNPs dissolution starts when the solution enters the barrier film and reaches the surface of the particles. At the long exposure times one can also detect a saturation point of the water uptake.

(a)

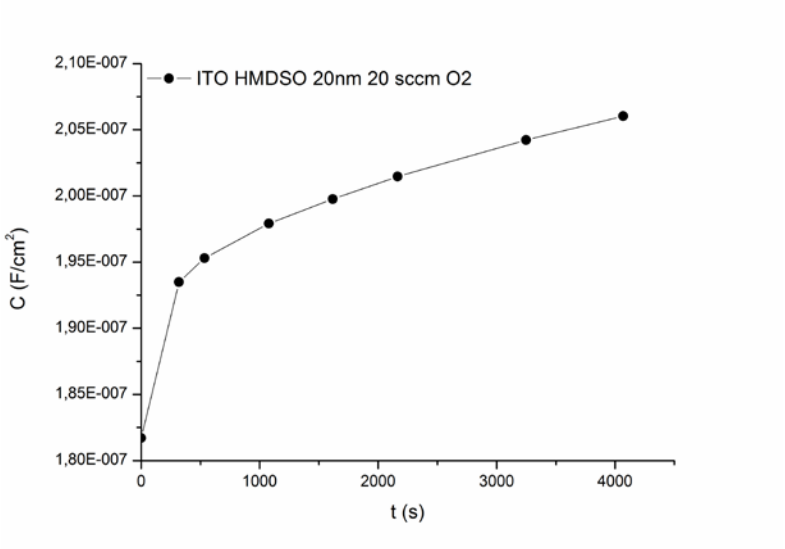

(b)

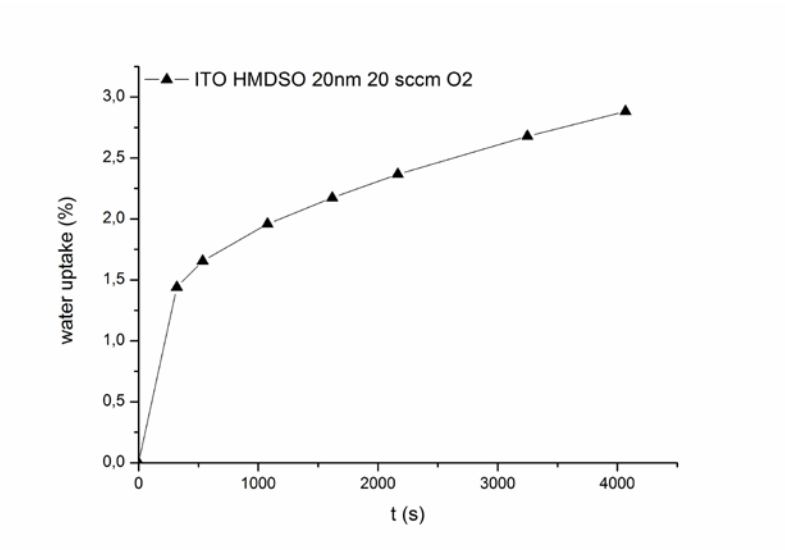

Figure 7.7 Capacitance (a) and water uptake (b) over exposure time to phosphate buffer for plasma polymerized HMDSO with 20 sccm O_2

(a)

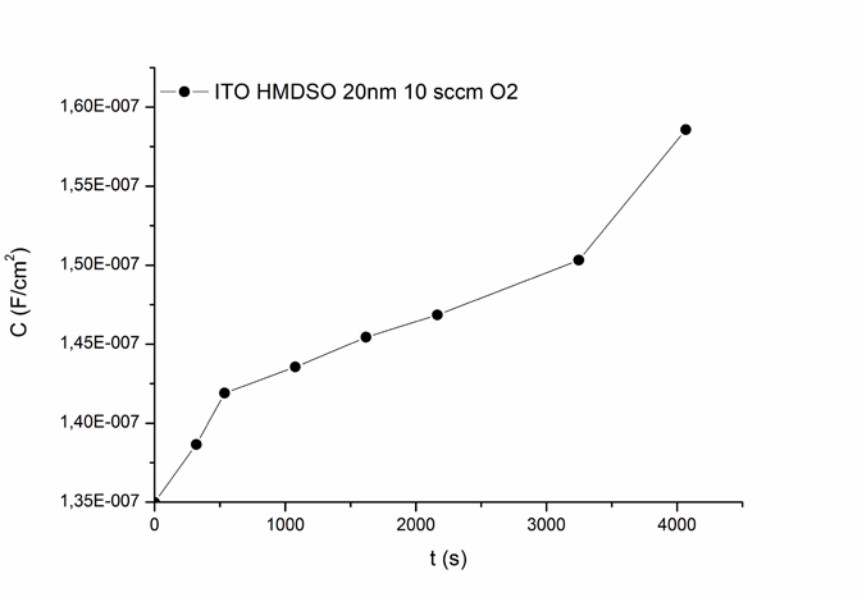

(b)

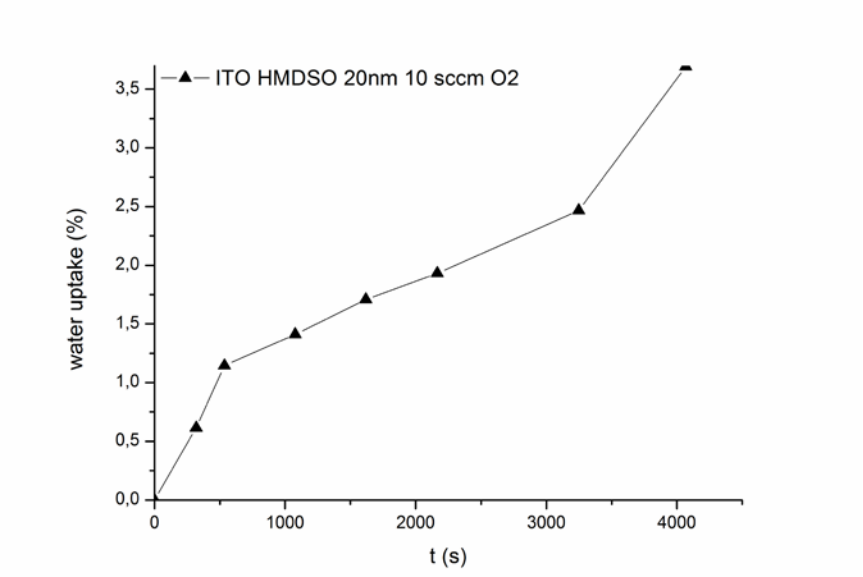

Figure 7.8 Capacitance (a) and water uptake (b) over exposure time to phosphate buffer for plasma polymerized HMDSO with 10 sccm O_2

To study the effect of the thickness of the plasma polymerized HMDSO barrier, samples of Ag/PTFE nanocomposites were covered by plasma polymerized HMDSO barriers of similar oxygen content (20 sccm) but two different barrier thickness (20 and 40 nm).

Samples were then immersed in water and the cumulative concentration of the released Ag ions in water was measured by ICP-MS as shown in Figure 7.9.

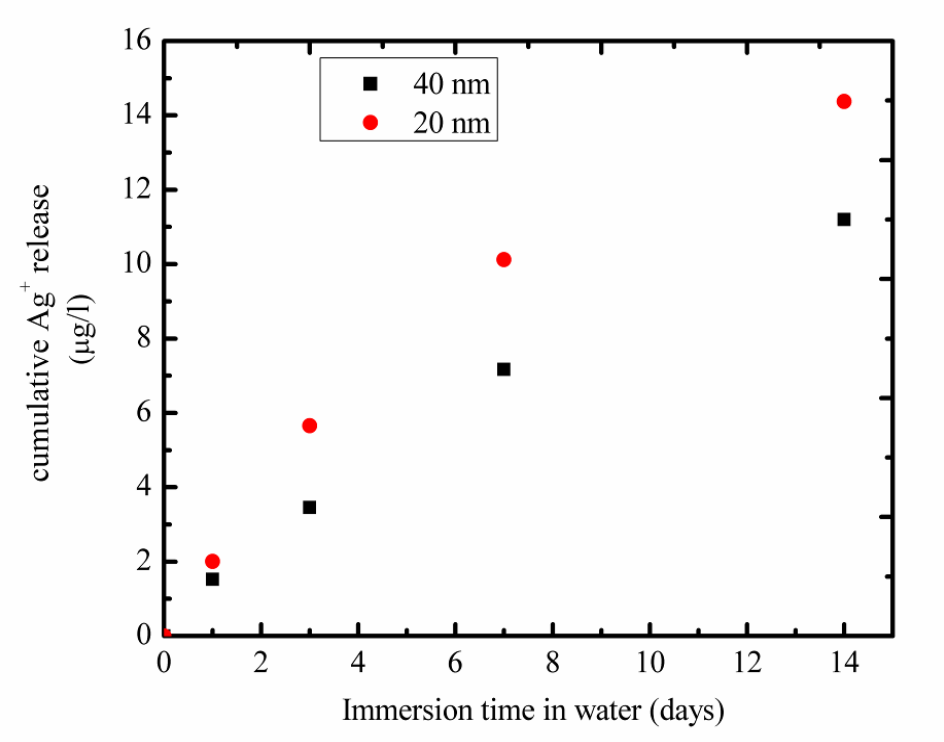

Figure 7.9 Cumulative Ag^+ released from Ag/PTFE nanocomposites coated by plasma polymerized HMDSO barriers prepared with same O_2 flow (20 sccm) but with two different thicknesses

One notices that the concentration of the ions in water gets less as the thickness of the barrier increases. The main reason is that as the thickness of the top layer increases, the water penetration through the barrier into the surface of the NPs gets slower. For the samples with 40 nm barrier thickness, water uptake is as high as for the samples with 20 nm barrier since both coatings were prepared with the same oxygen flow of 20 sccm, so they are both highly hydrophilic. However, the water mobility was to some extent retarded by increasing the thickness of the coatings. This implies that the diffusion of water molecules through the coatings must be taken into account to explain the silver ion release potential as we have shown previously for the Ag/PTFE nanocomposites coated with barriers of RF sputtered PTFE films.

7.2 Conclusions

The silver ion release kinetics and the water uptake properties of plasma polymerized HMDSO coatings were investigated. The technique of plasma polymerization was used to deposit HMDSO thin films on top of Ag/PTFE nanocomposites that consist of 2D ensembles of AgNPs with nominal thickness of 2 nm deposited on a 20 nm sputtered PTFE thin film. The nature of the plasma polymerized HMDSO barrier were varied by varying the oxygen flow during the deposition process from 0 to 20 sccm and the thickness of the films was varied as well. A strong relation has been found between the oxygen flow and the barrier properties of the plasma polymerized HMDSO films. ICP-MS results showed that the silver ion release potential was depending strongly on the oxygen content in the plasma polymerized HMDSO films as the released amount of Ag ions and the kinetics of the Ag ion release process increased by increasing the oxygen flow. Besides, the contact angle analysis was used to investigate the effect of the oxygen flow on the resulting structure of the plasma polymerized HMDSO coatings. Plasma polymerization with a high oxygen flow leads to the formation of hydrophilic thin films. In contrast, thin films obtained without oxygen flow have a polymeric chemical structure and are therefore highly hydrophobic making them exhibit high barrier properties. EIS results showed also a water diffusion dependence on the oxygen content in the coating films. From this point of view, the capability of controlling the film composition by varying the deposition conditions open interesting perspectives.

Changing the thickness of the barrier showed also another way of tuning the release of silver ions from the nanocomposites. By increasing the thickness of the coatings, the amount of the released ions decreases and the rate of the release process slows down. These results indicate that by tailoring the properties of the plasma polymerized coatings film and the thickness, the silver ion release properties of Ag/polymer nanocomposites can be tuned.

Chapter 8

Summary and outlook

Different nanocomposites were developed using several PVD techniques such as RF sputtering of PTFE, thermal evaporation of AgNPs or Ag-Au alloy NPs, and plasma polymerization sputtering of HMDSO using home-made deposition chambers under high vacuum conditions. The metal NPs were deposited on the surface of the polymer films instead of being embedded into the matrix in order to be directly accessible concerning their interfacial structure and reactivity. Morphology, composition and optical properties of these nanocomposites were studied. Various surface-sensitive analytical methods, such as UV-vis spectroscopy, XPS, TEM, and SEM were intensively applied to characterize the thin functional films and to study the potential of the silver ion release of the samples after immersion in DI water for several periods of time. ICP-MS technique was used to measure the concentration of Ag ions in water.

Well defined ensembles of AgNPs with narrow size distribution were generated by means of thermal evaporation of silver on top of RF sputtered crosslinked PTFE thin films in chapter 5. The formation of nanoparticles upon evaporation of a metal on top of a dielectric matrix can be understood in terms of the high cohesive energy of the metal and the low metal-matrix interaction energy which leads to high metal atom mobility on the matrix surface and metal aggregation whenever metal atoms encounter each other or a metal cluster. The average diameter of the nanoparticles increased from 4 to 8 nm and the

size distribution broadened with increasing amount of deposited silver with a nominal thickness ranges from 1.3 to 8.3 nm. The change in the Ag content has resulted in a SPR shift and a broadening and increasing of the absorbance peak which corresponds to an increasing particle size and a decrease in interparticle distance from the TEM analysis. Changes in the microstructure of the nanocomposite film upon immersion in water allowed demonstrating the kinetics of the silver ion release. Besides, as it was suggested, that the SPR depends on the original microstructure, the change in optical properties with immersion in water time was also a good way to study the silver ion release potential. The change in the morphology was attributed to the dissolution of the AgNPs after immersion in water and also to Ostwald ripening phenomena which led to particle coarsening. The results indicated that the silver ion release increases with increasing the silver content of the nanocomposites and it is faster for smaller particles as a reason of the higher surface area to volume ratio and the higher chemical potential which increase their tendency to dissolute, which shows the possibility of controlling the silver ion release properties of Ag/PTFE nanocomposites by tuning the amount and the particle size of the AgNPs. In order to hinder the mobility of the NPs on the polymer surface, the NPs were stabilized by a top layer of PTFE and the change in the silver ion release was studied with respect to the thickness of the barrier. Results showed that PTFE thin coatings reduce the amount of the released Ag ions and the release rate due to the slow water diffusion through the polymer layer. Moreover, it was found that tailoring the thickness of the polymer barrier, allows tuning of the kinetics of the Ag ion release process. Thus, the present geometrical way of either directly accessed 2D ensembles of AgNPs with different amount and size on PTFE nanocomposites or the nanocomposites based on the sandwich geometry, provides a unique means of tailoring the silver ion release.

In chapter 6, PTFE based nanocomposites with Ag-Au alloy NPs with various compositions have been prepared by simultaneous thermal evaporation of silver and gold and a complete alloy was formed. A uniform distribution was observed with an average diameter of about 5 nm. The optical absorption spectra showed a single plasmon resonance peak between the absorption maximum of Ag and Au whose position depends linearly on the composition of the alloy particles when expressed in terms of the gold fraction, confirming the alloy formation of Ag-Au NPs. The Ag ion release kinetics was

studied by observing the changes as samples were immersed in water for different time intervals and ICP-MS results showed a negligible Au ion concentration. and that the release of the silver ions for short time is fast for all alloy nanocomposites due to the first interaction of the nanoparticles with water and due to the entropic contributions. However, for long time, the relative silver release scales with the amount of silver present in the alloys and the slowing down of the silver release is directly correlated with the gold fraction in the alloy. Therefore, as the composition of the alloy NPs becomes Au rich a saturation state is approached. The decrease in the Ag amount in the alloy after immersion in water and that no gold shell was formed subsequently by the gold that is left behind were confirmed by XPS studies. The results from TEM studies showed also less dissolution of Ag along with a slight agglomeration of nanoparticles at higher Au fraction comparing to the pure AgNPs, and no Au shell formation was observed here either. Additionally, after immersion in water, SPR peak positions and absorbance maxima values were changed due to the release of silver ions into aqueous media. However, the changes were in a slower rate than that for the pure silver due to the increase of the Au fraction on the expense of Ag in the alloy.

In chapter 7, plasma polymerized HMDSO thin films were deposited on top of the 2D Ag/PTFE nanocomposites and the effect of varying the oxygen flow during the deposition process on the properties of the HMDSO coatings and the silver ion release potential of the nanocomposites was investigated. ICP-MS results showed that the concentration of the released ions is less for samples coated by HMDSO prepared with less oxygen flow, indicating that the oxygen flow during the plasma polymerization process changes the composition and the properties of the formed films as they become more hydrophilic by increasing the oxygen flow. This was confirmed by the contact angle analysis which showed that plasma polymerization with a high oxygen flow leads to the formation of more hydrophilic films. In contrast, thin films obtained without oxygen flow have a polymeric chemical structure and are therefore highly hydrophobic making them exhibit high barrier properties. The silver release process was connected to measurements of water uptake of the films and results were in agreement with the conclusion that the water permeability of the HMDSO barrier was altered by changing the oxygen flow.

Changing the thickness of the HMDS barriers showed also another way of tuning the release of silver ions from the nanocomposites.

The development of polymer/stabilized AgNPs is considered to be one of the most promising solutions to the issue of nanoparticles stability and to reduce the chances of their appearance in the environment. Present results obtained here for 2D Ag/PTFE nanocomposites provide both good understanding of the key parameters affecting the silver ion release and guidelines to produce 3D silver/polymer nanocomposites where the filling factor profiles can be tailored to tune the silver ion release behavior so it can be adjusted according the desired applications for short or long-term release.

Additional fine tuning of the initial particle content in order to optimize the parameters required for calculating the normalized Ag ion released would be much helpful. The changes in the silver ion release properties of the nanocomposites resulting from the changes in the morphology of the nanocomposite is an interesting point to investigate not only by using TEM but also by using different methods like, e.g., small-angle scattering (SAXS) and x-ray absorption spectroscopy where the structure and the dissolution of the nanoparticles could be monitored *in situ* and the ion transfer kinetics could be also checked.

The release of silver ions and the antibacterial properties and the cytocompatibility of the thin Ag/polymer nanocomposite films should be studied for their applications in household or medical field as antibacterial materials. Especially the quantitative determination of the silver release rate during the ageing process in humidity or in water-based solution would provide more reliable database for the long-term technological applications of such silver/fluorocarbon plasma polymer nanocomposite films as antibacterial coatings.

Finally, as one can see that the fabrication of Ag/polymer nanocomposites by PVD techniques requires many sophisticated equipments: a high vacuum chambers, deposition materials, a means of evaporating these materials, thermal control, a mechanism for monitoring the thickness of the materials deposited and many characterization techniques.

Thus, more effective efforts through the application of vapor phase deposition techniques should be in practice.

Bibliography

[1] C. Marambio-Jones and E. M. V. Hoek, “A review of the antibacterial effects of silver nanomaterials and potential implications for human health and the environment,” *Journal of Nanoparticle Research*, 12, 5, pp. 1531-1551 (**2010**).

[2] D. R. Monteiro, L. F. Gorup, A. S. Takamiya, A. C. Ruvollo-Filho, E. R. de Camargo, and D. B. Barbosa, “The growing importance of materials that prevent microbial adhesion: antimicrobial effect of medical devices containing silver,” *International journal of antimicrobial agents*, 34, 2, pp. 103-110 (**2009**).

[3] J. Fabrega, S. N. Luoma, C. R. Tyler, T. S. Galloway, and J. R. Lead, “Silver nanoparticles: behavior and effects in the aquatic environment,” *Environment international*, 37, 2, pp. 517-531, (**2011**).

[4] B. Nowack, H. F. Krug, and M. Height, “120 Years of Nanosilver History: implications for policy makers,” *Environmental science & technology*, 45, pp. 1177-1183 (**2011**).

[5] C. Greulich, D. Braun, A. Peetsch, J. Diendorf, B. Siebers, M. Epple, and M. Köller, “The toxic effect of silver ions and silver nanoparticles towards bacteria and human cells occurs in the same concentration range,” *RSC Advances*, 2, 17, pp. 6981-6987 (**2012**).

[6] V. Rotello (Ed.), *Nanoparticles: Building Blocks for Nanotechnology*, Springer, Springer international ed. (**2004**).

[7] M. Rai, A. Yadav, and A. Gade, “Silver nanoparticles as a new generation of antimicrobials,” *Biotechnology advances*, 27, 1, pp. 76-83 (**2009**).

[8] C. Damm, H. Münstedt, and A. Rösch, “Long-term antimicrobial polyamide 6/silver-nanocomposites,” *Journal of Materials Science*, 42, 15, pp. 6067-6073 (**2007**).

[9] J. Liu and R. H. Hurt, “Ion release kinetics and particle persistence in aqueous nano-silver colloids,” *Environmental science & technology*, 44, 6, pp. 2169-2175 (**2010**).

[10] J. Liu, D. A. Sonshine, S. Shervani, and R. H. Hurt, “Controlled release of biologically active silver from nanosilver surfaces,” *ACS nano*, 4, 11, pp. 6903-6913 (**2010**).

[11] Y.-J. Lee, J. Kim, J. Oh, S. Bae, S. Lee, I. S. Hong, and S.-H. Kim, “Ion-release kinetics and ecotoxicity effects of silver nanoparticles,” *Environmental toxicology and chemistry*, 31, 1, pp. 155-159 (**2012**).

[12] G. A. Sotiriou and S. E. Pratsinis, “Antibacterial activity of nanosilver ions and particles,” *Environmental science & technology*, 44, 14, pp. 5649-5654 (**2010**).

[13] H.-L. Liu, S. A. Dai, K.-Y. Fu, and S.-H. Hsu, “Antibacterial properties of silver nanoparticles in three different sizes and their nanocomposites with a new waterborne polyurethane,” *International journal of nanomedicine*, 5, pp. 1017-1028 (**2010**).

[14] G. A. Martínez-Castañón, N. Niño-Martínez, F. Martínez-Gutierrez, J. R. Martínez-Mendoza, and F. Ruiz, “Synthesis and antibacterial activity of silver nanoparticles with different sizes,” *Journal of Nanoparticle Research*, 10, 8, pp. 1343-1348 (**2008**).

[15] S. Rana and P. T. Kalaichelvan, “Ecotoxicity of nanoparticles,” *ISRN Toxicology*, 2013, pp. 1-11 (**2013**).

[16] C. Radheshkumar and H. Münstedt, “Antimicrobial polymers from polypropylene/silver composites—Ag^+ release measured by anode stripping voltammetry,” *Reactive and Functional Polymers*, 66, 7, pp. 780-788 (**2006**).

[17] V. K. Sharma, R. A. Yngard, and Y. Lin, “Silver nanoparticles: green synthesis and their antimicrobial activities,” *Advances in colloid and interface science*, 145, 1-2, pp. 83-96 (**2009**).

[18] C. Damm and H. Münstedt, “Kinetic aspects of the silver ion release from antimicrobial polyamide/silver nanocomposites,” *Applied Physics A*, 91, 3, pp. 479-486 (**2008**).

[19] V. Zaporojtchenko, R. Podschun, U. Schürmann, A. Kulkarni, and F. Faupel, “Physico-chemical and antimicrobial properties of co-sputtered Ag-Au/PTFE nanocomposite coatings,” *Nanotechnology*, 17, 19, pp. 4904-4908 (**2006**).

[20] F. Faupel, V. Zaporojtchenko, H. Greve, U. Schürmann, V. S. K. Chakravadhanula, Ch. Hanisch, A. Kulkarni, A. Gerber, E. Quandt, and R. Podschun, “Deposition of nanocomposites by plasmas,” *Contributions to Plasma Physics*, 47, 7, pp. 537-544 (**2007**).

[21] F. Faupel, V. Zaporojtchenko, T. Strunskus, and M. Elbahri, “Metal-polymer nanocomposites for functional applications,” *Advanced Engineering Materials*, 12, 12, pp. 1177-1190 (**2010**).

[22] N. Alissawi, V. Zaporojtchenko, T. Strunskus, T. Hrkac, I. Kocabas, B. Erkartal, V. S. K. Chakravadhanula, L. Kienle, G. Grundmeier, D. Garbe-Schönberg, and F. Faupel, “Tuning of the ion release properties of silver nanoparticles buried under a hydrophobic polymer barrier,” *Journal of Nanoparticle Research*, 14, 7, pp. 928-939 (2012).

[23] K. Vasilev, V. Sah, K. Anselme, C. Ndi, M. Mateescu, B. Dollmann, P. Martinek, H. Ys, L. Ploux, and H. J. Griesser, “Tunable antibacterial coatings that support mammalian cell growth,” *Nano letters*, 10, 1, pp. 202-207 (**2010**).

[24] V. Zaporojtchenko, V. S. K. Chakravadhanula, F. Faupel, S. Tamulevičius, M. Andrulevičius, A. Tamulevičienė, and L. Augulis, “Residual stress in polytetrafluoroethylene-metal nanocomposite films prepared by magnetron sputtering,” *Thin Solid Films*, 518, 21, pp. 5944-5949 (**2010**).

[25] V. S. K. Chakravadhanula, T. Hrkac, V. Zaporojtchenko, R. Podschun, V. G. Kotnur, A. Kulkarni, T. Strunskus, L. Kienle, and F. Faupel, “Nanostructural and functional properties of Ag-TiO_2 coatings prepared by co-sputtering deposition technique,” *Journal of Nanoscience and Nanotechnology*, 11, 6, pp. 4893-4899 (**2011**).

[26] N. Alissawi, V. Zaporojtchenko, T. Strunskus, I. Kocabas, V. S. K. Chakravadhanula, L. Kienle, D. Garbe-Schönberg, and F. Faupel, “Effect of gold alloying on stability of silver nanoparticles and control of silver ion release from vapor-deposited Ag-Au/polytetrafluoroethylene nanocomposites,” *Gold Bulletin*, 46, 1, pp. 3-11 (**2013**).

[27] W. Zhang, Y. Yao, N. Sullivan, and Y. Chen, “Modeling the primary size effects of citrate-coated silver nanoparticles on their ion release kinetics,” *Environmental science & technology*, 45, 10, pp. 4422-4428 (**2011**).

[28] T. Hrkac, C. Röhl, R. Podschun, V. Zaporojtchenko, T. Strunskus, H. Papavlassopoulos, D. Garbe-Schönberg, and F. Faupel, “Huge increase of therapeutic window at a bioactive silver/titania nanocomposite coating surface compared to solution,” *Materials science & engineering. C, Materials for biological applications*, 33, 4, pp. 2367-2375 (**2013**).

[29] O. S. Ivanova and F. P. Zamborini, “Size-dependent electrochemical oxidation of silver nanoparticles,” *Journal of the American Chemical Society*, 132, 1, pp. 70-72 (**2010**).

[30] K. Vasilev, S. Simovic, D. Losic, H. J. Griesser, S. Griesser, K. Anselme, and L. Ploux, “Platforms for controlled release of antibacterial agents facilitated by plasma polymerization,” *Engineering in Medicine and Biology Society (EMBC), 2010 Annual International Conference of the IEEE*, pp. 811-814 (**2010**)

[31] E. Körner, M. H. Aguirre, G. Fortunato, A. Ritter, J. Rühe, and D. Hegemann, “Formation and distribution of silver nanoparticles in a functional plasma polymer matrix and related Ag^+ release properties,” *Plasma Processes and Polymers*, 7, 7, pp. 619-625 (**2010**).

[32] D. Dowling, A. Betts, C. Pope, M. McConnell, R. Eloy, and M. Arnaud, “Anti-bacterial silver coatings exhibiting enhanced activity through the addition of platinum,” *Surface and Coatings Technology*, 163-164, pp. 637-640 (**2003**).

[33] A. J. Betts, D. P. Dowling, M. L. McConnell, and C. Pope, “The influence of platinum on the performance of silver-platinum anti-bacterial coatings,” *Materials & Design*, 26, 3, pp. 217-222 (**2005**).

[34] R. Kumar and H. Münstedt, “Silver ion release from antimicrobial polyamide/silver composites,” *Biomaterials*, 26, 14, pp. 2081-2088 (**2005**).

[35] K. Yliniemi, B. Özkaya, N. Alissawi, V. Zaporojtchenko, T. Strunskus, B. P. Wilson, F. Faupel, and G. Grundmeier, “Combined in situ electrochemical impedance spectroscopy-UV/Vis and AFM studies of Ag nanoparticle stability in perfluorinated films,” *Materials Chemistry and Physics*, 134, 1, pp. 302-308 (**2012**).

[36] U. Schürmann, W. Hartung, H. Takele, V. Zaporojtchenko, and F. Faupel, “Controlled syntheses of Ag-polytetrafluoroethylene nanocomposite thin films by

co-sputtering from two magnetron sources," *Nanotechnology*, 16, 8, pp. 1078-1082 (**2005**).

[37] Y. Fu, M. Hou, H. Xu, Z. Hou, P. Ming, Z. Shao, and B. Yi, "Ag-polytetrafluoroethylene composite coating on stainless steel as bipolar plate of proton exchange membrane fuel cell," *Journal of Power Sources*, 182, 2, pp. 580-584 (**2008**).

[38] Q. Zhao, Y. Liu, and C. Wang, "Development and evaluation of electroless Ag-PTFE composite coatings with anti-microbial and anti-corrosion properties," *Applied Surface Science*, 252, 5, pp. 1620-1627 (**2005**).

[39] C. You, C. Han, X. Wang, Y. Zheng, Q. Li, X. Hu, and H. Sun, "The progress of silver nanoparticles in the antibacterial mechanism, clinical application and cytotoxicity," *Molecular Biology Reports*, 39, 9, pp. 9193-9201 (**2012**).

[40] K. Chaloupka, Y. Malam, and A. M. Seifalian, "Nanosilver as a new generation of nanoproduct in biomedical applications," *Trends in biotechnology*, 28, 11, pp. 580-588 (**2010**).

[41] H. Cao and X. Liu, "Silver nanoparticles-modified films versus biomedical device-associated infections," *Nanomedicine and nanobiotechnology*, 2, 6, pp. 670-684 (**2010**).

[42] D. B. Warheit, C. M. Sayes, K. L. Reed, and K. A. Swain, "Health effects related to nanoparticle exposures: environmental, health and safety considerations for assessing hazards and risks," *Pharmacology & therapeutics*, 120, 1, pp. 35-42 (**2008**).

[43] C. Beer, R. Foldbjerg, Y. Hayashi, D. S. Sutherland, and H. Autrup, "Toxicity of silver nanoparticles - nanoparticle or silver ion?," *Toxicology letters*, 208, 3, pp. 286-292 (**2012**).

[44] R. Rudolf, M. Anzel, E. Markovic, M. Colic, and D. Stamenkovic, “Gold in the past, today and future,” *Metalurgija*, 51, 2, pp. 261-264 (**2012**).

[45] R. C. Edelstein, A. S. and Cammarata (Eds.), *Nanomaterials: Synthesis, properties and applications.* IOP Publishing Ltd (**1996**).

[46] E. Roduner, “Size matters: why nanomaterials are different,” *Chemical Society reviews*, 35, 7, pp. 583-592 (**2006**).

[47] M. Wautelet and D. Duvivier, “The characteristic dimensions of the nanoworld,” *European Journal of Physics*, 28, 5, pp. 953-959 (**2007**).

[48] T. A. H. R Nagarajan, *Nanoparticles: synthesis, stabilization, passivation, and functionalization*. American Chemical Society, Division of Colloid and Surface Chemistry (**2008**).

[49] I. A. Mudunkotuwa and V. H. Grassian, “The devil is in the details (or the surface): impact of surface structure and surface energetics on understanding the behavior of nanomaterials in the environment,” *Journal of Environmental Monitoring*, 13, 5, pp. 1135-1144 (**2011**).

[50] N. S. Wigginton, K. L. Haus, and M. F. Hochella, “Aquatic environmental nanoparticles,” *Journal of Environmental Monitoring*, 9, 12, pp. 1306-1316 (**2007**).

[51] D. R Gaskell, *Introduction to the thermodynamics of materials*, Taylor & Francis group, 4th ed. (**2003**).

[52] L. V. Stebounova, E. Guio, and V. H. Grassian, “Silver nanoparticles in simulated biological media: a study of aggregation, sedimentation, and dissolution,” *Journal of Nanoparticle Research*, 13, 1, pp. 233-244 (**2010**).

[53] C. A. Johnson, “Generalization of the Gibbs-Thomson equation,” *Surface Science*, 3, 5, pp. 429-444 (**1965**).

[54] V. M. Samsonov, A. N. Bazulev, and N. Yu. Sdobnyakov, “On applicability of Gibbs thermodynamics to nanoparticles,” *Central european journal of physics*, 3, pp. 474-484 (**2003**).

[55] G. Schmid (Ed.), *Nanoparticles: from theory to application*. Wiley-VCH Verlag GmbH & Co. KGaA, Weinheim (**2004**).

[56] Y. Xia and N. J. Halas, “Shape-controlled synthesis and surface plasmonic properties of metallic nanostructures,” *MRS Bulletin*, 30, 5, pp. 338-348 (**2011**).

[57] K. L. Kelly, E. Coronado, L. L. Zhao, and G. C. Schatz, “The optical properties of metal nanoparticles: the influence of size, shape, and dielectric environment,” *The Journal of Physical Chemistry B*, 107, 3, pp. 668-677 (**2003**).

[58] W. A. Murray and W. L. Barnes, “Plasmonic materials,” *Advanced Materials*, 19, 22, pp. 3771-3782 (**2007**).

[59] U. Kreibig and M. Vollmer, *Optical properties of metal clusters, Vol. 25*. Springer series in Material Sciences, Berlin (**1995**).

[60] P. K. Jain, X. Huang, I. H. El-Sayed, and M. A. El-Sayed, “Review of some interesting surface plasmon resonance-enhanced properties of noble metal nanoparticles and their applications to biosystems,” *Plasmonics*, 2, 3, pp. 107-118 (**2007**).

[61] L. M. Liz-Marzán, “Tailoring surface plasmons through the morphology and assembly of metal nanoparticles,” *Langmuir*, 22, 1, pp. 32-41 (**2006**).

[62] M. F. Ashby, P. J. Ferreira, and D. L. Schodek, *Nanomaterials, nanotechnologies and design: an introduction for engineers and architects*. Elsevier Ltd (**2009**).

[63] X. Jin, M. Li, J. Wang, C. Marambio-Jones, F. Peng, X. Huang, R. Damoiseaux, and E. M. V. Hoek, “High-throughput screening of silver nanoparticle stability and

bacterial inactivation in aquatic media: influence of specific ions," *Environmental science & technology*, 44, 19, pp. 7321-7328 (**2010**).

[64] S. A. Cumberland and J. R. Lead, "Particle size distributions of silver nanoparticles at environmentally relevant conditions," *Journal of chromatography A*, 1216, 52, pp. 9099-9105 (**2009**).

[65] A. M. El Badawy, T. P. Luxton, R. G. Silva, K. G. Scheckel, M. T. Suidan, and T. M. Tolaymat, "Impact of environmental conditions (pH, ionic strength, and electrolyte type) on the surface charge and aggregation of silver nanoparticles suspensions," *Environmental science & technology*, 44, 4, pp. 1260-1266 (**2010**).

[66] A. Dokoumetzidis, V. Papadopoulou, G. Valsami, and P. Macheras, "Development of a reaction-limited model of dissolution: application to official dissolution tests experiments," *International journal of pharmaceutics*, 355, 1-2, pp. 114-125 (**2008**).

[67] C. Levard, E. M. Hotze, G. V Lowry, and G. E. Brown, "Environmental transformations of silver nanoparticles: impact on stability and toxicity," *Environmental science & technology*, 46, 13, pp. 6900-6914 (**2012**).

[68] C.-M. Ho, C.-K. Wong, S. K.-W. Yau, C.-N. Lok, and C.-M. Che, "Oxidative dissolution of silver nanoparticles by dioxygen: a kinetic and mechanistic study," *Chemistry, an Asian journal*, 6, 9, pp. 2506-2511 (**2011**).

[69] X. Li, J. J. Lenhart, and H. W. Walker, "Aggregation kinetics and dissolution of coated silver nanoparticles.," *Langmuir*, 28, 2, pp. 1095-1104 (**2012**).

[70] S. Elzey and V. H. Grassian, "Agglomeration, isolation and dissolution of commercially manufactured silver nanoparticles in aqueous environments," *Journal of Nanoparticle Research*, 12, 5, pp. 1945-1958 (**2009**).

[71] S. Kittler, C. Greulich, J. Diendorf, M. Köller, and M. Epple, “Toxicity of silver nanoparticles increases during storage because of slow dissolution under release of silver ions,” *Chemistry of Materials*, 22, 16, pp. 4548-4554 (**2010**).

[72] P. Dallas, V. K. Sharma, and R. Zboril, “Silver polymeric nanocomposites as advanced antimicrobial agents: classification, synthetic paths, applications, and perspectives,” *Advances in colloid and interface science*, 166, 1-2, pp. 119-135 (**2011**).

[73] A. D. Politano, K. T. Campbell, L. H. Rosenberger, and R. G. Sawyer, “Use of silver in the prevention and treatment of infections: Silver review,” *Surgical infections*, 14, 1, pp. 1-13 (**2013**).

[74] E. Navarro, F. Piccapietra, B. Wagner, F. Marconi, R. Kaegi, N. Odzak, L. Sigg, and R. Behra, “Toxicity of silver nanoparticles to Chlamydomonas reinhardtii,” *Environmental Science & Technology*, 42, 23, pp. 8959-8964 (**2008**).

[75] L. Kvitek, A. Panacek, R. Prucek, J. Soukupova, M. Vanickova, M. Kolar, and R. Zboril, “Antibacterial activity and toxicity of silver - nanosilver versus ionic silver,” *Journal of Physics: Conference Series*, 304, p. 012029 (**2011**).

[76] S. P. Dhas, P. J. Shiny, S. Khan, A. Mukherjee, and N. Chandrasekaran, “Toxic behavior of silver and zinc oxide nanoparticles on environmental microorganisms,” *Journal of basic microbiology*, 53, pp. 1-12 (**2013**).

[77] Z. Xiu, Q. Zhang, H. L. Puppala, V. L. Colvin, and P. J. J. Alvarez, “Negligible particle-specific antibacterial activity of silver nanoparticles,” *Nano letters*, 12, 8, pp. 4271-4275 (**2012**).

[78] I. Chopra, “The increasing use of silver-based products as antimicrobial agents: a useful development or a cause for concern?,” *The Journal of antimicrobial chemotherapy*, 59, 4, pp. 587-590 (**2007**).

[79] J. R. Morones, J. L. Elechiguerra, A. Camacho, K. Holt, J. B. Kouri, J. T. Ramírez, and M. J. Yacaman, "The bactericidal effect of silver nanoparticles," *Nanotechnology*, 16, 10, pp. 2346-2353 (**2005**).

[80] S. Pal, Y. K. Tak, and J. M. Song, "Does the antibacterial activity of silver nanoparticles depend on the shape of the nanoparticle? A study of the Gram-negative bacterium Escherichia coli," *Applied and environmental microbiology*, 73, 6, pp. 1712-1720 (**2007**).

[81] K.-T. Kim, L. Truong, L. Wehmas, and R. L. Tanguay, "Silver nanoparticle toxicity in the embryonic zebrafish is governed by particle dispersion and ionic environment," *Nanotechnology*, 24, 11, pp. 115101-115108 (**2013**).

[82] N. Simonetti, G. Simonetti, F. Bougnol, and M. Scalzo, "Electrochemical Ag^{+} for preservative use," *Applied & Environmental Microbiology*, 58, 12, pp. 3834-3836 (**1992**).

[83] J. Fabrega, S. R. Fawcett, J. C. Renshaw, and J. R. Lead, "Silver nanoparticle impact on bacterial growth: effect of pH, concentration, and organic matter," *Environmental Science & Technology*, 43, 19, pp. 7285-7290 (**2009**).

[84] C.-N. Lok, C.-M. Ho, R. Chen, Q.-Y. He, W.-Y. Yu, H. Sun, P. K.-H. Tam, J.-F. Chiu, and C.-M. Che, "Silver nanoparticles: partial oxidation and antibacterial activities," *Journal of biological inorganic chemistry*, 12, 4, pp. 527-534 (**2007**).

[85] S. A. Blaser, M. Scheringer, M. Macleod, and K. Hungerbühler, "Estimation of cumulative aquatic exposure and risk due to silver: contribution of nano-functionalized plastics and textiles," *The Science of the total environment*, 390, 2-3, pp. 396-409 (**2008**).

[86] X. Chen and H. J. Schluesener, "Nanosilver: a nanoproduct in medical application," *Toxicology letters*, 176, 1, pp. 1-12 (**2008**).

[87] O. Palanna, *Engineering chemistry*. Tata McGraw-Hill Pvt. Ltd (**2009**).

[88] P. Haasen, *Physical Metallurgy*. Cambridge University Press, 3rd ed. (**1996**).

[89] S. C. Yeo, D. H. Kim, K. Shin, and H. M. Lee, "Phase diagram and structural evolution of Ag-Au bimetallic nanoparticles: molecular dynamics simulations," *Physical chemistry chemical physics*, 14, 8, pp. 2791-2796 (**2012**).

[90] S. Link, Z. L. Wang, and M. A. El-Sayed, "Alloy formation of gold-silver nanoparticles and the dependence of the plasmon absorption on their composition," *The Journal of Physical Chemistry B*, 103, 18, pp. 3529-3533 (**1999**).

[91] Y. Fleger and M. Rosenbluh, "Surface plasmons and surface enhanced Raman spectra of aggregated and alloyed gold-silver nanoparticles," *Advances in Nonlinear Optics*, 2009, pp. 1-5 (**2009**).

[92] F. Hubenthal, T. Ziegler, C. Hendrich, M. Alschinger, and F. Träger, "Tuning the surface plasmon resonance by preparation of gold-core/silver-shell and alloy nanoparticles," *The European Physical Journal D*, 34, 1-3, pp. 165-168 (**2005**).

[93] H. T. Beyene, V. S. K. Chakravadhanula, C. Hanisch, M. Elbahri, T. Strunskus, V. Zaporojtchenko, L. Kienle, and F. Faupel, "Preparation and plasmonic properties of polymer-based composites containing Ag-Au alloy nanoparticles produced by vapor phase co-deposition," *Journal of Materials Science*, 45, 21, pp. 5865-5871 (**2010**).

[94] L. Feng, G. Gao, P. Huang, K. Wang, X. Wang, T. Luo, and C. Zhang, "Optical properties and catalytic activity of bimetallic gold-silver nanoparticles," *Nano Biomedicine and Engineering*, 2, 4, pp. 258-267 (**2010**).

[95] Y. Chen, H. Wu, Z. Li, P. Wang, L. Yang, and Y. Fang, "The study of surface plasmon in Au/Ag Core/Shell compound nanoparticles," *Plasmonics*, 7, 3, pp. 509-513 (**2012**).

[96] T. Shibata, B. a Bunker, Z. Zhang, D. Meisel, C. F. Vardeman, and J. D. Gezelter, "Size-dependent spontaneous alloying of Au-Ag nanoparticles.," *Journal of the American Chemical Society*, 124, 40, pp. 11989-11996 (**2002**).

[97] A. Eremenko and N. Smirnoval, "Silver and gold nanoparticles in silica matrices: synthesis, properties, and application," *Theoretical and Experimental Chemistry*, 46, 2, pp. 67-88 (**2010**).

[98] M. B. Cortie and A. M. McDonagh, "Synthesis and optical properties of hybrid and alloy plasmonic nanoparticles," *Chemical reviews*, 111, 6, pp. 3713-3735 (**2011**).

[99] S. Besner and M. Meunier, "Femtosecond laser synthesis of AuAg nanoalloys: photoinduced oxidation and ions release," *The Journal of Physical Chemistry C*, 114, 23, pp. 10403-10409 (**2010**).

[100] D.-H. Chen and C.-J. Chen, "Formation and characterization of Au-Ag bimetallic nanoparticles in water-in-oil microemulsions," *Journal of Materials Chemistry*, 12, 5, pp. 1557-1562 (**2002**).

[101] A. J. Forty, "Micromorphological studies of the corrosion of gold alloys," *Gold Bulletin*,14, 1, pp. 25-35 (**1981**).

[102] N. Perez, *Electrochemistry and corrosion science*. Kluwer Academic Publishers (**2004**).

[103] A. Hahn, G. Brandes, P. Wagener, and S. Barcikowski, "Metal ion release kinetics from nanoparticle silicone composites," *Journal of controlled release*, 154, 2, pp. 164-170 (**2011**).

[104] A. Hahn, S. Günther, P. Wagener, and S. Barcikowski, "Electrochemistry-controlled metal ion release from silicone elastomer nanocomposites through combination of different metal nanoparticles," *Journal of Materials Chemistry*, 21, 28, pp. 10287-10289 (**2011**).

[105] A. Heilmann, *Polymer films with embedded metal nanoparticles*. Springer-Verlag (**2003**).

[106] F. Faupel, V. Zaporojtchenko, T. Strunskus, J. Erichsen, K. Dolgner, A. Thran, and M. Kiene, "Fundamental aspects of polymer metallization," *Metallization of Polymers 2*, E. Sacher (Ed.), Kluwer Academic/Plenum Publishers, pp. 73-96 (**2002**)

[107] V. Zaporojtchenko, T. Strunskus, K. Behnke, C. Von Bechtolsheim, M. Kiene, and F. Faupel, "Metal/polymer interfaces with designed morphologies," *Journal of Adhesion Science and Technology*, 14, 3, pp. 467-490 (**2000**).

[108] V. Zaporojtchenko, K. Behnke, T. Strunskus, and F. Faupel, "Determination of condensation coefficients of metals on polymer surfaces," *Surface Science*, 454-456, 1-2, pp. 412-416 (**2000**).

[109] V. Zaporojtchenko, K. Behnke, T. Strunskus, and F. Faupel, "Condensation coefficients of noble metals on polymers: a novel method of determination by x-ray photoelectron spectroscopy," *Surface and Interface Analysis*, 30, pp. 439-443 (**2000**).

[110] M. Ohring, *Materials science of thin films: deposition and structure*. Academic Press, 2nd ed. (**2002**).

[111] C. G. Granqvist, *Spectrally selective surfaces for heating and cooling applications*. SPIE Press (**1989**).

[112] H. Wasa, K., Kitabatake, M, Adachi, *Thin film materials technology: sputtering of compound materials*. Springer-Verlag Gmbh & Co (**2004**).

[113] D. L. Smith, *Thin film deposition: principles & practice*. McGraw-Hill (**1995**).

[114] S. Ebnesajjad, *Fluoroplastics, Vol. 2: Melt processible fluoroplastics*. William Andrew (**2003**).

[115] H. Biederman, “Organic films prepared by polymer sputtering,” *Journal of Vacuum Science & Technology A*, 18, 4, pp. 1642-1648 (**2000**).

[116] H. Biederman, “RF sputtering of polymers and its potential application,” *Vacuum*, 59, 2-3, pp. 594-599 (**2000**).

[117] L. Holland, H. Biederman, and S. M. Ojha, “Sputtered and plasma polymerized fluorocarbon films,” *Thin Solid Films*, 35, 2, pp. L19-L21 (**1976**).

[118] H. Biederman, “The properties of films prepared of PTFE and plasma polymerization by the RF sputtering of some freons,” *Vacuum*, 31, 7, pp. 285-289 (**1981**).

[119] H. Biederman, P. Bilkova, J. Jezek, P. Hlidek, and D. Slavinska, “RF magnetron sputtering of polymers,” *Journal of Non-Crystalline Solids*, 218, pp. 44-49 (**1997**).

[120] H. Biederman, M. Zeuner, J. Zalman, P. Bílková, D. Slavínská, V. Stelmasuk, and A. Boldyreva, “RF magnetron sputtering of polytetrafluoroethylene under various conditions,” *Thin Solid Films*, 392, 2, pp. 208-213 (**2001**).

[121] H. Biederman, S. M. Ojha, and L. Holland, “The properties of fluorocarbon films prepared by RF sputtering and plasma polymerization in inert and active gas,” *Thin Solid Films*, 41, pp. 329-339 (**1977**).

[122] Y. Zhang, G. H. Yang, E. T. Kang, K. G. Neoh, W. Huang, A. C. H. Huan, and S. Y. Wu, “Deposition of fluoropolymer films on Si(100) surfaces by RF magnetron sputtering of poly(tetrafluoroethylene),” *Langmuir*, 18, 16, pp. 6373-6380 (**2002**).

[123] L. Li, P. M. Jones, and Y.-T. Hsia, “Characterization of a nanometer-thick sputtered polytetrafluoroethylene film,” *Applied Surface Science*, 257, 9, pp. 4478-4485 (**2011**).

[124] A. W. Hassel, S. Milenkovic, U. Schürmann, H. Greve, V. Zaporojtchenko, R. Adelung, and F. Faupel, “Model systems with extreme aspect ratio, tunable

geometry, and surface functionality for a quantitative investigation of the Lotus effect," *Langmuir*, 23, 4, pp. 2091-2094 (**2007**).

[125] R. Morent, N. De Geyter, S. Van Vlierberghe, P. Dubruel, C. Leys, and E. Schacht, "Organic-inorganic behavior of HMDSO films plasma-polymerized at atmospheric pressure," *Surface and Coatings Technology*, 203, 10-11, pp. 1366-1372 (**2009**).

[126] C. Vautrin-Ul, C. Boisse-Laporte, N. Benissad, A. Chausse, P. Leprince, and R. Messina, "Plasma-polymerized coatings using HMDSO precursor for iron protection," *Progress in Organic Coatings*, 38, 1, pp. 9-15 (**2000**).

[127] R. Morent, N. De Geyter, S. Van Vlierberghe, P. Dubruel, C. Leys, L. Gengembre, E. Schacht, and E. Payen, "Deposition of HMDSO-based coatings on PET substrates using an atmospheric pressure dielectric barrier discharge," *Progress in Organic Coatings*, 64, 2-3, pp. 304-310 (**2009**).

[128] C. Saulou, B. Despax, P. Raynaud, S. Zanna, P. Marcus, and M. Mercier-Bonin, "Plasma deposition of organosilicon polymer thin films with embedded nanosilver for prevention of microbial adhesion," *Applied Surface Science*, 256, 3, pp. S35-S39 (**2009**).

[129] J. Schäfer, S. Horn, R. Foest, R. Brandenburg, P. Vašina, and K.-D. Weltmann, "Complex analysis of $SiO_xC_yH_z$ films deposited by an atmospheric pressure dielectric barrier discharge," *Surface and Coatings Technology*, 205, pp. S330-S334 (**2011**).

[130] T. Peter, "Tailoring of nanocomposite materials by embeding of gas phase grown nanoclusters," PhD thesis, Christian-Albrechts-University, Kiel (**2013**).

[131] A. Lakhtakia and R. Messier, *Sculptured thin films: nanoengineered morphology and optics*. SPIE Press (**2005**).

[132] G. L. Weissler (Ed.) and W. R. Carlson (Ed.), *Vacuum physics and technology: methods in experimental physics, vol. 14*. Academic Press, 1st ed. (**1979**).

[133] V. S. K. Chakravadhanula, "Vapor phase deposition of functional nanocomposite thin films and their modification by ion beam irradiation," PhD thesis, Christian-Albrechts-University, Kiel (**2011**).

[134] H. Yasuda, *Plasma polymerization*. Academic Press (**1985**).

[135] *Sycon Instruments, STM-100/MF, Thicknes/Rate monitor, User's Manual* (**2010**)

[136] D. A. Skoog, D. M. West, F. J. Holler, and S. R. Crouch, *Fundamentals of analytical chemistry*. Thomson Brooks/Cole, 8th ed. (**2004**).

[137] C. A. Brundle, C. A., Evans and J. S. Wilson (Eds.), *Encyclopedia of materials characterization: surfaces, interfaces, thin films*. Butterworth-Heinemann (**1992**).

[138] P. von der Heide, *X-ray photoelectron spectroscopy: An introduction to principles and practices.* John Wiley & Sons Inc. (**2012**).

[139] K. Moulder, F, Stickle, W F, Sobol, P E, Bomben, *Handbook of X-ray photoelectron spectroscopy*, Prairie, MN:Perkin-Elmer Corporation, 2nd ed. (**1992**).

[140] R. H. Fuchs, E., Oppolzer H., *Particle beam microanalysis: fundamentals, methods and applications*. VCH Verlagsgesellschaft mbH (**1990**).

[141] A. Lasia, *Electrochemical Impedance Spectroscopy and its Applications: Modern Aspects of Electrochemistry, vol. 32*. Kluwer Academic/Plenum (**1999**).

[142] S. Peng, J. M. McMahon, G. C. Schatz, S. K. Gray, and Y. Sun, "Reversing the size-dependence of surface plasmon resonances," *PNAS*, 107, 33, pp. 14530-14534 (**2010**).

[143] P. L. Redmond, A. J. Hallock, and L. E. Brus, “Electrochemical Ostwald ripening of colloidal ag particles on conductive substrates,” *Nano letters*, 5, 1, pp. 131-135 (**2005**).

[144] H. Takele, A. Kulkarni, S. Jebril, V. S. K. Chakravadhanula, C. Hanisch, T. Strunskus, V. Zaporojtchenko, and F. Faupel, “Plasmonic properties of vapor-deposited polymer composites containing Ag nanoparticles and their changes upon annealing,” *Journal of Physics D: Applied Physics*, 41, 12, pp. 125409-125414 (**2008**).

[145] J. Liu, D. M. Aruguete, M. Murayama, and M. F. Hochella, “Influence of size and aggregation on the reactivity of an environmentally and industrially relevant nanomaterial (PbS),” *Environmental science & technology*, 43, 21, pp. 8178-8183 (**2009**).

[146] M. V. Petri, R. A. Ando, and P. H. C. Camargo, “Tailoring the structure, composition, optical properties and catalytic activity of Ag-Au nanoparticles by the galvanic replacement reaction,” *Chemical Physics Letters*, 531, pp. 188-192 (**2012**).

[147] A. Kuzma, M. Weis, S. Flickyngerova, J. Jakabovic, A. Satka, E. Dobrocka, J. Chlpik, J. Cirak, M. Donoval, P. Telek, F. Uherek, and D. Donoval, “Influence of surface oxidation on plasmon resonance in monolayer of gold and silver nanoparticles,” *Journal of Applied Physics*, 112, 10, pp. 103531-103535 (**2012**).

[148] R. Lamendola, R. D. Agostino, and F. Fracassi, “Thin film deposition from hexamethyldisiloxane fed glow discharges,” *Plasmas and Polymers*, 2, 3, pp. 147-164 (**1997**).

[149] C. Damm, H. Münstedt, and A. Rösch, “The antimicrobial efficacy of polyamide 6/silver-nano- and microcomposites,” *Materials Chemistry and Physics*, 108, 1, pp. 61-66 (**2008**).

[150] K. Yliniemi, M. Vahvaselkä, Y. Van Ingelgem, K. Baert, B. P. Wilson, H. Terryn, and K. Kontturi, “The formation and characterisation of ultra-thin films containing Ag nanoparticles,” *Journal of Materials Chemistry*, 18, 2, pp. 199-206 (**2008**).

[151] S. Tanuma, T. Shiratori, T. Kimura, K. Goto, S. Ichimura, and C. J. Powell, “Experimental determination of electron inelastic mean free paths in 13 elemental solids in the 50 to 5000 eV energy range by elastic-peak electron spectroscopy,” *Surface and Interface Analysis*, 37, 11, pp. 833-845 (**2005**).